Electrical Conductivity of Binary PMMA/carbon-based filler and Ternary Poly(alkyl methacrylate)/PS/carbon-based filler composite films

Elektrische Leitfähigkeit von binären PMMA / Kohlenstoff-basierten Füllstoffen und ternären Poly (alkylmethacrylat) / PS / Kohlenstoff-basierten Füllstoff-Verbundfilmen

Der Technischen Fakultät
der Friedrich-Alexander-Universität Erlangen-Nürnberg
zur
Erlangung des Doktorgrades Doktor-Ingenieur
vorgelegt von

Huagen Xu
aus Jiangxi, China

Als Dissertation genehmigt von der

Technischen Fakultät der

Friedrich-Alexander-Universität Erlangen Nürnberg

Tag der mündlichen Prüfung: 12/November/2020

Vorsitzender des Promotionsorgans:	**Prof. Dr.-Ing. habil. Andreas Paul Fröba**
Gutachter:	**Prof. Dr. rer. nat. habil. Dirk W. Schubert**
	Prof. Dr.-Ing. Gregor Lang

List of publications

A. Peer-reviewed Papers

1. Xu, H., Qu, M., & Schubert, D. W. (2019). Conductivity of poly (methyl methacrylate) composite films filled with ultra-high aspect ratio carbon fibers. Composites Science and Technology, 181, 107690.

2. Xu, H., Qu, M. C., Pan, Y. M., & Schubert, D. W. (2019). Conductivity of Poly (methyl methacrylate)/Polystyrene/Carbon Black and Poly (ethyl methacrylate)/Polystyrene/Carbon Black Ternary Composite Films. Chinese Journal of Polymer Science, 38(3), 288-297.

3. Xu, H., Schubert, D. W. (2020). Perpendicular and in-plane conductivity of poly(methyl methacrylate) composite films filled with carbon-based fillers prepared from solution casting process. Macromolecular Materials and Engineering, DOI:10.1002/mame.202000107.

4. Xu, H., Schubert, D. W. (2020). Electrical Conductivity of Polystyrene/Poly(n-alkyl methacrylate)s/Carbon nanotube ternary composite casting films. Journal of Polymer Research, 27, 153.

5. Xu, H., Qu, M, & Schubert, D. W. (2020). Investigating electrical percolation threshold of various poly(alkyl methacrylate) /polystyrene/carbon black ternary composite films. Submitted.

6. Qu, M., Qin, Y., Sun, Y., **Xu, H**., Schubert, D. W., Zheng, K., & Nilsson, F. (2020). Biocompatible, Flexible Strain Sensor Fabricated with Polydopamine-Coated Nanocomposites of Nitrile Rubber and Carbon Black. ACS Applied Materials & Interfaces, 12(37), 42140-42152.

B. Conference contributions

1. Xu H., Qu M., Schubert DW. Conductivity of PMMA composite casting films filled with ultra-high aspect ratio of carbon fibers. The 2019 International Conference on Materials and Nanomaterials (MNs-19), in Paris, France, 2019.

2. Xu H., Qu M., Schubert DW. Double percolation effect on conductivity of PMMA/PS/CB and PEMA/PS/CB ternary composite films. The 2019 International Conference on Materials and Nanomaterials (MNs-19), in Paris, France, 2019.

3. **Xu H.,** Qu M., Schubert DW. Conductivity of PMMA composite casting films filled with ultra-high aspect ratio of carbon fibers. Polychar-27 World Forum on Advanced Materials, in Naples, Italy, 2019.

Table of contents

1

Introduction

Conductive polymer composite (CPC) films have been used in many fields, such as electromagnetic interfaces or shields against electrostatic as well as wearable sensors [1-4]. These CPC films can be obtained by adding carbon-based fillers to polymers. Conductive carbon-based fillers, such as carbon fibers (CFs), carbon black (CB) as well as carbon nanotubes (CNTs) are generally added into a polymer matrix [5-7]. Reaching a certain critical filler concentration, the electrical conductivity of the CPC films increases by several orders of magnitude. This critical concentration can be treated as the percolation threshold (ϕ_c), which indicates the formation of conductive filler pathways passing through the polymer matrix [8].

One of the important characteristics of the CPC films obtained from the solution casting method [9-12] is the filler alignment of the film. In most cases, the fillers like CNTs or CF are randomly oriented in CPC films along the substrate on which they are deposited [13,14]. Both from the theoretical and experimental point of view, there are plenty of researches focused on filler alignment. Apart from the filler alignment in-plane direction of the film, another significant factor for the ϕ_c is the perpendicular direction to the film.

Composites with high contents of fillers usually present poor mechanical properties, poor processability and high cost. Therefore, it is meaningful to manufacture CPC films with a lower ϕ_c [15,16]. It has been proved that the double percolation effect is an effective way to reduce the ϕ_c [17]. Moreover, thermal annealing under the quiescent condition is another effective method to lower the ϕ_c. During the annealing procedure, the fillers re-aggregate and form a pathway of filler particles in the polymer matrix [18].

In this thesis, binary composite films poly(methyl methacrylate) (PMMA)/CF with different CFs concentrations were obtained through the solution casting method. Considering different measure directions of the films, the pre-factors $K_\perp$ and $K_\parallel$ were revealed based on the existing Balberg's excluded volume theory for the first time.

In addition, binary composite films PMMA/CB and PMMA/CNT were obtained utilizing solution casting to reveal the electrically conductive behaviors of CPC films towards in-plane and perpendicular directions. The ϕ_c of all the binary composite films PMMA/CF, PMMA/CB and PMMA/CNT as well as different measurement directions were investigated. For different filler types (CF, CB, CNT), a power-law behavior was revealed correlating ϕ_c for perpendicular and in-plane directions and the corresponding exponent t for McLachlan theory.

To reveal the relationship between the compatibility of polymer blends in double percolation structure and corresponding ϕ_c of CPC films, polystyrene (PS), poly (alkyl methacrylate) (PalkylMA) and poly (cyclohexyl methacrylate) (PChMA) were selected as the polymer matrix in this thesis. The conductive PalkylMA/PS/CB and PChMA/PS/CB ternary composite films were obtained through the solution casting method. The ϕ_c of all the films before and after thermal annealing have been investigated. Moreover, scanning electron microscopy (SEM) was applied to characterize phase morphology of different kinds of PalkylMA/PS blends and PChMA/PS blend before and after annealing.

To further reveal how the different kinds of PalkylMA in PalkylMA/PS blends affect the conductivity of PalkylMA/PS/filler films, CNT was chosen as another kind of filler. Thus, PMMA/PS/CNT and PEMA/PS/CNT ternary composite films were presented as well.

For the solution cast films in this work, a series of ϕ_c and exponent t pairs could be obtained from the percolation curves of different carbon-based fillers utilizing the McLachlan equation. In particular, pairs derived perpendicular and in-plane to the films for binary composite films with CF of different AR as well as pairs derived perpendicular for ternary composite films with different polymer blends and different polymer blend ratios for both CB and CNT filler were investigated. In these systems, the exponent t for all three fillers is different from the value of 2.0 often referred to as “universal”. For the first time a relationship between ϕ_c and exponent t following a linear behavior $t = 2.0 + a \cdot \phi_c$ is proposed, indicating there is an intersection with the t-axis at t=2.0 when ϕ_c approaches 0.

2

Literature review

2.1 Conductive polymer composite (CPC) films

Conductive polymer composite (CPC) films are widely used in many fields like electromagnetic interference shielding, electrostatic dissipation as well as sensor [19-21]. Conductive fillers such as carbon fibers (CFs), carbon black (CB) as well as carbon nanotubes (CNTs) are often added to an insulating polymer matrix [22-24]. A percolation threshold (ϕ_c) is defined as a certain critical filler concentration when the electrical conductivity of the composites increases by several orders of magnitude, corresponding to the formation of a conductive filler pathway in the polymer matrix [8].

Many models are used to predict the conductivity of the CPCs system [25-28]. The most classical percolation theory for the percolation threshold of CPCs is [27]:

$$\sigma=\sigma_0 (\phi-\phi_c)^t \quad \text{for} \quad (\phi>\phi_c) \tag{2.1}$$

where ϕ is the volume concentration of fillers and ϕ_c is the percolation threshold of

fillers. σ_0 and σ are the electrical conductivities of filler and the composites, respectively. For composites with $\phi > \phi_c$, the experimental data are fitted by plotting log ($\phi-\phi_c$) against the log σ and adjusting ϕ_c to achieve the best linear fit.

McLachlan's general effective media (GEM) theory as following:

$$(1-\phi)\frac{\sigma_m^{1/s}-\sigma_c^{1/s}}{\sigma_m^{1/s}+\frac{1-\phi_c}{\phi_c}\cdot\sigma_c^{1/s}}+\phi\frac{\sigma_f^{1/t}-\sigma_c^{1/t}}{\sigma_f^{1/t}+\frac{1-\phi_c}{\phi_c}\cdot\sigma_c^{1/t}}=0 \quad (2.2)$$

where ϕ is the volume fraction of conductive filler and ϕ_c is the percolation volume fraction. σ_c, σ_m, σ_f are the conductivities of composite, the polymer matrix and the filler. The exponents t and s values are generally taken to be 2 and 0.87, respectively [28].

Additionally, A theory describing the ϕ_c of the cylindrical filler with the average angle between two cylinder fillers was presented by Balberg [29,30]. The cylinder orientation is considered in a 2-D system, where the cylindrical fillers contacted together, and thus the excluded volume of the cylindrical fillers as follows:

$$V_{ex}=\left(\frac{4}{3}\right)\pi W^3+2\pi W^2L+2WL^2\langle sin\ \gamma\rangle \quad (2.3)$$

where W is width of the filler, L is length of the filler, γ is the angle between two fillers. For each pair of fillers was presented by average sinusoidal value <sin γ>.

The percolation threshold is thus presented as follows:

$$\phi_c=K\times\frac{V_f}{V_{ex}}=K\times\frac{\frac{1}{6}\pi W^3+\frac{1}{4}\pi W^2L}{\left(\frac{4}{3}\right)\pi W^3+2\pi W^2L+2WL^2\langle sin\gamma\rangle} \quad (2.4)$$

An equation between aspect ratio AR=L/W and ϕ_c can be obtained through dividing by W^3,

Therefore, in this model, the percolation threshold can be presented as follows:

$$\phi_c = K \times \frac{\frac{1}{6}\pi+\frac{1}{4}\pi AR}{\frac{4}{3}\pi+2\pi AR+2AR^2\langle sin\gamma\rangle} \quad (2.5)$$

It can be noted that the percolation threshold of CPCs with CF as filler depends on the AR of CF and the internal orientation of CF.

2.2 Conductivity models for conductive polymer composite

A great number of models were applied to reveal the relationship between conductivity and filler concentration for conductive polymer composites which consisted of conductive fillers and polymer matrix.

2.2.1 Thermodynamic models

Mamunya et al. [31, 32] reported the conductivity of composites versus the filler volume concentration for different polymers to predict the influence of different parameters on the conductivity. These factors include surface energies of polymers and fillers as well as viscosities. The electrical conductivity of CPCs is presented based on this model is:

$$\log\sigma = \log\sigma_c + (\log\sigma_F - \log\sigma_c) \times \left(\frac{\phi-\phi_c}{F-\phi_c}\right)^k \quad (2.6)$$

$$k = \frac{K\phi_c}{(\phi-\phi_c)^n} \quad (2.7)$$

$$K = A - B\Upsilon_{pf} \quad (2.8)$$

where σ_c is the conductivity when filler fraction is exactly at the ϕ_c; σ_F is the conductivity when ϕ is at F; F is the maximum volume concentration; γ_{pf} is the surface energy; A, B and n are fixed values. This model only predicts the data point that the volume fraction above the percolation threshold. Therefore, in this thesis, this model is not utilized to obtain the percolation threshold.

2.2.2 Geometrical percolation models

A well-known theory, in this case, is the model presented by Turner and Malliaris [33]:

$$\sigma_B(max) \approx \left({}^{2}/_{300}\right)V_A\sigma_m \tag{2.9}$$

$$\rho_B(min) \cong 150\left({}^{\rho_m}/_{V_B}\right) \tag{2.10}$$

where V_A is a monolayer volume percent, V_B is a double layer volume percent, σ_m and ρ_m are the conductivity and resistivity of a bulk sample of metal, respectively.

However, in this study, after the experimental results, it was proved that the models cannot be able to reveal the volume fractions accurately.

2.2.3 Structure-oriented models

Kamal and Weber [34] have proposed two models considering the filler dimensions, volume fraction, aspect ratio as well as orientation. The corresponding equations for the contact can as follows:

$$\rho_{c,long} = \frac{\pi r^2 \rho_f X}{4\phi_p d_c l \cos^2\theta} \tag{2.11}$$

$$X = \frac{1}{0.59+0.15m} \tag{2.12}$$

$$\phi_p = \beta\phi \tag{2.13}$$

$$\beta = \frac{\phi-\phi_c}{\phi_t-\phi_c} \tag{2.14}$$

where $\rho_{c,\,long}$ is the longitudinal resistivity, ρ_f is the resistivity of fiber, l is the length, m is the contact numbers, ϕ_p is the volume concentration of fiber, d_c is the diameter for the contact circle, d is diameter of the fiber, θ is the angle of orientation, X is the contact numbers and ϕ_t is

threshold value, respectively.

A major restriction of these theories is that they do not account for predicting the surface energies that have been proved which has a noteworthy effect on the conductivity of the composite in this case.

McCullough et al. [35] combined thermal and electrical conductivity, diffusion coefficients as well as dielectric constant. Which generated a more precise equation:

$$\sigma_c = \phi\sigma_f + (1-\phi)\sigma_m - \left[\phi(1-\phi)S\left(\sigma_f - \sigma_m\right)^2 / \left(V_f\sigma_f + V_m\sigma_m\right)\right] \quad (2.15)$$

$$\mathrm{V}_f = (1-\mathrm{S})\cdot\phi + \mathrm{S}\cdot(1-\phi) \quad (2.16)$$

$$\mathrm{V}_p = \mathrm{S}\cdot\phi + (1-\mathrm{S})\cdot(1-\phi) \quad (2.17)$$

where σ_m, σ_f and σ_c are the electrical conductivities of the polymer matrix, the conductive fillers and the composites, respectively. S is a reference factor and ϕ is the volume fraction of filler. However, the geometry as well as the orientation of the fillers, are not considered in this model.

In terms of the GEM equation, Barton et al. [36] proved that critical exponent t (Figure 2.1) is influenced by the morphology and structure of the conductive fillers. If the filler in CPCs is graphite flake structure material, a large exponent t value between 6 and 8 is determined. This proved that exponent t value is influenced by the geometry of conductive filler [36]. Moreover, the t value is also affected by single filler as well as multiple fillers.

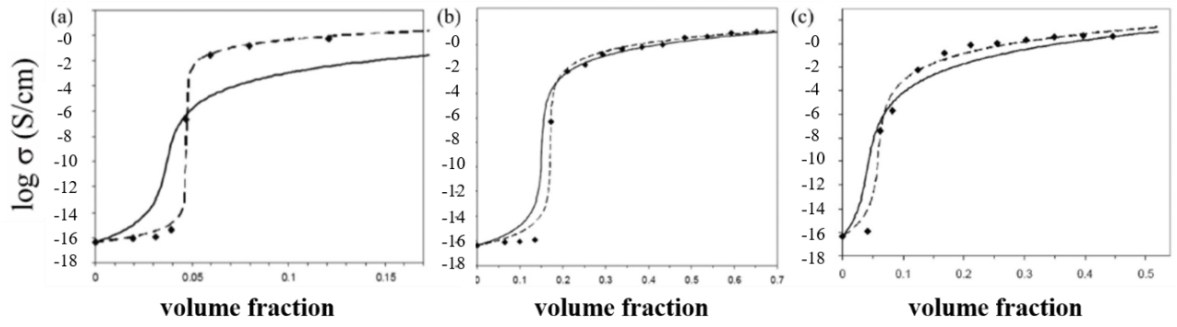

Figure 2.1 Electrical conductivity and GEM theory fitting results from experimental data: (a) CB ϕ_c =3.7%, t=4.2 and ϕ_c =4.7%, t=1.85; (b) synthetic graphite ϕ_c =1.51%, t=3.43 and ϕ_c =1.71%, t=2.75; (c) CF ϕ_c =4.1, t=5.77 and ϕ_c =5.9, t=4.38 [36].

2.3 Perpendicular and in-plane conductivity of CPC films

One of the important characteristics of the CPC films obtained from the solution casting method [37-40] is the electrical filler alignment of the film. In most cases, the fillers like CNTs or CF are randomly oriented in CPC films along the substrate on which they are deposited [13,14]. From both the theoretical and experimental point of view, there are plenty of researches concentrated on filler alignment. It has been revealed that the percolation threshold (ϕ_c) is strongly influenced by the internal orientation of the fillers or filler alignment [30, 43-46]. Gao et al. have fabricated anisotropic CPC films through the distribution of CNTs parallel to the substrate [43]. Additionally, Kocabas et al. [46] proved that perfect alignment of CNT is not good for the conductivity in the thin film.

Apart from the filler alignment along the in-plane direction of the film, another significant factor for the ϕ_c is the perpendicular direction to the film. A large number of researchers have been proved that the electrically conductive behaviors would be different at through-plane and in-plane directions of the film [47-49]. Bertolotti et al. revealed that electrically conductive behavior along the through-plane direction is much worse than that in-plane direction [47]. Stankovich et al. demonstrated that there is no remarkable difference in the through-plane conductivity and in-plane conductivity for the graphene-based composites [48].

Ding et al. revealed that the percolation behavior of the through-plane direction of the CPC films was almost ten times lower than that of in-plane direction [49]. Suherman et al. [50] also proved that the in-plane direction conductivity is different from the through-plane conductivity in Exopy/graphite/CB ternary composites.

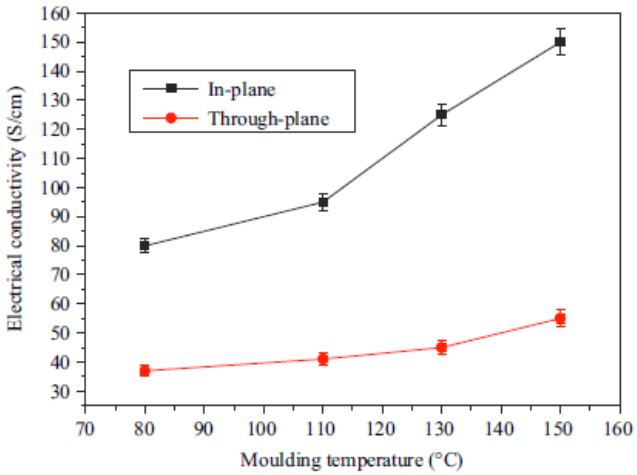

Figure 2.2 The through-plane and in-plane conductivities of the SG/EP/CB composites [50].

2.4 Polymer blends

Mixing polymers known as polymer blends is one of the most effective as well as economical methods to produce polymeric materials. This method can meet complex demands as well [51]. Polymer blends can be categorized as an immiscible system, partially miscible as well as miscible depending on the mutual interactions between the polymers [52].

A homogeneous phase can be observed in miscible polymer blends, which means polymers are mutually soluble. In this condition, only one glass transition temperature (T_g) would be observed. However, only a single-phase structure can be shown. There is always a level of heterogeneity at the thermodynamically miscible systems. Therefore, these blends are regarded as partially miscible instead of fully miscible. The partially miscible blends would be characterized by a broad interface with excellent interfacial adhesion while the immiscible system would be characterized by a sharp interface and a coarse morphology [53].

Immiscible polymer blends system would form different phase morphologies like co-continuous, fiber, sea-island as well as laminar (Figure 2.3) based on the processing conditions and blend ratios. The blend properties are greatly influenced by phase morphologies.

In general, an immiscible polymers system can be segregated into mainly two parts: (a) one phase that forms a dispersed phase while the other forms a continuous phase, which shows a sea-island structure; (b) the sections that form continuous phases and interlocked with each other or interpenetrated state of dispersion, forming a co-continuous structure [53].

Paul and Barlow [52,53] presented that the state from a sea-island to a co-continuous is:

$$\frac{\eta_{\gamma_1}}{\eta_{\gamma_2}} = \frac{\phi_1}{\phi_2} \tag{2.18}$$

where ϕ_i and η_{γ_i} are volume concentration and viscosity of component i, respectively.

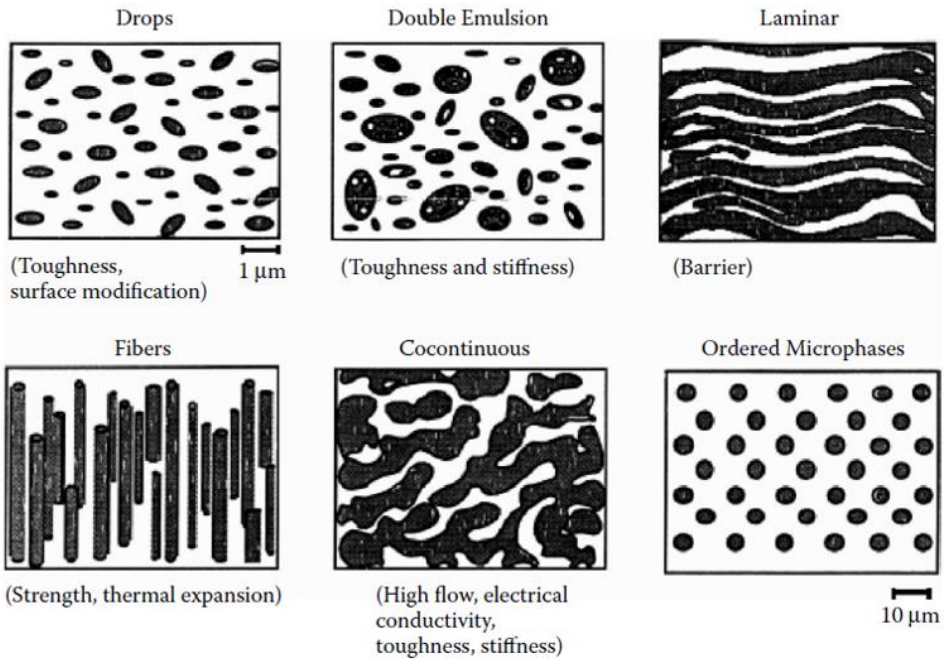

Figure 2.3 Schematic of phase morphologies of the polymer blends system. [53]

Poly(alkyl methacrylate) (PalkylMA)/polystyrene (PS) blends are widely investigated in the literature [54-56]. Friedrich et al. investigated thermodynamic study and rheological of the PChMA/PS blend, they found that the PChMA/PS blend system exhibits the LCST behavior

with a lower critical solution temperature of about 245°C. Only one T_g was revealed by DSC measurements. The range of the transition is small enough to conclude that they are miscible. [57]. Chang et al. [58] investigated the miscibility in blends of PChMA/PS with thermal, morphology and NMR characterizations. They revealed that mixtures of all compositions were miscible with all microscopic and thermal observations. The further evidence of LCST behavior with the thermodynamic transition in this blend system indicated that the transition of an originally miscible mixture, at higher temperatures, would be going through phase separation.

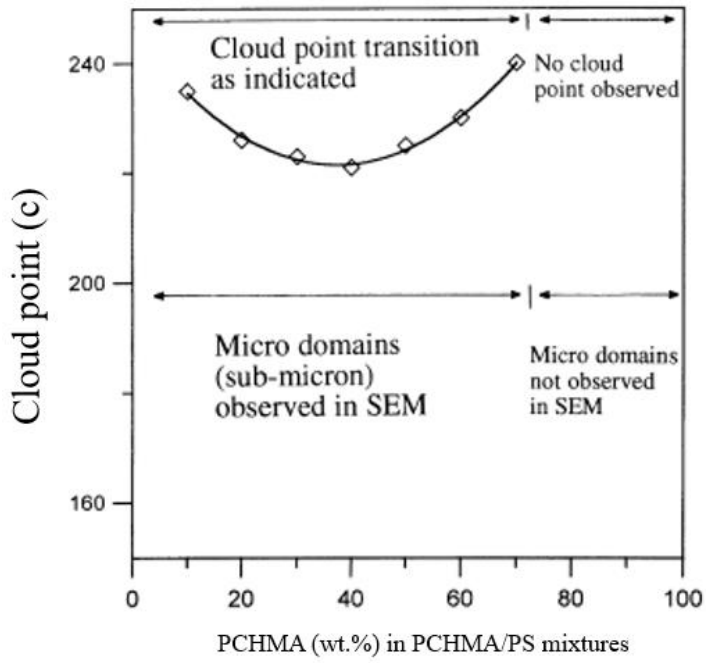

Figure 2.4 Cloud point of PChMA/PS blend as a function of composition. [59]

Voulgaris et al. [60] revealed that PEMA/PS blends show two T_g which are attributed to the two phases from PEMA and PS phase. The approach of the two T_g is ascribed to the partial mixing of the two polymers.

Affrossman et al. [61] revealed that in PBMA/PS mixtures, interfacial segregation would be caused and thus depletion of PBMA thin film by the lower surface energy of the butyl ester is in contrast to PMMA/PS blends.

The miscibility between PalkylMA and PS changes with alkyl lengths increasing because the

interaction energies between various methacrylate and PS are different. Schubert et al. [54] proposed a scheme (Figure 2.5) representing the compatibility of PalkylMA with PS and PMMA by investigating the interaction parameter between polymer blends. In the diagram, distances mirror the square root of the respective interaction parameters.

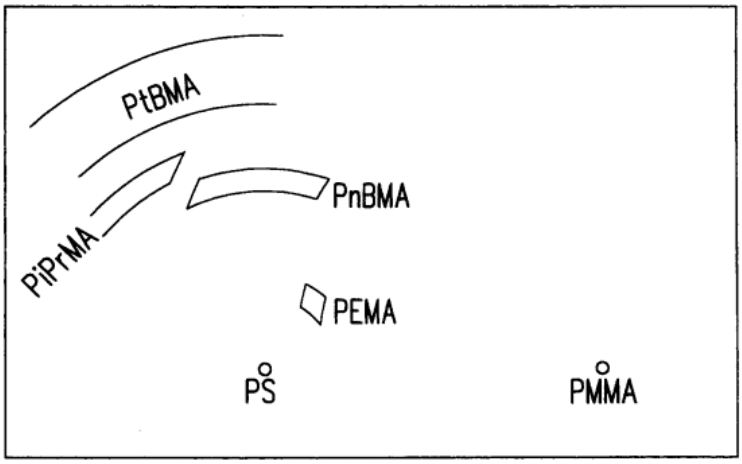

Figure 2.5 Scheme representing the compatibility of PalkylMA with PS and PMMA. distances mirror the square root of the respective interaction parameters. [54]

Kim et al. [55] reported that the immiscibility of PS with different methacrylate follows as PMMA>PBMA>PEMA>PChMA.

2.5 Double percolation effect

The double percolation method is a productive way of reducing ϕ_c [62]. It is essential that the filler selectively stays at the interface of a co-continuous structure or in one phase because of the affinity of filler with each polymer in this double percolation structure [63-68]. It is a typical method to evaluate the filler distribution in polymer blends using the wetting coefficient. According to the calculation of the interfacial tensions between all the components in the system, the theoretical prediction of the filler distribution is confirmed in many studies [69-72].

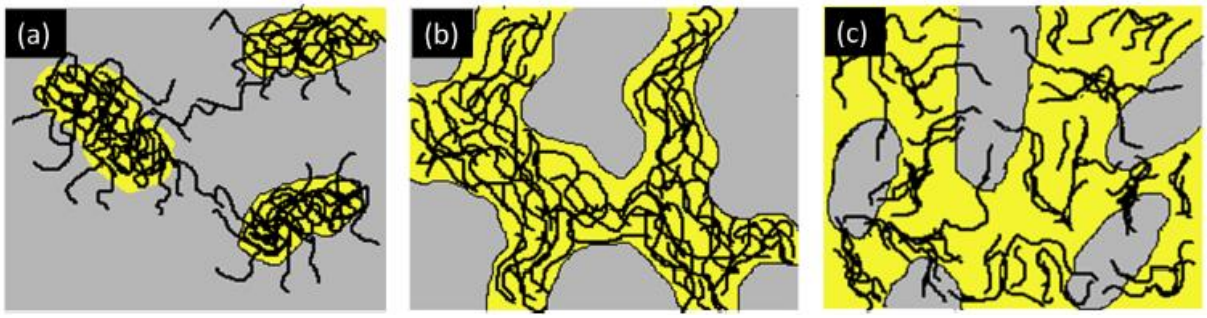

Figure 2.6 Schematic diagram showing the morphologies in (a) 3 wt% MWCNT+ 80/20 PP/NR, (b) 3 wt% MWCNT + 50/50 PP/NR and (c) 3 wt% MWCNT + 20/80 PP/NR (the grey region represents the PP phase, the yellow region represents the NR phase and the hairy-like structures represent MWCNTs).[5]

A lower ϕ_c could be obtained if the distribution of conductive fillers is at the interface of the co-continuous structure. This is probably due to a small number of fillers, which is enough to form a network at the continuous interface [72]. Two different methods have been investigated to achieve a double percolation effect: (a) kinetic control. The fillers, at least for a workable period, are "immobilized" at the polymer blend interface during processing conditions. Huang et al. identified PLA/PCL blend filled with MWCNT ternary composite. The ϕ_c of MWCNT/PLA/PCL composites was decreased by two orders of magnitude through adjusting the MWCNT only located at interface between PCL and PLA phases. (b) thermodynamic method. To make the filler at the interface of the polymer blend, the conductive fillers were modified or a compatibilizer was introduced. An extremely low ϕ_c of 0.05 wt % was obtained by Chen et al. They controlled MWCNT at the interface of immiscible PC/ABS by adding compatibilizer, and then an appropriate processing procedure was applied.

In addition, thermal annealing under the quiescent condition is another useful method for reducing the ϕ_c. During the annealing procedure, the particles re-aggregate and form a pathway in the polymer matrix [18]. Cipriano et al. [73] investigated MWCNT/PS and carbon nanofiber /PS composites obtained through melt blending, it was revealed that conductivities of the composites, through thermal annealing above the T_g, can be improved. This was probably

attributed to the aggregation of the MWCNT network.

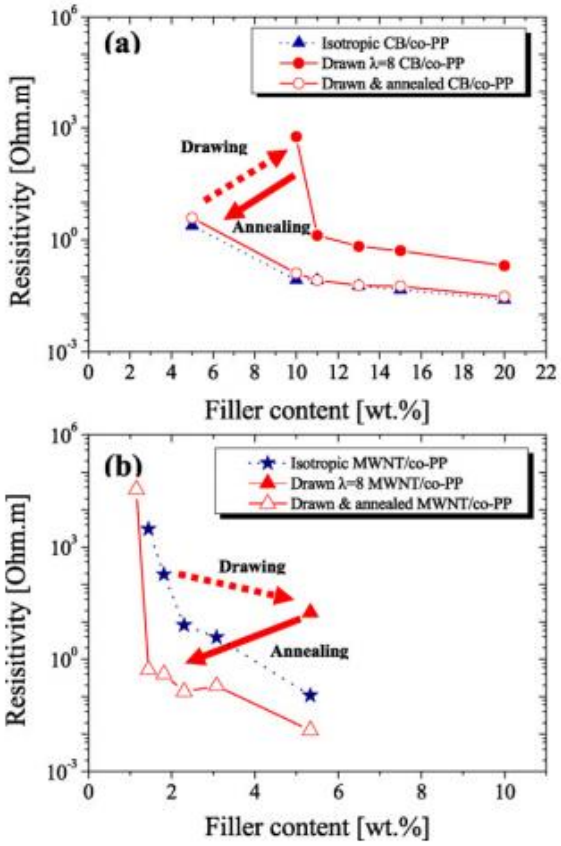

Figure 2.7 Effect of annealing (solid arrows) and solid-state drawing (dasher arrows) on the percolation threshold of CPCs revealed (a) co-PP with CB; (b) co-PP with MWCNT.[74]

2.6 Outline of the thesis

In this thesis, the electrical and morphology behaviors of PMMA/carbon-based fillers binary composite films will be investigated. Moreover, PalkylMA/PS/CB, PChMA/PS/CB and PalkylMA/PS/CNT ternary composite films. In chapter 2, background information about conductive polymer composite, phase morphologies, as well as PalkylMA/PS blends were presented. In Chapter 3, the materials, the processing as well as characterization methods involved in the thesis were presented. In chapter 4, PMMA/CF, PMMA/CB and PMMA/CB binary composite films have been investigated to show the influence of aspect ratio of conductive filler as well as the orientation of fillers on both the in-plane and perpendicular direction electrical conductivity of the CPC films. Not only the development of the existing

theory for electrical conductivity, but a power-law behavior was presented as well for different carbon-based filler types (CF, CB, CNT) correlating ϕ_c for perpendicular and in-plane directions and corresponding exponent t for McLachlan theory. In chapter 5, the PalkylMA/PS/CB and PChMA/PS/CB ternary composite films have been researched. The electrical conductivity behaviors of PalkylMA/PS/CB with different kinds of PalkylMA was revealed. In chapter 6, the electrical conductivity of PalkylMA/PS/CNT ternary composite films was investigated. In chapter 7, the relationship between percolation threshold and exponent t was investigated. The conclusions of this thesis are summarized in Chapters 8 and 9 (German version). Additional information is presented in the Appendix in Chapter 10.

3

Experimental section

3.1 Materials

In this thesis, polystyrene (PS), poly (alkyl methacrylate) (PalkylMA) and poly (cyclohexyl methacrylate) (PChMA) was selected as a polymer matrix. The PalkylMA matrix represents poly(methyl methacrylate) (PMMA), poly(butyl methacrylate) (PBMA), poly(ethyl methacrylate) (PEMA), respectively. PMMA is a kind of optically clear plastic. Owing to its lightweight, high impact strength as well as favorable processing conditions, it has been broadly applied as a substitute for inorganic glass. PS is another most broadly used polymer and is generally rigid and inexpensive. The miscibility between PalkylMA and PS changes with alkyl lengths increasing because the interaction energies between various methacrylates and PS are different, Therefore, PEMA/PS, PBMA/PS and PChMA/PS blends are used as the polymer matrix as well. PS 158N and PMMA Plexiglas 7N were got from Evonik Röhm GmbH. PEMA, PBMA and PChMA were obtained from Sigma Aldrich. Finally, Table 3.1 presents the material properties of PS, PalkylMA and PChMA used in this work.

The carbon-based filler utilized in this thesis are carbon black (CB), carbon fiber (CF) as

well as carbon nanotube (CNT), respectively. The CB particles (Figure 3.1 (a)), with a specific surface area of 900 m^2/g measured by the BET-method, is Printex XE2 from Evonik industries. The density of the primary CB particles is 2.13 g/cm^3 and the mean diameter is around 35 nm. The CF (Figure 3.1 (b)) is got from Tenax® - JHT C493 (Toho Tenax Europe GmbH, Wuppertal, Germany) with a specific resistance of 1.7×10^{-3} Ω/cm, a diameter of 7 μm, an initial length of 6 mm, and a density of 1.79 g/cm^3. The CNT (Figure 3.1 (c)) is Bayertubes® C 150 P, with an inner diameter of 4 nm, an outer diameter of 13 nm, an average length of 1 μm and a bulk density of 130-150 kg/m^3.

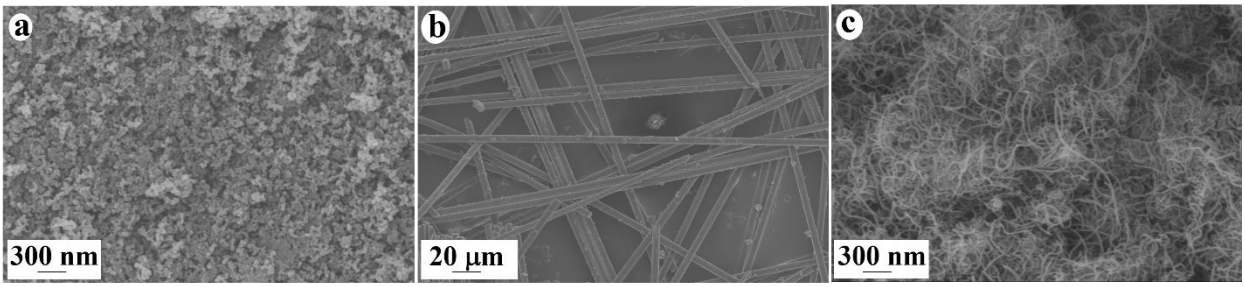

Figure 3.1 Morphological images of the carbon-based fillers (a) CB; (b) CF; (c) CNT.

Table 3.1 Properties of the PalkylMA and PS.

Polymer	T_g (°C)	Density (g/cm^3)	M_w (kg/mol)	M_w/M_n
PS	109	1.05	268	2.5
PMMA	101	1.19	92	2.1
PBMA	20	1.07	227	2.3
PEMA	65	1.16	281	2.5
PChMA	104	1.10	147	2.8

3.2 Composite films preparation

3.2.1 Binary composite films

To reduce aggregations, aqua regia was used to oxidize both CNT and CF for 24h. And then

washed with acetone to PH value around 7. Afterward, the CF and CNT were put into the oven for 48h to be completely dried.

Utilizing a scissor, the CFs with different aspect ratios (AR) were obtained through cutting the original CFs to the desired length of 4.5 mm, 3.75 mm, 3.0 mm, 2.25mm, 1.5 mm, 0.75 mm and 0.375 mm, respectively. A nonius caliper was applied to control the cut length of CFs. Afterward, the real lengths of CF are determined by a light microscope.

Before processing, all the materials were dried in an oven for twelve hours at 80 °C. All binary PMMA/CF, PMMA/CB as well as PMMA/CNT composite films were obtained through the solution casting method (Figure 3.2). Carbon fillers were sonicated in THF for one hour for a better dispersion before mixing with the polymer. In this work, the concentration of polymer in solution was roughly kept at 4 wt. %. Afterward, PMMA was put into a prepared solution. And then PMMA/carbon-based filler mixtures were obtained after the previous mixtures stirred 24 h at room temperature. PMMA/carbon-based filler solutions were deposited onto rectangular glass plates (75 × 25 mm^2) (Figure 3.3). Let it stand still for 96 h and then peel it off from the substrate. The films were firstly dried by vacuum absorption drying for 6 h. Finally, the films were put into an oven after the evaporation of THF (Figure 3.3) at 80 °C to remove the residual THF. The thickness of the film is about 200 μm can be obtained through this method.

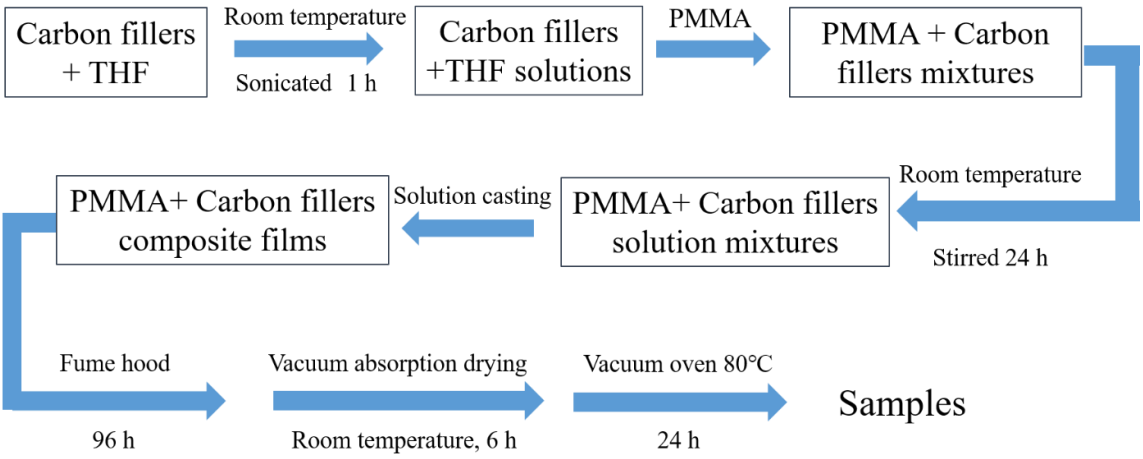

Figure 3.2 Sample preparation flow chart. Carbon fillers represent CB, CF as well as CNT in this thesis.

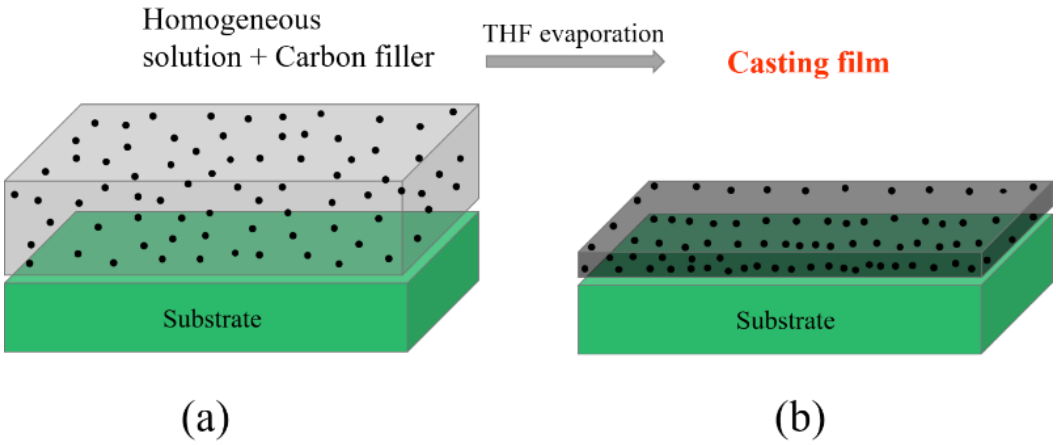

Figure 3.3 Schematic diagram of the solution casting method: (a) homogeneous solution with carbon filler and polymer; (b) casting film after THF evaporated.

3.2.2 Ternary composite films

Before processing, all materials were dried in an oven for twelve hours at 80 °C. PalkylMA/PS/Filler films were obtained through the solution casting as well (Figure 3.4). CNT and CB were sonicated in THF for one hour before mixed with polymers for better dispersion. Afterward, PalkylMA and PS with a certain ratio (pure PalkylMA and PS also included) were put into the THF solution. Next, PalkylMA/PS/Filler solution mixtures were prepared after the previous mixtures were stirred 24 h at room temperature. PalkylMA/PS/Filler solutions were

deposited by solution casting onto rectangular glass plates (75 × 25 mm^2). A schematic diagram for ternary composite films was presented to simply describe the solution casting process (Figure 3.5). Thermal annealing treatment of the PalkylMA/PS/CB films was conducted at 143°C in the hot press for 120 minutes.

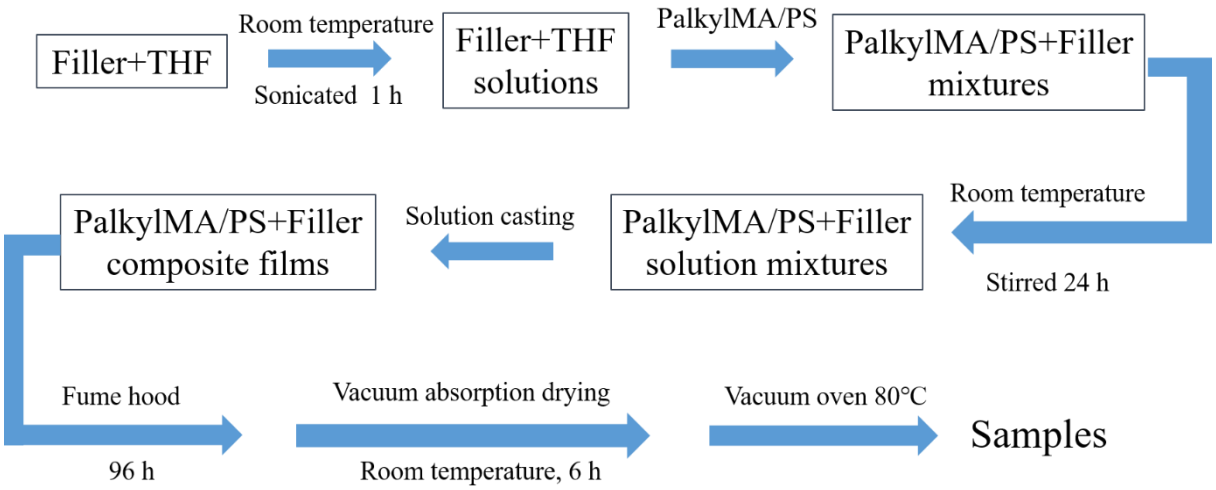

Figure 3.4 Sample preparation process. Fillers represent CB and CNT in this work.

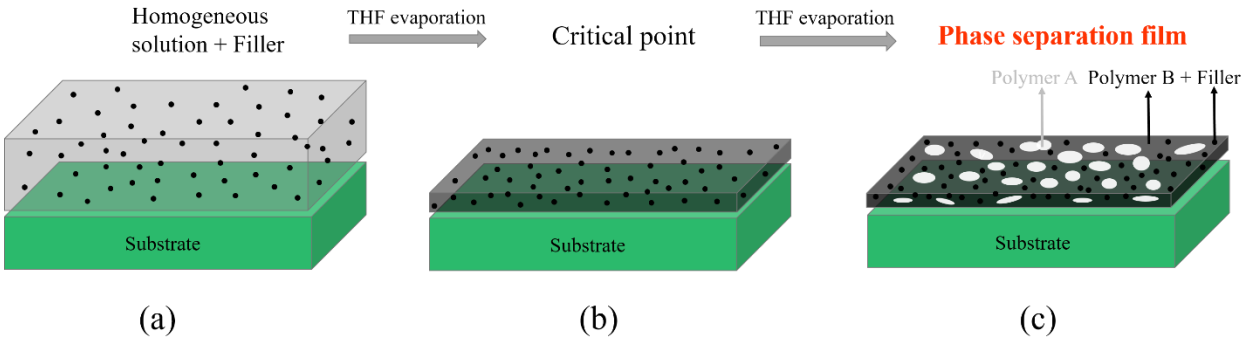

Figure 3.5 Schematic diagram of solution casting process: (a) homogeneous solution consists of polymer A, polymer B, solvent as well as CNT; (b) critical point; (c) phase separation with THF still evaporates and enables sufficient mobility to form phase-separated structure.

3.3 Analytical characterization

3.3.1 Morphology

The light microscope (Leitz, Orthoplan P) was applied to observe surfaces of the composite

films. The dispersion and orientation of CFs can be evaluated.

The cross-section morphology of the films was observed through the scanning electron microscope (SEM) (Carl Zeiss Microscopy, Germany). The accelerating voltage is 5 kV. Firstly, the films were fractured in liquid nitrogen. Afterward, the fracture surfaces were coated by gold through the Sputter Coater S150B from Edwards.

3.3.2 Electrical conductivity

For the perpendicular direction conductivity, as shown in Figure 3.6 (a), a stack of rubber foam, aluminum foil, sample and a counter of aluminum foil and rubber foam was used. This kind of device ensured a reliable resistance measurement [75]. The thickness of the CPC films was measured through a digital test device (TESA Digico, TESA SA, Renes, Swiss).

The perpendicular direction resistance of the films was measured utilizing a Keithley 6487 picoammeter with a fixed voltage (1 V) at room temperature. The perpendicular direction conductivity σ was calculated as follows:

$$\sigma_{\perp} = \frac{d}{R_{\perp} \cdot \pi \cdot r^2} \tag{3.1}$$

where $R_{\perp}$ is the perpendicular direction resistance of the film, d is the thickness of the film and r is the radius of the rubber foam which is covered by aluminum foils.

For the in-plane direction conductivity measurement (Figure 3.6 (b)), the composite films were cut to the rectangular shape of ca. 20×25 mm^2 and both edges of each sample were slightly polished and coated with Ag-paste for better contact between electrode and samples. The length of the sample L (distance between both coated edges) and the width of composite films were measured.

The in-plane direction electrical conductivity σ was calculated as follows:

$$\sigma_{\parallel} = \frac{L}{R_{\parallel} \cdot W \cdot d} \tag{3.2}$$

where L is the distance between both coated ends, d is the thickness of the film, $R_{\parallel}$ is the in-plane direction resistance and W is the width of the film.

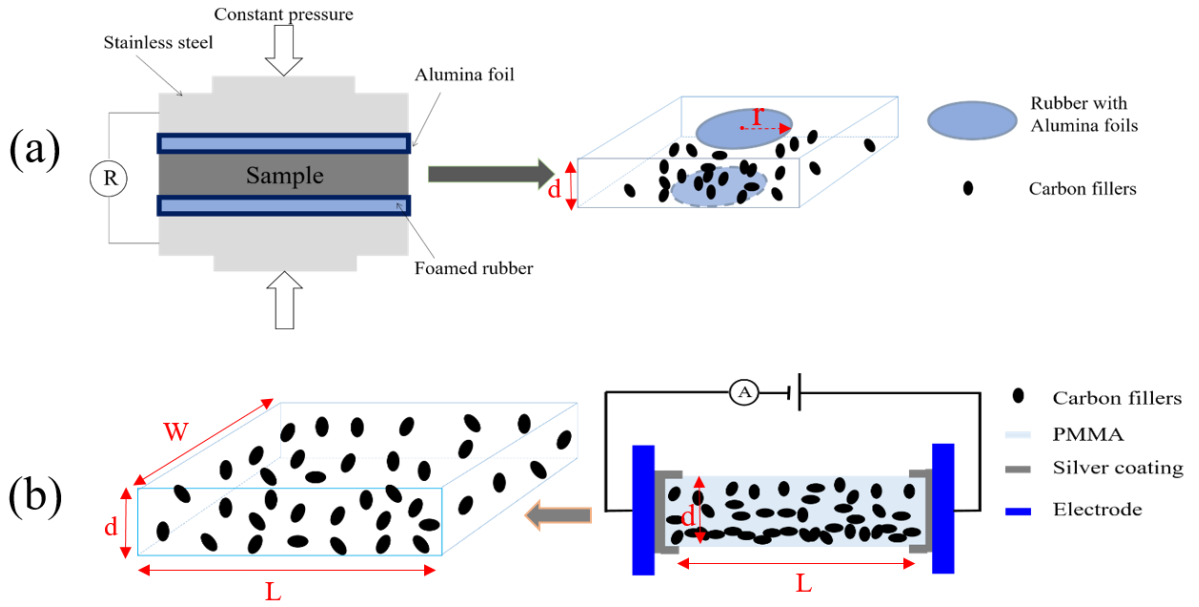

Figure 3.6 Schematic diagrams for conductivity measurement: (a) For perpendicular direction; (b) For in-plane direction. Ten samples were tested for each measurement to ensure reproducibility.

3.3.3 Size exclusion chromatography (SEC)

M_w of PBMA and PChMA were determined through Size exclusion chromatography (GPCmax, Malvern). THF solution is used to dissolve the polymers with a constant flow rate of 1.0 ml/min at 35°C. Based on GPC results, polymerization degrees can be determined for these polymers.

3.3.4 Fourier Transform infrared spectrometer (FTIR)

The FTIR spectra of the composite films were recorded through a Nicolet 6700 FTIR spectrophotometer with a resolution of 4 cm^{-1} for four scans in the wavenumber range of 4000–550 cm^{-1} by the attenuated total reflection method.

4

PMMA/Carbon-based filler binary system

For CF: $\phi_{c,\parallel} \approx 7.65 \times \phi_{c,\perp}$

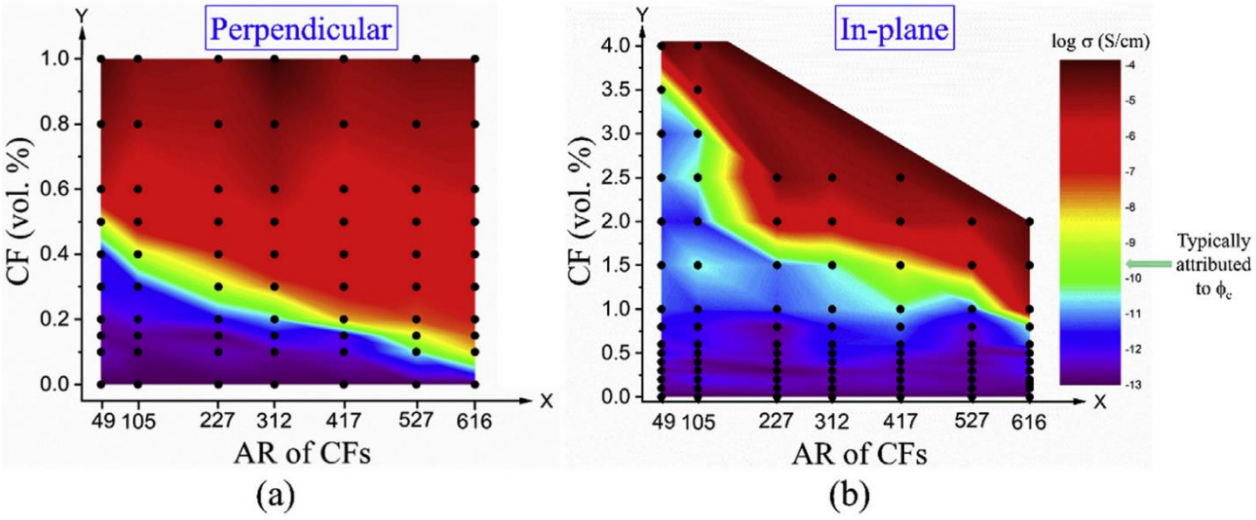

4.1 Introduction

As a conductive filler, in both engineering and academic contexts, carbon fiber (CF) with a high aspect ratio (AR) as well as high conductivity is the most widely used carbon filler [76-78]. It was revealed that forming a conductive network is strongly affected by oriented of the fillers, filler volume fraction as well as the AR of the filler [79].

The orientation of CF in PMMA/CF films is an important factor in terms of the percolation threshold (ϕ_c) of the composite films [80,81]. With the increasing orientation of CFs, the ϕ_c of composites would be shifted to a higher filler concentration. A great deal of researches has concentrated on polymer/CF composites with CF randomly oriented in the polymer matrix [82,83], even from a purely theoretical point of view [84]. The probability of contact between the fibers increases with AR of CF increasing, which means that the CPC with a larger AR of CF shows a higher electrical conductivity at the same CF concentration. That is to say, the ϕ_c of CPC films would be the lowest with the highest AR of CFs [85-87].

4.2 Oxidation of CFs

To determine the oxidation result of CFs, the pristine CF and oxidation CF were characterized with FTIR-spectrum. And the result as Figure 4.1.

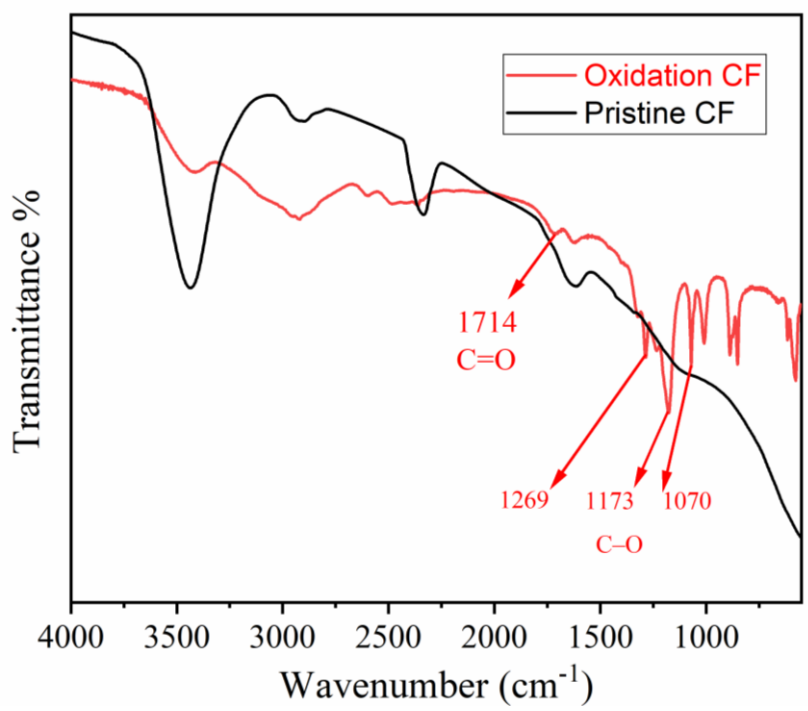

Figure 4.1 FTIR of pristine and oxidation carbon fibers

It can be clearly found that the spectrum gave rise to a new peak located at 1714 cm^{-1} after oxidation, which was attributable to C=O. Moreover, the new peak located at 1269, 1173 and 1070 cm^{-1} was also found after oxidation, which was attribute to C–O. Combined with these different peaks, it indicates that surface oxidation of CFs (COOH) was successful [88,89].

4.3 Length of carbon fibers

To reveal the CF lengths after film processing, the CPC films were dissolved into acetone to evaluate CF length. 200 CFs were chosen randomly with the light microscope, and JMicrovision software was used to analyze. The lengths of CF prior to (Fig. 4.2(a-c)) and next to (Fig. 4.2(d-f)) the film processing was observed and analyzed directly. The desired lengths of 0.375mm, 2.25mm, 4.5mm are presented as typical examples. The frequency distributions of the CF lengths prior to (Fig.4.3, a-c) and next to (Fig.4.3, d-f) film processing for the corresponding desired lengths are shown in Figure 4.3.

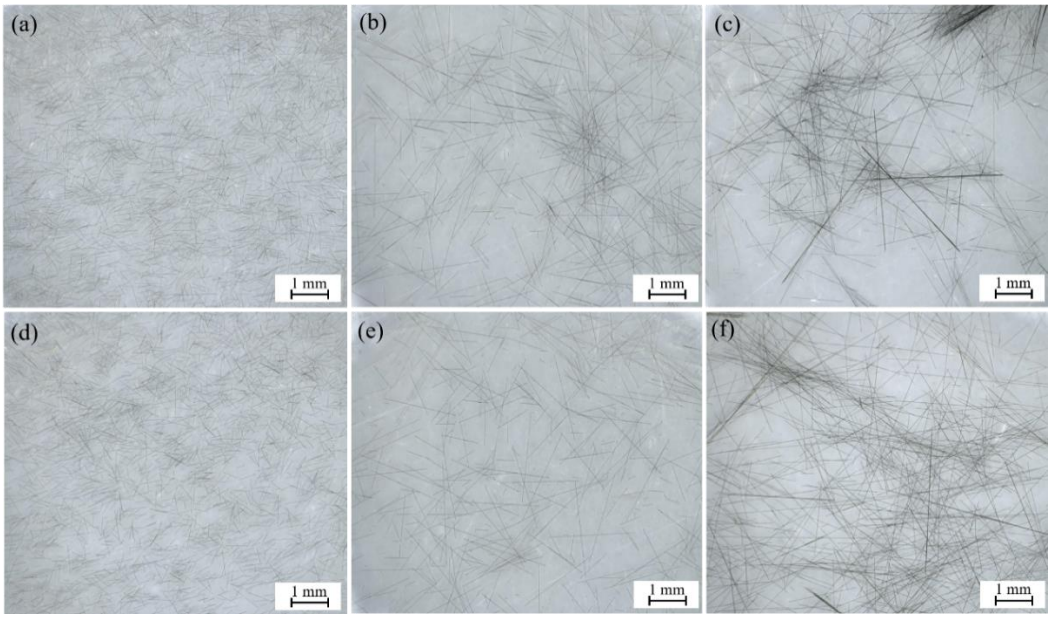

Figure 4.2 CF Lengths prior to (a, b, c) and next to (d, e, f) film processing for the desired lengths of 0.375 mm (a, d), 2.25 mm (b, e), 4.5 mm (c, f), respectively.

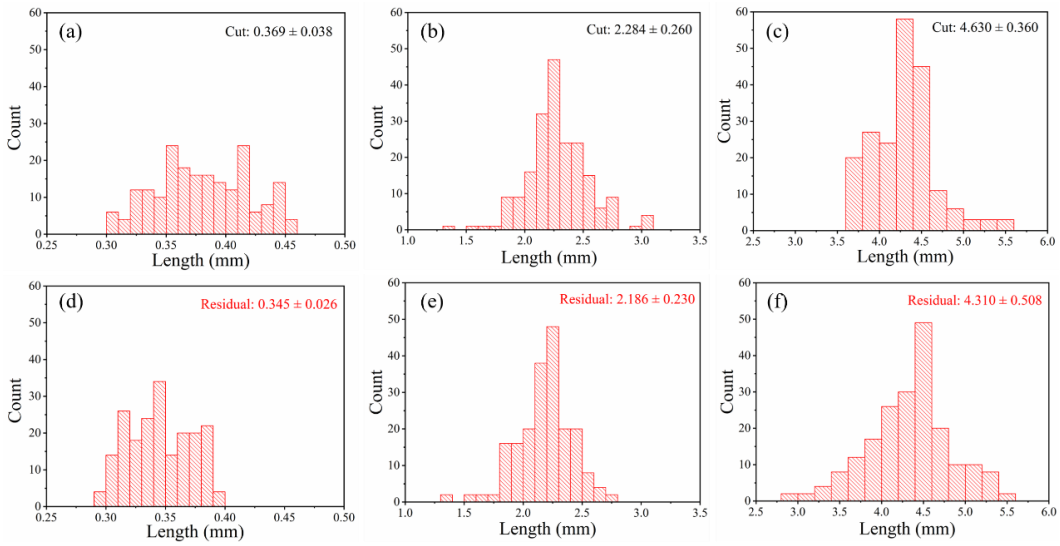

Figure 4.3 Lengths distribution of CFs prior to (a, b, c) and next to (d, e, f) film processing for the desired lengths of 0.375 mm (a, d), 2.25 mm (b, e), 4.5 mm (c, f), respectively.

Figure 4.4 shows the average CFs lengths prior to and next to film processing. The difference between the CF lengths prior to and next to film processing is negligible, which means a stable length of CFs during film processing. Moreover, the deviation between the experimental length and the desired lengths of the CF is presented by the dashed line, which is located within the

error bars. Thus, the corresponding AR of CF, in this study, were calculated based on the lengths after film processing. The results for AR of CFs are 49, 105, 227, 312, 417, 527 and 616, respectively.

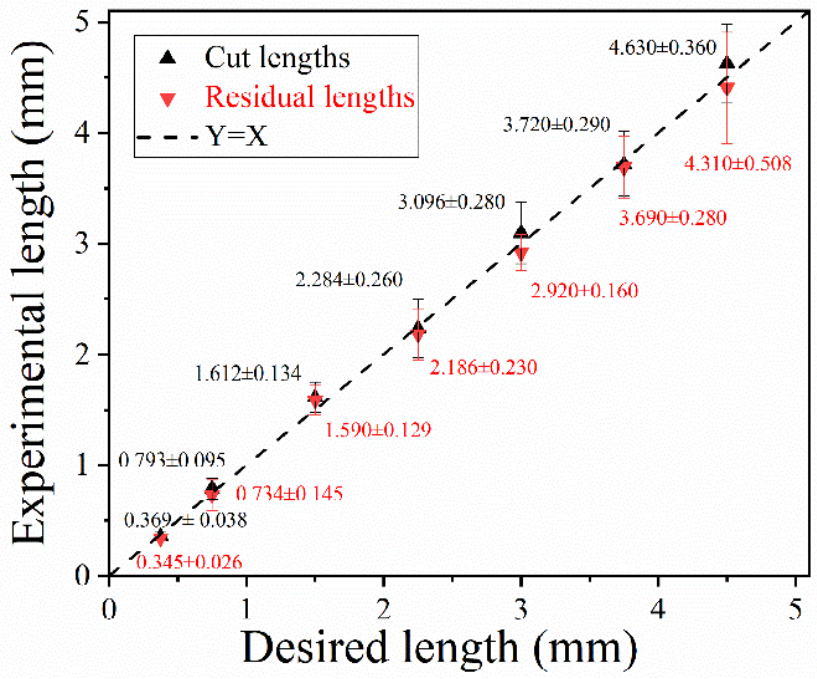

Figure 4.4 The average lengths of the CFs prior and next to film preparation versus the desired length.

4.4 Morphology of PMMA/CF composite films

A distribution of CFs with AR at 227 in the binary PMMA/CF composite films prepared from the solution casting method is shown in Figure 4.5. The volume CF concentration in (a)-(d) are 0.1; 0.2; 0.5; 1.0 vol. %, respectively. It is well known that the conductive pathway is formed through the CF gets contacted with each other. In this study, there is a subsidence effect during film processing. Therefore, the CF would be get contacted with each other easily due to gravity. In other words, the isolated polymer matrix between CF can be neglected. Thus, the only parameter that would affect the electrical conductivity of CPC films is supposed to be the CF length. Due to the extremely high CF length, at high magnification, the whole single CF cannot be shown in one graph. The connection between the CFs is easily achieved because of the high

CF length in polymer composite films, which means the conductive filler pathway in the matrix is easy to form.

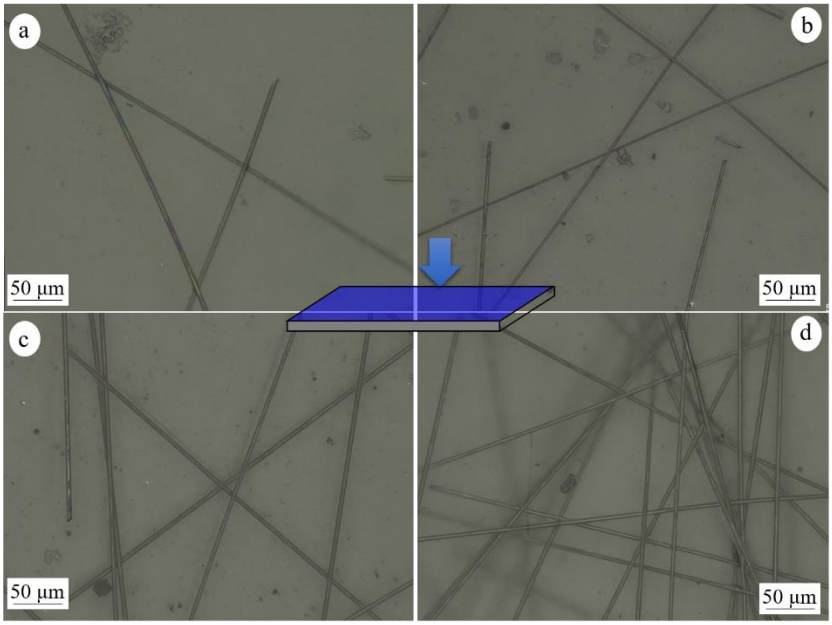

Figure 4.5 CFs distribution in the binary PMMA/CF composite films prepared from solution casting method: (a) CF vol. 0.1%; (b) CF vol. 0.2%; (c) CF vol. 0.5% (d) CF vol. 1.0%. The direction of the blue arrow shows the observation direction under the microscope.

SEM micrographs of CPC films with AR of CF at 227 are shown in Figure 4.6, The volume fractions of CF are 0.1; 0.2; 0.5; 1.0 vol. %, respectively. The graphs are taken of the cross-section of the films, that is to say, this is perpendicular to the surface observed by light microscopy. The increasing CFs concentration in Figure 4.6 brings a higher probability for CFs contacted with each other, which means the conductive pathway between the CFs in the polymer matrix is formed when CF concentration high enough. Moreover, the oxidized CFs are evenly dispersed in CPC films without forming a cluster.

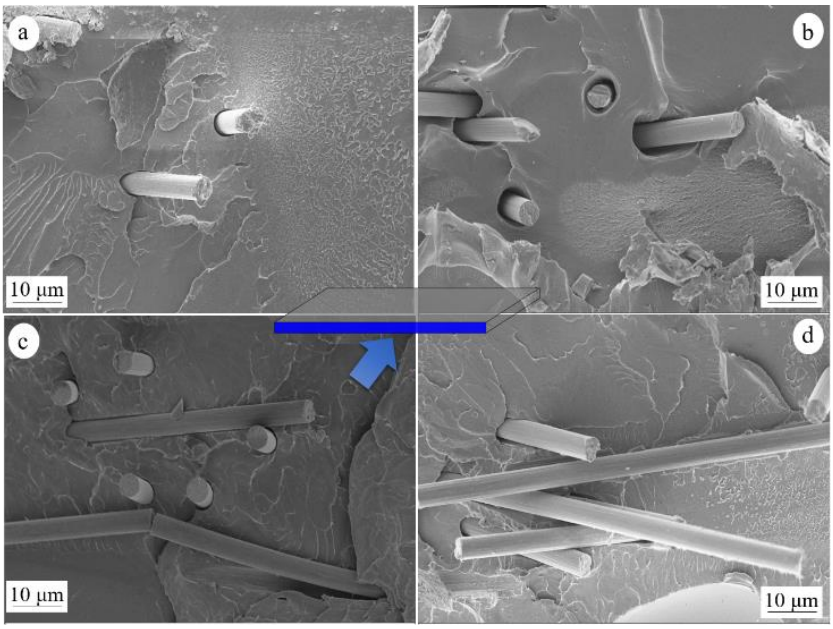

Figure 4.6 SEM graphs of PMMA/CF composite films: (a) CF vol. 0.1%; (b) CF vol. 0.2%; (c) CF vol. 0.5%; (d) CF vol. 1.0%. The direction of the blue arrow shows the observation direction under the microscope.

4.5 Electrical conductivity of the PMMA/CF composite films

The in-plane and perpendicular electrical conductivity of the CPC films versus CF concentration with different AR are shown in Figure 4.7 and Figure 4.8, respectively. With ARs of CFs from 49 to 616, the corresponding electrical conductivities of CPC films are shown with different symbols. Each data point is obtained from an average of 10 measurements, and vertical error bars represent standard deviations. All curves show a steep increase in electrical conductivity on reaching a critical concentration, which is corresponding to ϕ_c.

The electrical conductivity of pure PMMA was measured to σ_m (1.0×10^{-13} S·cm^{-1}) and was taken as a constant. The σ_f, electrical conductivity of the CF, was taken from the manufacturer's datasheet which is 5.89×10^2 S·cm^{-1}. The dashed lines in Figure 4.7 and Figure 4.8 represent the fits according to Eq. 2.2, where the ϕ_c and exponent t are used adjustable fitting parameters for all seven different ARs, respectively. The perpendicular percolation threshold $\phi_{c,\perp}$ results are shown in Table 4.1 and the in-plane percolation threshold $\phi_{c,\parallel}$ results are shown in Table 4.2.

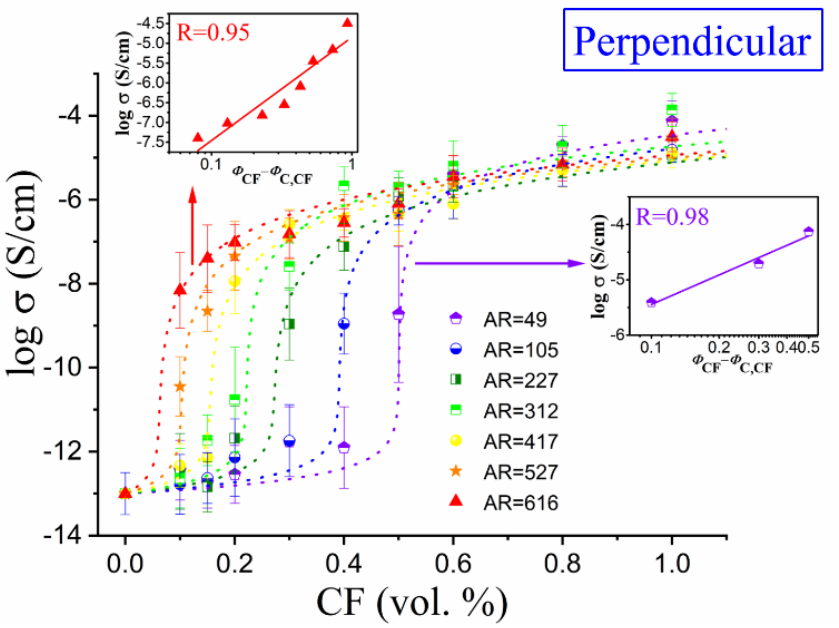

Figure 4.7 The logarithm value of the perpendicular conductivity of the CPC films versus CF concentration for binary PMMA/CF composite films obtained from the solution casting method with AR of CFs is 49, 105, 227, 312, 417, 527 and 616, respectively. The best fit utilizing the Mclachlan theory (Eq. 1) was shown by the dashed lines. The two insets illustrate the linear fit using (Eq. 2) for AR=49, AR=616, respectively.

Table 4.1. Perpendicular direction ϕ_c results of the fitting of experimental data utilizing the Mclachlan equation and classical percolation theory shown in Figure 4.7.

AR	49	105	227	312	417	527	616
ϕ_c (Eq.2.2)	0.50±0.36	0.39±0.09	0.27±0.06	0.22±0.09	0.15±0.05	0.10±0.06	0.07±0.04
ϕ_c (Eq.2.1)	0.57	0.43	0.25	0.24	0.14	0.11	0.06
t (Eq.2.1)	3.38	3.28	2.7	2.26	2.27	1.63	1.17

The experimental results, for filler concentration $\phi>\phi_c$, were fitted (Eq. 2.1) by plotting log $(\phi-\phi_c)$ against the log σ and adjusting ϕ_c until the best linear fit was achieved. In each Figure 4.7 and Figure 4.8 present two of them as the insets. Table 4.1 shows the fitted $\phi_{c,\perp}$ and exponent t value, and Table 4.2 shows $\phi_{c,\parallel}$ and t value. The ϕ_c towards a lower concentration with

increasing AR of CF. And the t value is decreasing accordingly. There is no significant difference between the ϕ_c obtained from Eq. 2.1 and Eq. 2.2. Therefore, all the ϕ_c results discussed in this thesis are obtained from Eq. 2.2.

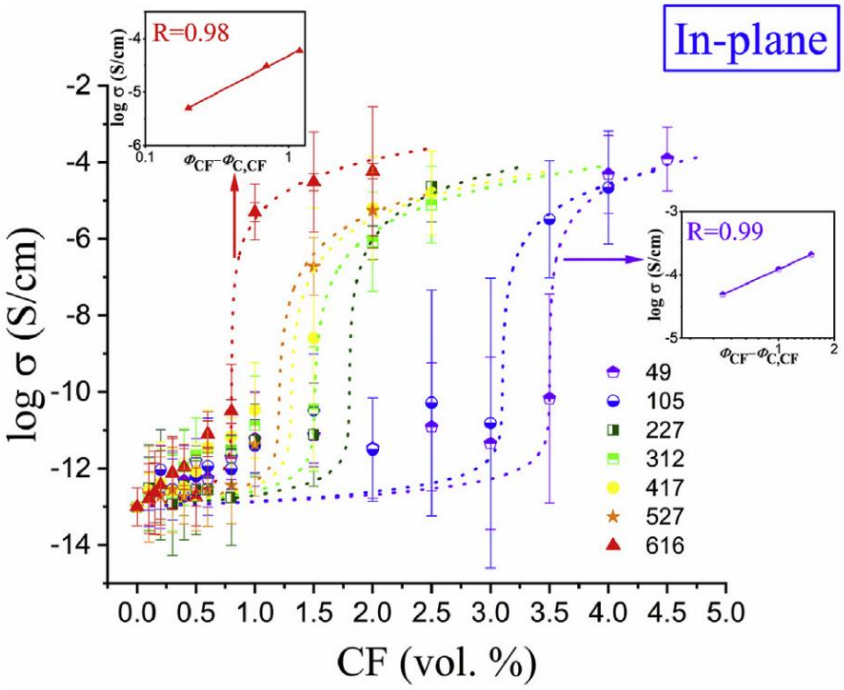

Figure 4.8 The logarithm value of in-plane direction conductivity versus CF concentration for binary PMMA/CF composite films (all other information is the same as Fig. 4.7).

Table 4.2. In-plane direction ϕ_c results of the fitting of experimental data utilizing the Mclachlan theory and classical percolation theory shown in Figure 4.8.

AR	49	105	227	312	417	527	616
ϕ_c (Eq.2.2)	3.50±0.60	3.10±0.50	1.80±0.30	1.51±0.25	1.30±0.35	1.10±0.18	0.80±0.20
ϕ_c (Eq.2.1)	3.87	3.25	1.92	1.47	1.12	1.09	0.72
t (Eq.2.1)	4.22	3.61	3.19	2.67	2.59	2.31	2.26

4.6 Contour plot of conductivity on PMMA/CF composite films

Figure 4.9 presents a conductivity contour plot diagram according to all conductivity data of

PMMA/CF films with different CF concentrations and different ARs of CF. In the contour plot, the X-axis and Y-axis respectively correspond to AR of CFs and volume fraction of CF. The experimental data are presented by black dots in the contour plot. The colors in the contour plot represent the logarithm value of conductivity.

The electrical conductivity of binary PMMA/CF composite films is obviously influenced by the AR of CFs (along the X-axis). Moreover, the electrical conductivity increases with an increasing volume fraction of CFs (along the Y-axis). Furthermore, the ϕ_c area typically corresponds to the green area in the contour plot starts with a lower volume fraction of CF, this means the ϕ_c towards a lower concentration as well with increasing AR of CF.

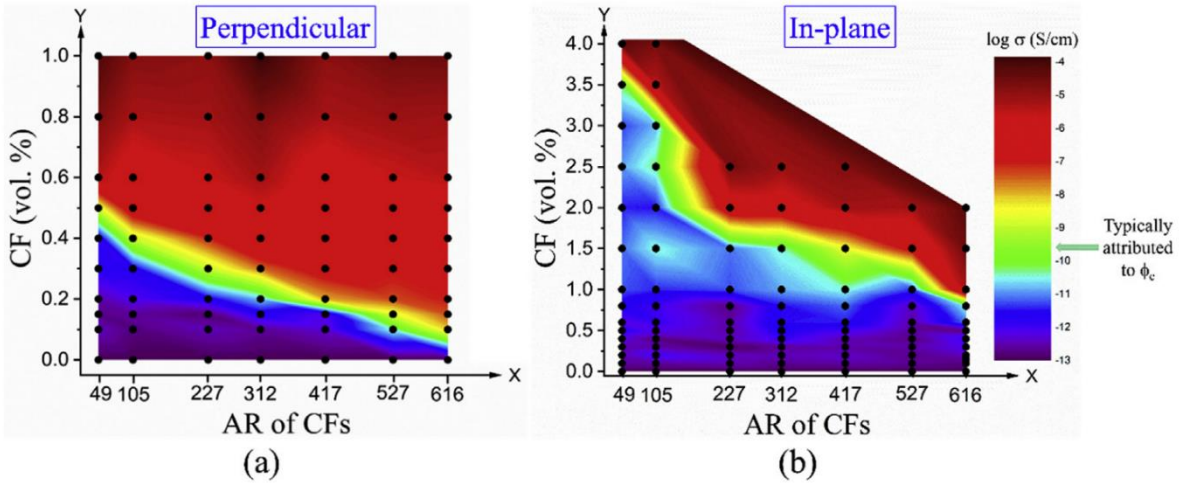

Figure 4.9 The logarithm value of electrical conductivity of binary PMMA/CF composite films versus different ARs of CF and volume fraction of CF: (a) Perpendicular direction of film; (b) In-plane direction of the film.

A schematic diagram for a conductive filler pathway (perpendicular direction) is presented in Figure 4.10. The AR of CF and CF concentrations are increasing. The CPC films are represented by cuboids in this study, CFs are represented by the black sticks and the conductive pathway is represented by the red lines. The high AR of CF can contact with each other, and thus the conductive pathway was only formed in Fig. 10 (c) with low CF content (a, b, c). The conductive pathway of CF can form at a lower AR (e, f) with increasing CF concentrations (d,

e, f). Finally, all conductive pathways can be formed in the composite films with different AR when the CF concentration is high enough (g, h, i). Therefore, all composite films with high CF concentration and with different AR of CF are shown in the red area in the contour plot, this means they all have achieved high conductivity (above 10^{-7} S/cm).

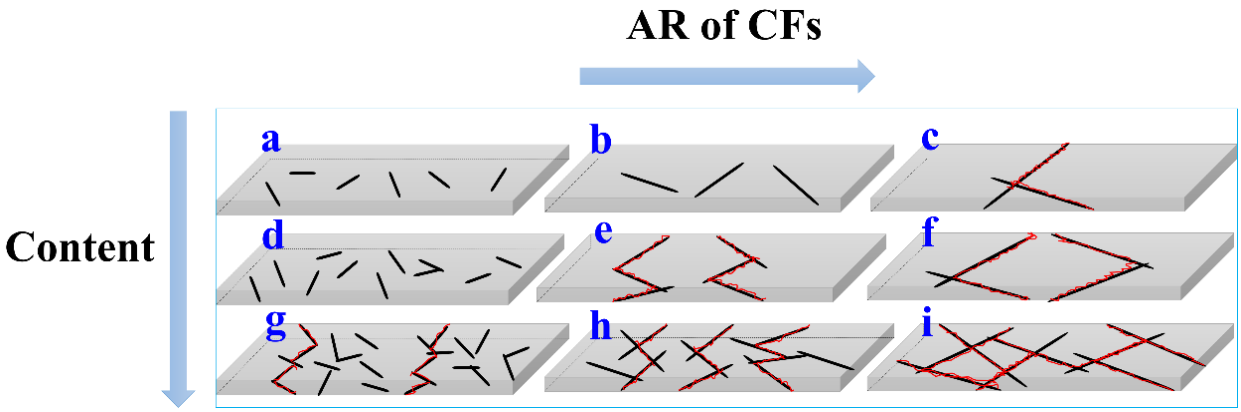

Figure 4.10 The schematic diagram of the conductive CFs pathway with different concentrations and different AR (perpendicular direction).

4.7 Model explanation

Two adjustable parameters (an orientation related <sin γ>, and a pre-factor K) were utilized to reveal the relation between ϕ_c and AR in the Balberg excluded volume theory (Eq. 2.5). It was dominated by AR^2 in Eq. 2.5 because of the large AR in this thesis, this yields equation 4.1 as follows [90]:

$$\phi_c = K' \times \frac{1}{AR} \tag{4.1}$$

Table 4.1 and Table 4.2 can show the ϕ_c versus 1/AR as well. Figure 4.11shows that Eq. 4.1 is not an approximate description of the relationship between AR and ϕ_c. However, two regimes can be assumed for the relation of ϕ_c and 1/AR at both in-plane and perpendicular direction of the film. The consequence might be the confined geometry of CPC films in the present work.

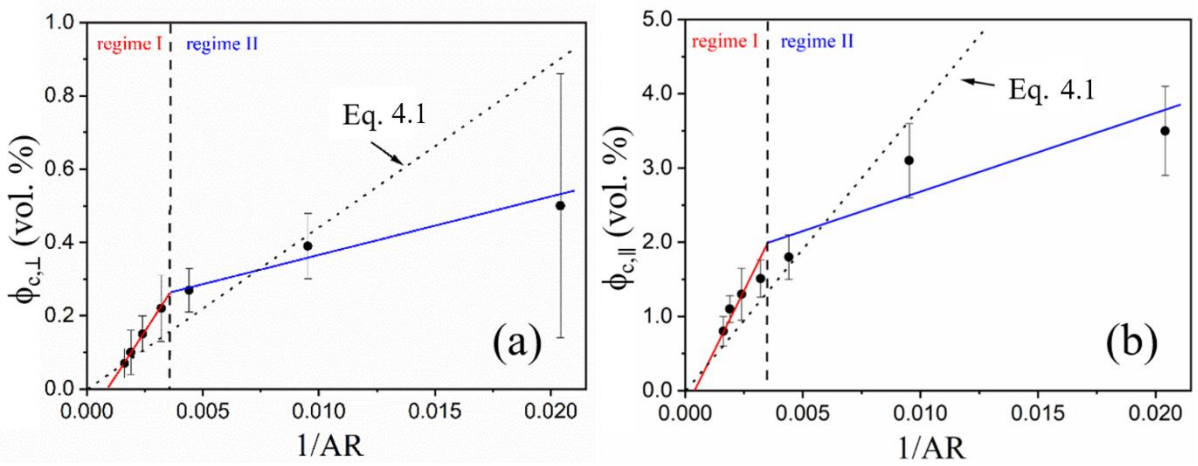

Figure 4.11 Relationship between ϕ_c and 1/AR: (a) Perpendicular direction of the film; (b) In-plane direction of the film.

With randomly oriented CFs, utilizing a spherical coordinate system, the corresponding <sin γ> in an isotropic 3-D system can be calculated as follows:

$$<\sin\gamma> = \frac{\int_0^{\pi} \sin\Upsilon \cdot \sin\Upsilon \, d\Upsilon}{\int_0^{\pi} \sin\Upsilon \, d\Upsilon} = \frac{\pi}{4} \approx 0.78 \tag{4.2}$$

which has been reported by the literature [84,91].

With CFs randomly oriented in a 2-D system, however, the <sin γ> under specific experimental conditions can be calculated as follows:

$$<\sin\gamma> = \frac{\int_0^{\pi} \sin\Upsilon \, d\Upsilon}{\int_0^{\pi} d\Upsilon} = \frac{2}{\pi} \approx 0.64 \tag{4.3}$$

which should describe the CPC films perfectly in this study. For the excluded volume theory, the pre-factor K value in Eq. 2.5 has been revealed to be 3.4 in the work from Qu et al. [45] through mastering all available data from the literature. Therefore, K=3.4 was utilized, the equation for the randomly oriented 2-D system would as follows:

$$\phi_c = 3.4 \times \frac{\frac{1}{6}\pi + \frac{1}{4}\pi AR}{\frac{4}{3}\pi + 2\pi AR + 1.28AR^2} \tag{4.4}$$

Equation 4.4 is illustrated by the dashed curve in Figure 4.12, where experimental data from this study both in-plane and perpendicular direction of the film are presented as red squares. It can be seen that Eq. 4.4 cannot describe the data. Therefore, for the randomly oriented 2-D system, the pre-factor K value in the CPC films must be different from K=3.4.

In the literature, the only data representing a large AR carbon filler in accordance with our results are from Grujicic et al. [92], where the relationship between AR of CNTs and ϕ_c was revealed in polymer composites by computational simulation, as shown by Figure 4.12.

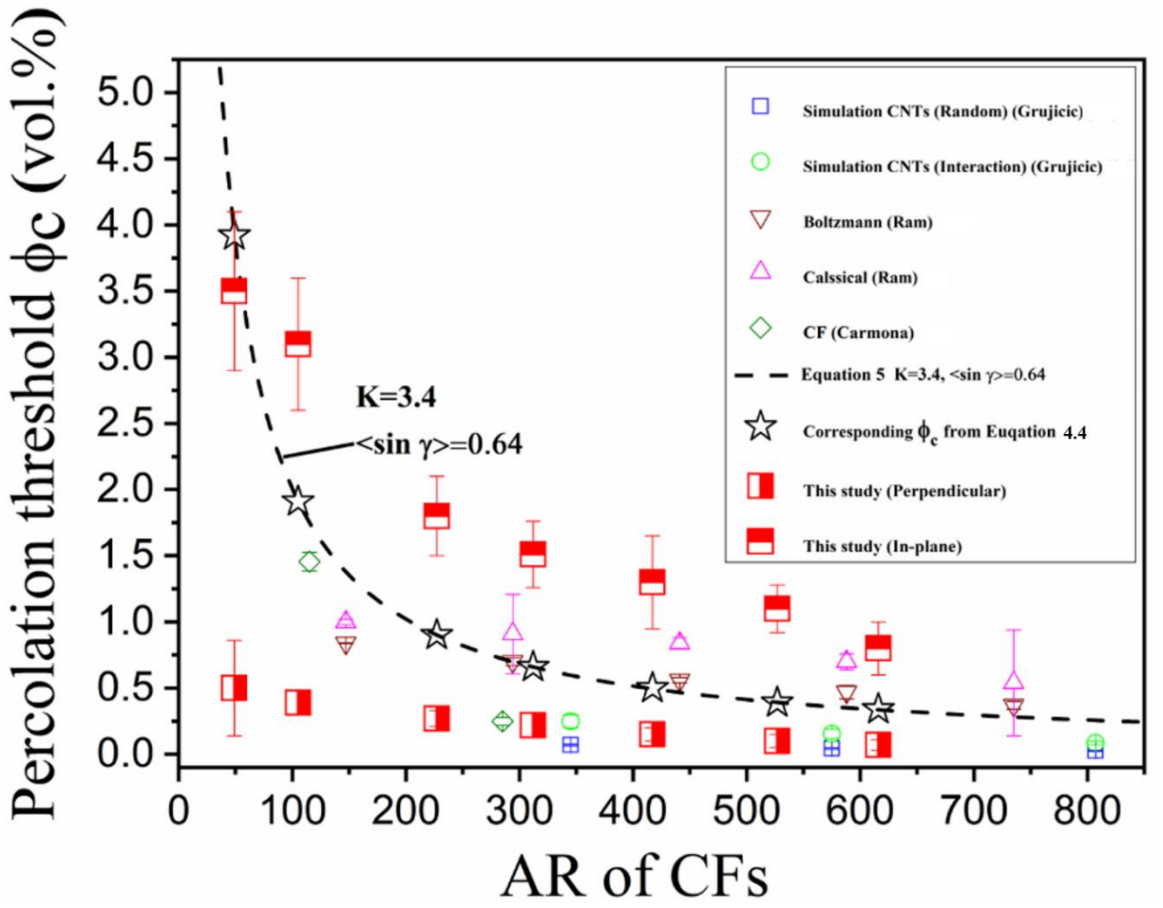

Figure 4.12 Relationship between percolation threshold and aspect ratio of the fillers found for PMMA/CF composite films investigated and its comparison with the data (both experimental and prediction) from the literature [92-94].

However, with the <sin γ> already revealed as 0.64 in Eq. 4.3, a straight forward analysis utilizing Eq. 4.4, but K as an adjustable parameter yields the equation as follows:

$$\phi_c = K \times \frac{\frac{1}{6}\pi+\frac{1}{4}\pi AR}{\frac{4}{3}\pi+2\pi AR+1.28AR^2} \quad (4.5)$$

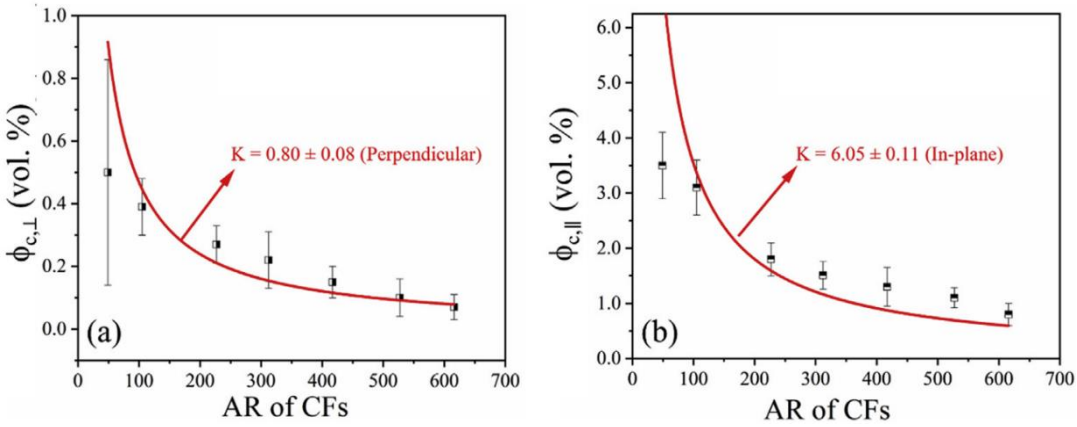

Figure 4.13 Fitted result of the relationship between percolation threshold and aspect ratio with Balberg excluded volume theory (<sin γ> =0.64, K were fitted using Eq. 4.5): (a) Perpendicular direction; (b) In-plane direction.

From Figure 4.13, a pre-factor $K_\perp$=0.80 and $K_\parallel$=6.05 of Eq. 4.5 were respectively determined for the perpendicular and in-plane direction of the film from the fitting results.

A significant difference between the pre-factor $K_\perp$ and $K_\parallel$ was shown in this work. All the $\phi_{c,\perp}$ are smaller than the $\phi_{c,\parallel}$, which is different from other work [92-94]. Moreover, to reveal the relationship between the two directions ϕ_c, Figure 4.14 shows the $\phi_{c,\parallel}$ as a function of $\phi_{c,\perp}$. Two directions ϕ_c is proportional to each other was shown from the result and the ratio is 7.65 was revealed. Presumably, because the orientation of CFs in the film is restricted in the confined geometry.

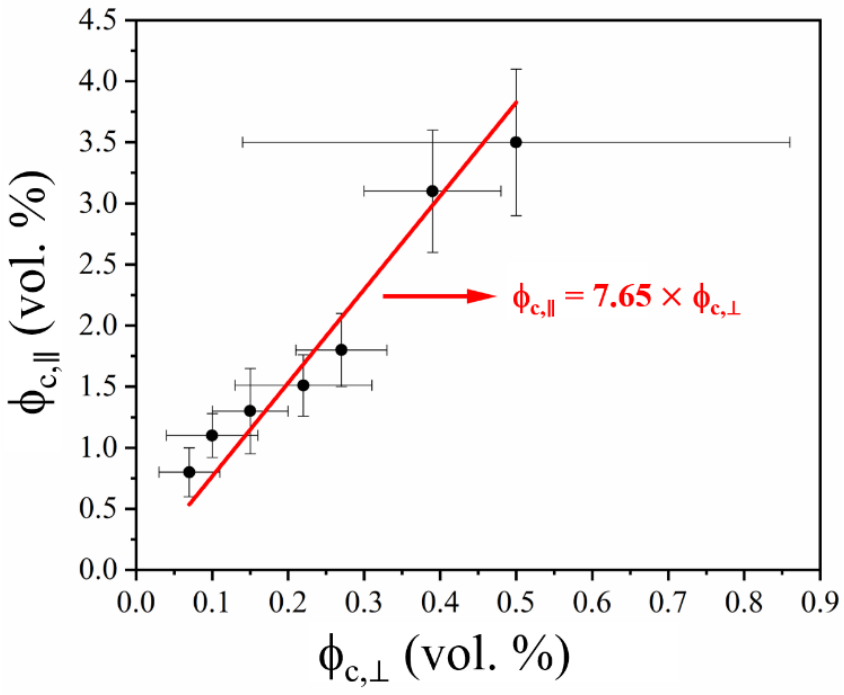

Figure 4.14 The $\phi_{c,\parallel}$ as a function of $\phi_{c,\perp}$. The corresponds to the proportionality of $\phi_{c,\parallel}$ and $\phi_{c,\perp}$ was shown by the red line.

4.8 Comparison with CB and CNT

To investigate in-plane and perpendicular directions of other binary PMMA/carbon-based filler composite films, binary PMMA/CB as well as PMMA/CNT composite films were prepared through the solution casting method as well.

4.8.1 Morphology of binary PMMA/CF, PMMA/CB and PMMA/CNT composite films

SEM images of binary PMMA/CB composite films with CB volume fraction at (a) 0.5 vol. %, (b) 1.5 vol. %; binary PMMA/CF composite films with CF concentration at (c) 0.5 vol. %, (d) 1.5 vol. %; binary PMMA/CNT composite films with CNT volume fraction at (e) 0.5 vol. %; (f) 1.5 vol. % were shown in Figure 4.15, respectively. The graphs of binary composite films are a cross-section of the CPC films. In this thesis, the top of the film presents the surface toward air which corresponds to the top of the SEM graphs. The bottom of the film means the interface contact with the substrate during the film casting process which corresponds to the bottom of the SEM graphs.

Firstly, Fig. 3.1(a) shows that the dispersion of the CB particles is mainly as small CB aggregations. And it is in the range of approximately 20-200 nm, this is small in comparison with the thickness of the CPC film (≈200 μm). Moreover, due to the gravity effect, the CB particles prefer to locate at the bottom of the film when CB concentration at 0.5 vol. % as shown in Fig. 4.15(a). However, such an effect disappears when CB volume fraction up to 1.5 vol. % (Fig. 4.15(b)).

As discussed before, the whole CF cannot be presented in Fig. 3.1(b) because of the CF used in this thesis is extremely long (≈1.5 mm). Therefore, the obvious difference between Fig. 4.15(c) and (d) which corresponds to the CF volume fraction at 0.5 vol. % and 1.5 vol. % cannot be observed. The thickness of the CPC film is only 200 μm while the length of CF used in this part is roughly 1.5 mm, it is clear that the thickness of the CPC film is much smaller than the length of CF. Thus, in this case, there is no significant difference can be found between the bottom and top of the CPC film due to the confined geometry for CF.

Finally, Fig. 3.1(c) shows that pristine CNT aggregated together with each other, and the CNT is aggregated in binary PMMA/CNT composite films as well with volume fraction at both 0.5 vol. % (Fig. 4.15(e)) and 1.5 vol. % (Fig. 4(f)). Like CF, the CNT also has a high AR, however, the CNT is not straight and always entangled. Therefore, at low or high concentrations, there is no obvious difference that can be observed along with perpendicular and in-plane directions.

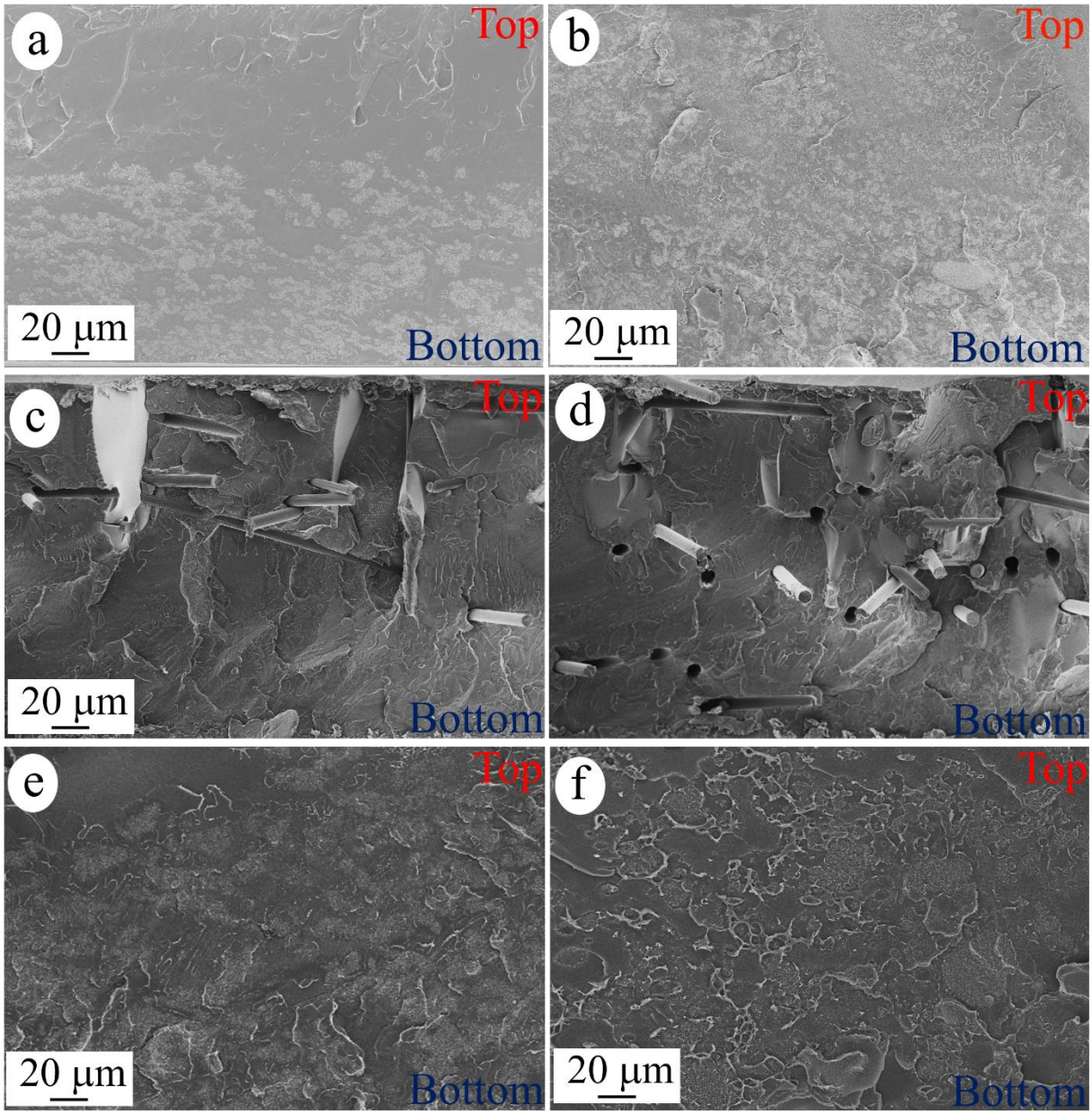

Figure 4.15 SEM graphs of: binary PMMA/CB composite films with CB volume fraction at (a) 0.5 vol. %, (b) 1.5 vol. %; binary PMMA/CF with CF volume fraction at (c) 0.5 vol. %, (d) 1.5 vol. %; binary PMMA/CNT with CNT volume fraction at (e) 0.5 vol. %; (f) 1.5 vol. %. (Cross-section of the films).

4.8.2 Conductivity of binary PMMA/CF, PMMA/CB and PMMA/CNT composite films

The logarithm value of in-plane and perpendicular conductivity as a function of the volume fraction of CF, CB and CNT are shown in Figure 4.16. The blue squares and red squares represent the in-plane and perpendicular conductivities of composite films, respectively. Each data point in the graph corresponds to the average of 10 experimental data, and vertical error

bars represent standard deviations.

Figure 4.16 shows the in-plane percolation threshold $\phi_{c,\parallel}$ and perpendicular percolation threshold $\phi_{c,\perp}$ of the binary PMMA/CF, PMMA/CB as well as PMMA/CNT composite films, which were obtained through fitting the experimental data with the GEM theory (Eq. 2.2). Figure 4.18 shows all the ϕ_c results. Moreover, the ϕ_c obtained from the GEM equation was also further checked using the classical percolation theory (Eq. 2.1).

(a)

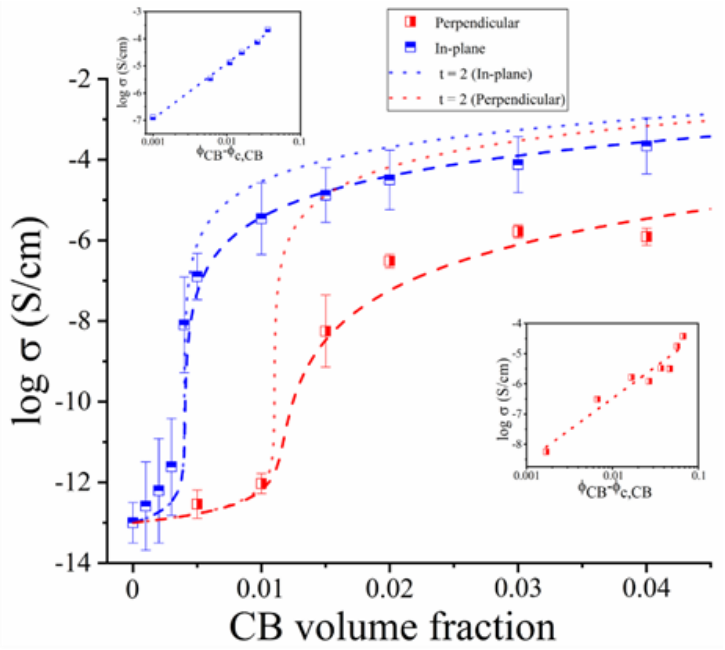
Perpendicular
In-plane
t = 2 (In-plane)
t = 2 (Perpendicular)
log σ (S/cm)
CB volume fraction
ϕCB-ϕc,CB

(b)

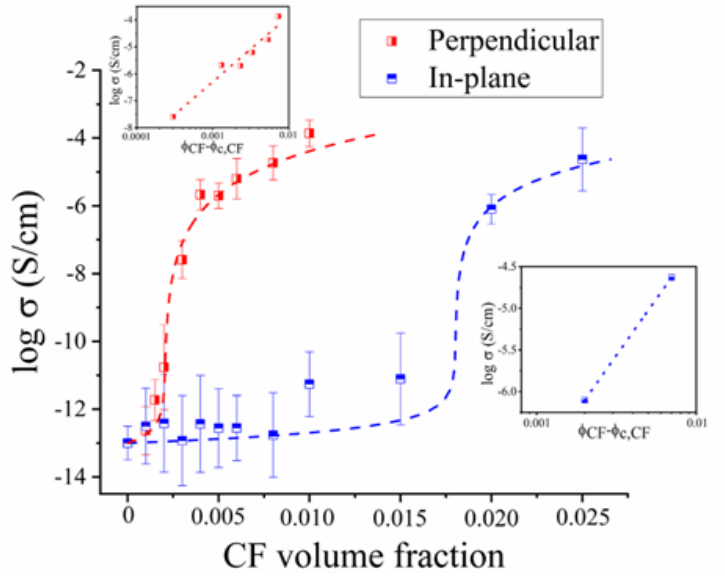
Perpendicular
In-plane
log σ (S/cm)
CF volume fraction
ϕCF-ϕc,CF

(c)

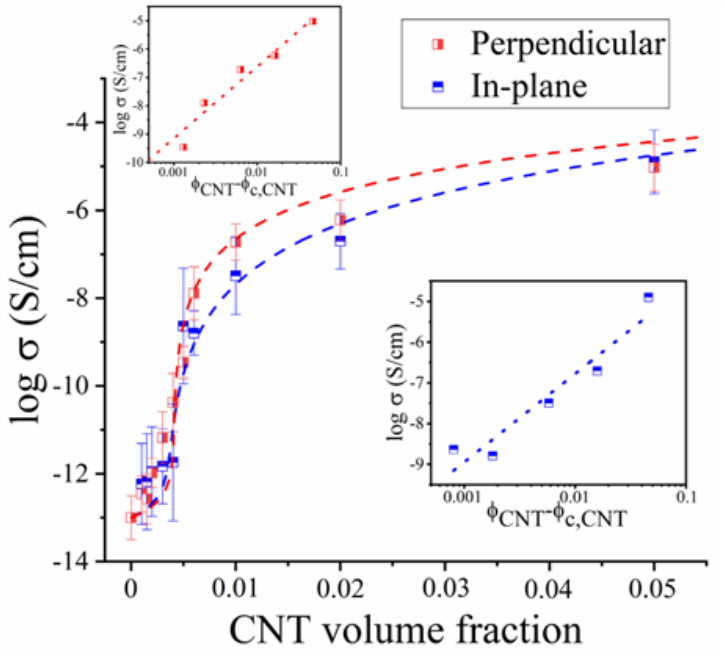
Perpendicular
In-plane
log σ (S/cm)
CNT volume fraction
ϕCNT-ϕc,CNT

Figure 4.16 The logarithm value of the in-plane and perpendicular conductivity versus CB, CF and CNT concentration for PMMA/CF, PMMA/CB as well as PMMA/CNT composite films, respectively. The best fit utilizing the McLachlan Eq. 2.2 with two adjustable parameters (ϕ_c and exponent t in Eq. 2.2) are shown with the dashed lines. The dot lines in Fig.5 (a) are the fitted curves using exponent t=2 in Eq. 2.2. The two insets illustrate the linear fit using Eq. 2.1 for the in-plane and perpendicular direction, respectively.

Table 4.3. ϕ_c of CPC films utilizing the McLachlan theory and corresponding exponent t.

	s (Fixed)	t (In-plane)	t (Perpendicular)	$\phi_{c,\text{ in-plane}}$ (%)	$\phi_{c,\text{ perpendicular}}$ (%)
PMMA/CB	0.87	2.40±0.20	3.55±0.30	0.40±0.07	1.33±0.10
PMMA/CF	0.87	3.10±0.25	2.22±0.15	1.80±0.40	0.27±0.06
PMMA/CNT	0.87	3.00±0.15	3.24±0.20	0.37±0.06	0.42±0.08

As shown in Table 4.3 and Fig. 4.16, the generally used exponent value of t=2 [28,95,96] is not always an approximate choice. Thus, in this thesis, the relationship between ϕ_c and its corresponding exponent t value is investigated.

4.8.3 Relationship between percolation threshold and exponent t.

For all CF, CB and CNT as fillers, the in-plane and perpendicular direction ϕ_c was determined, and corresponding exponent t from the McLachlan theory is revealed as well. It is noteworthy that $\phi_{c,\text{ perpendicular}} / \phi_{c,\text{ in-plane}}$ and $t_{\text{ perpendicular}} / t_{\text{ in-plane}}$ correlates for different conductive fillers. It is evident that $t_{\text{ perpendicular}} / t_{\text{ in-plane}}$ and $\phi_{c,\text{ perpendicular}} / \phi_{c,\text{ in-plane}}$ follows a power-law behavior from Fig. 4.17, the equation as follows:

$$\frac{t_{perpendicular}}{t_{in-plane}} = k \times \left(\frac{\Phi_{c,perpendicular}}{\Phi_{c,in-plane}}\right)^{m} \tag{4.6}$$

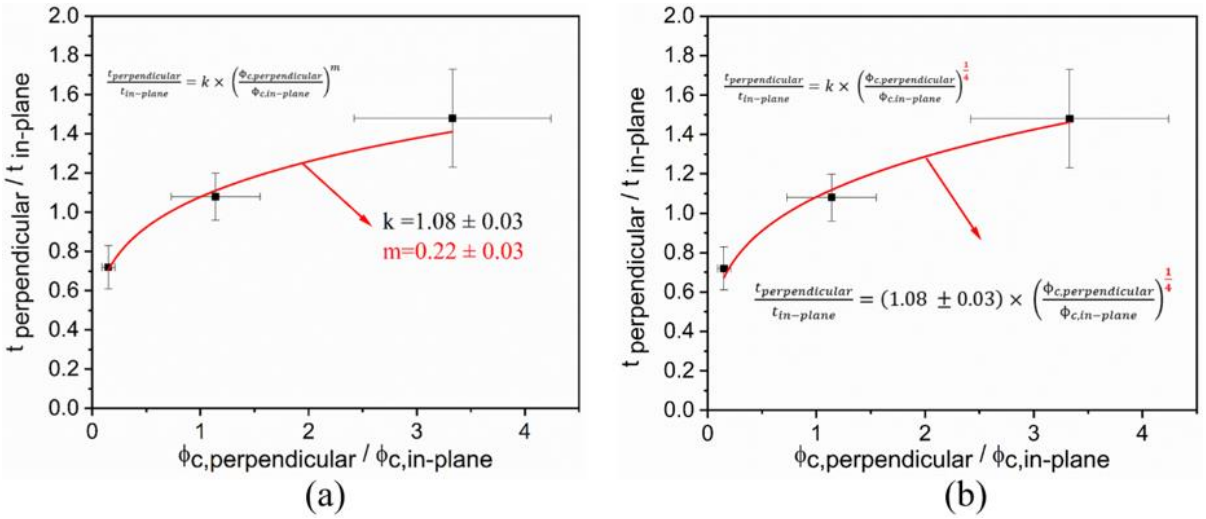

Figure 4.17 The ratio of $\phi_{c,\,perpendicular}/\phi_{c,\,in\text{-}plane}$ versus the ratio of corresponding exponent $t_{\,perpendicular}/t_{\,in\text{-}plane}$. The solid line corresponds to Eq. (4.6).

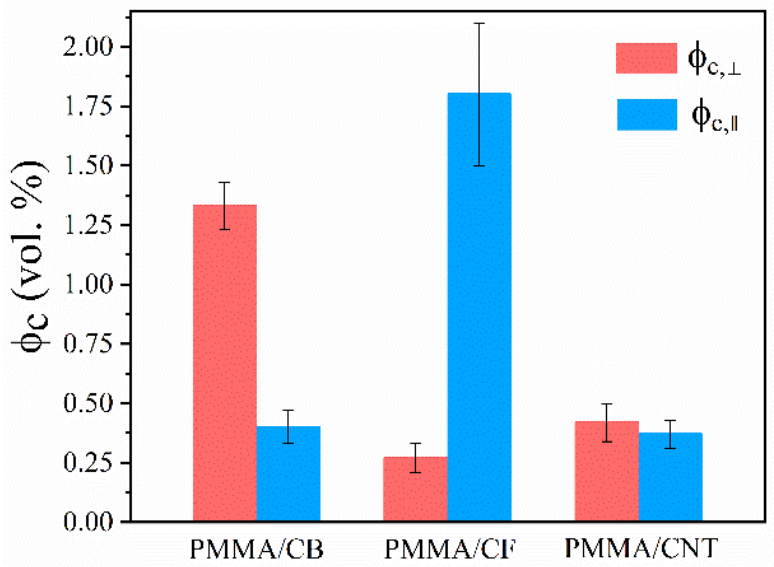

Figure 4.18 $\phi_{c,\parallel}$ and $\phi_{c,\perp}$ results obtained from fitting GEM theory for binary PMMA/CF, PMMA/CB as well as PMMA/CNT composite films.

Figure 4.18 shows that the $\phi_{c,\parallel}$ of binary PMMA/CB composite films, is much smaller than the corresponding $\phi_{c,\perp}$. At first of the casting process (Figure 3.3), a homogenous solution was formed, which consists of CB, THF and PMMA (Figure 3.3 (a)). With THF evaporating, the thickness of the homogenous system gradually reducing. When THF was completed evaporating, then the casting films were obtained. During this procedure, CB particles are influenced by the gravity effect and would towards the bottom of the films (Fig. 3.3(b)). The

distribution of CB particles in this situation can be regarded as a layer by layer from the bottom of the film to the top. Therefore, the filler conductive network along the perpendicular direction is more difficult to form in comparison to the in-plane direction of the film. As a result, the $\phi_{c,\perp}$ of the CPC film would be higher than the corresponding $\phi_{c,\parallel}$.

On the contrary, as shown in Fig. 4.18, the $\phi_{c,\parallel}$ of binary PMMA/CF composite films is much higher than $\phi_{c,\perp}$. As described before, the thickness of the CPC film is much smaller than the average CF length. In other words, the CF along the perpendicular direction of the film is confined which leads to the CPC film anisotropic. Supposing the CPC films from the bottom to the top was passed through by one single CF (as inserted schematic diagram), the angle γ between the film plane and the CF can be calculated as:

$$\sin\gamma = \frac{d}{L} \qquad (4.7)$$

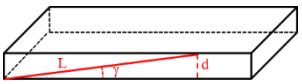

where L is the CF length and d is the thickness of the CPC film. Thus, the γ in this work can be calculated as 7.66°.

The gravity effect in this case still plays a role, while the CF conductive pathway can be formed as long as the CF upward 7.66° along the perpendicular direction. Furthermore, the CPC film was obtained from the solution casting method in which conductive filler would be easily aggregated during the casting process [97], thus, the CF is not parallel to the substrate exactly which means it is easy to upward to the top of the film. As a result, the filler conductive pathway is easy to form along the perpendicular direction. This would lead to an extremely low $\phi_{c,\perp}$ of binary PMMA/CF composite film.

Finally, as shown in Fig. 4.18, the relationship between $\phi_{c,\parallel}$ and $\phi_{c,\perp}$ of binary PMMA/CNT composite films, is different from both PMMA/CB ($\phi_{c,\perp} >> \phi_{c,\parallel}$) and PMMA/CF ($\phi_{c,\perp} << \phi_{c,\parallel}$) case. The $\phi_{c,\perp}$ and $\phi_{c,\parallel}$ of binary PMMA/CNT composite films did not show a big difference. Thus, in

terms of conductivity, the binary PMMA/CNT composite film towards the isotropic case. Even though the CNT is used in this thesis with a high AR, in the polymer matrix, the CNT is bent and tends to be entangled [98,99]. Therefore, the CNT is probably interconnected with each other after the film casting process. At both in-plane and perpendicular directions of the CPC film, in this case, the conductive filler pathway can be formed roughly at the same level. As a consequence, a tremendous difference between the $\phi_{c,\parallel}$ and $\phi_{c,\perp}$ of binary PMMA/CNT composite film cannot be observed.

4.8.4 Schematic illustration for casting films

The difference among PMMA/CF ($\phi_{c,\perp} << \phi_{c,\parallel}$), PMMA/CB ($\phi_{c,\perp} >> \phi_{c,\parallel}$) and PMMA/CNT ($\phi_{c(Perpendicular)} \approx \phi_{c(In\text{-}plane)}$) is probably because the carbon fillers distribution is different after the film casting process. A schematic illustration for different fillers location in the PMMA/CB, PMMA/CF as well as PMMA/CNT casting films is shown in Fig. 4.19(a) (b) (c), respectively. In the schematic diagram, the in-plane direction is parallel to the graph while the perpendicular direction is vertical to the graph.

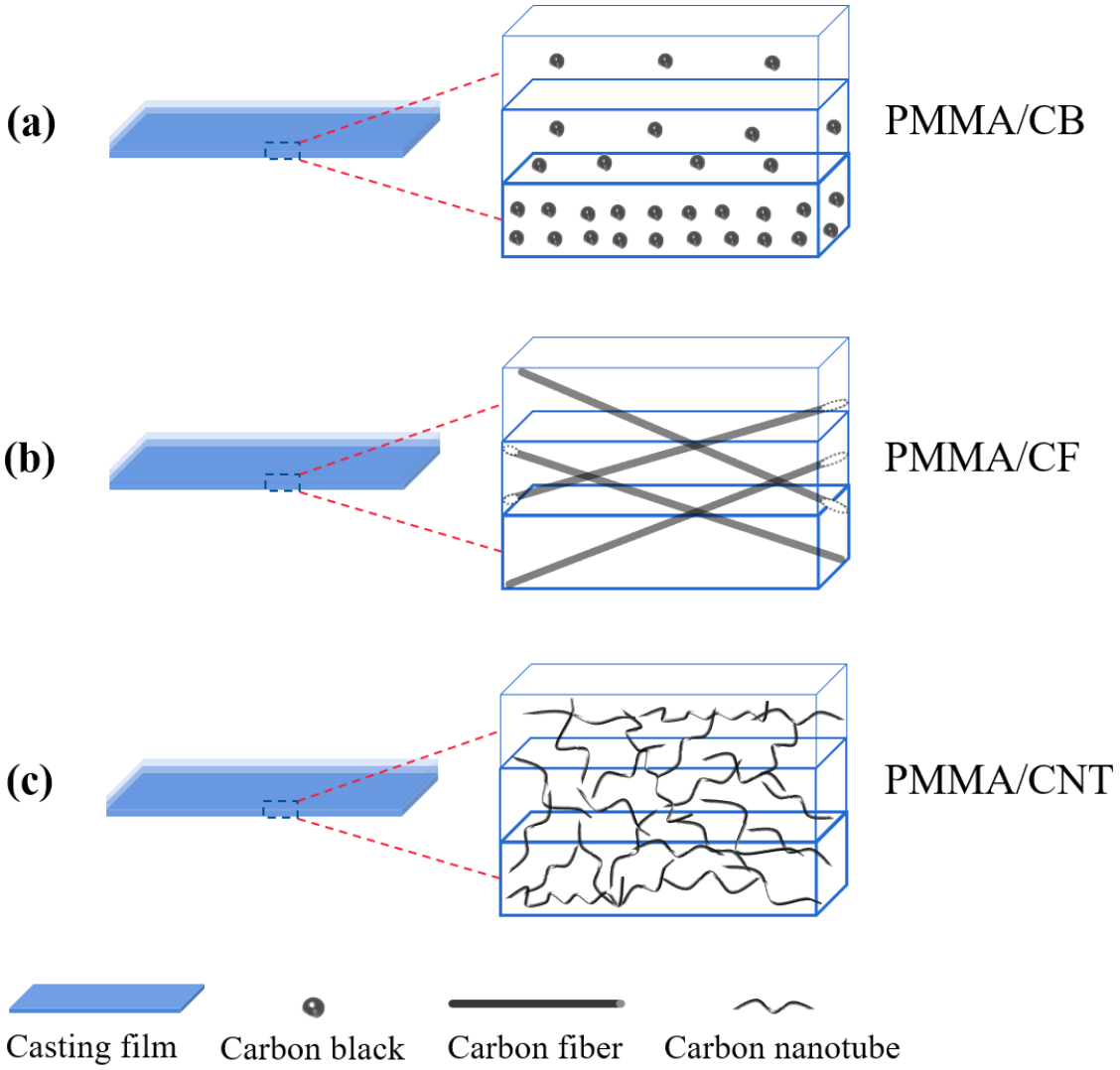

Figure 4.19 Schematic illustration of casting films with carbon black (a), carbon fiber (b) and carbon nanotube (c) as filler, respectively.

4.9 Conclusion

PMMA/CF binary composite films with seven ARs of CF from 49 to 616 and different CF volume fractions from 0.1 to 5.0 vol. % were prepared utilizing the solution casting method. As both AR of CF and CF volume fraction increases, in-plane and perpendicular directions conductivities of composite films increase. Two different pre-factors $K_{\parallel}=6.05$ and $K_{\perp}=0.80$ for Balberg excluded volume theory is revealed considering measurement directions for the in-plane and perpendicular direction of the film. A proportionality was revealed for $\phi_{c,\parallel}$ and $\phi_{c,\perp}$: $\phi_{c,\parallel} \approx 7.65 \times \phi_{c,\perp}$.

Binary PMMA/CB and PMMA/CNT composite films were obtained from solution casting as well. An obvious difference of CB distribution was observed between the bottom and the top of the PMMA/CB composite film when CB volume fraction at 0.5 vol. %. The in-plane $\phi_{c,\parallel}$ and perpendicular $\phi_{c,\perp}$ with different carbon fillers (CB, CF and CNT) show totally different behaviors. The $\phi_{c,\parallel}$ is much smaller than $\phi_{c,\perp}$ for binary PMMA/CB composite films. For PMMA/CF, the $\phi_{c,\parallel}$ is much higher than $\phi_{c,\perp}$, while the $\phi_{c,\parallel}$ and $\phi_{c,\perp}$ do not show a tremendous difference for PMMA/CNT. For different filler types (CB, CF, CNT), a power-law behavior is revealed as $t_{perpendicular}/t_{in\text{-}plane} = (1.08\pm0.03)\times(\phi_{c,\,perpendicular}/\phi_{c,\,in\text{-}plane})^{1/4}$ correlating the ϕ_c and corresponding exponent t in McLachlan theory for perpendicular and in-plane directions.

5

PalkylMA/PS/CB ternary system

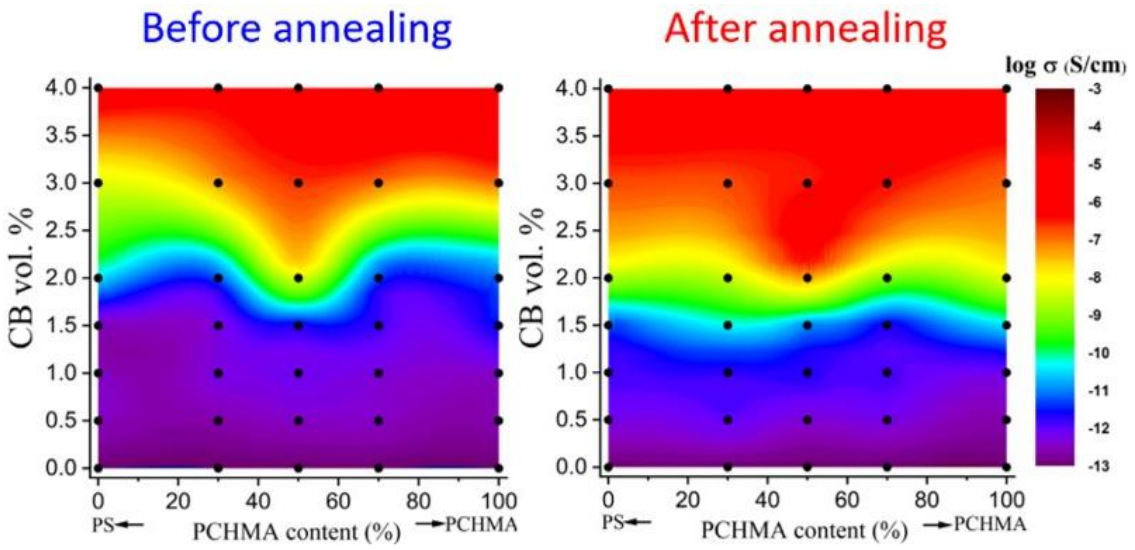

5.1 Introduction

It has been proved that the double percolation effect is an effective way to reduce the ϕ_c [17]. It is essential that the filler selectively stays at the interface of a co-continuous structure or only in one phase because of the affinity of filler with each polymer in this double percolation structure [100-104].

In the past few decades, extensive efforts have been concentrated on the double percolation structure to develop CPCs with an immiscible polymer blend. As far as we can tell, in the open literature, the compatibility between the two polymers in a double percolation structure was scarcely reported. However, the phase morphology of the polymer blend is tremendously affected by the compatibility between the two polymers [105-107]. Thus, the ϕ_c of CPCs in the double percolation structure is probably affected by the compatibility between the two polymer blends as well.

Poly(alkyl methacrylate) (PalkylMA)/polystyrene (PS) blends were widely investigated in the literature [54-56]. The miscibility between PalkylMA and PS changes with alkyl lengths increasing because the interaction energies between various methacrylates and PS are different. Schubert et al. [54] and Kim et al. [55] reported that the immiscibility of PS with various methacrylates was in the order PMMA>PBMA>PEMA>PChMA.

Therefore, it is meaningful to reveal the electrical percolation threshold ϕ_c of composite films using PalkylMA/PS blends as a matrix. In this thesis, PalkylMA/PS/CB ternary composite films were investigated. Additionally, the electrical conductivities of all the PalkylMA/PS/CB composite films after thermal annealing were investigated.

5.2 Calculating wetting coefficient

The wetting coefficient, ω_a, can be applied to predict the conductive filler location in polymer

blends, which is defined in Eq. (5.1) [68-71].

$$\omega_a = \frac{\gamma_{filler-polymer1} - \gamma_{filler-polymer2}}{\gamma_{polymer1,2}} \quad (5.1)$$

where $\gamma_{polymer1,2}$, $\gamma_{filler\text{-}polymer\ l,}$ and $\gamma_{filler\text{-}polymer\ 2}$ are the interfacial energies between polymer 1 and polymer 2, filler and polymer 1, filler and polymer 2, respectively.

Thus, in this work, the CB will be preferentially in PalkylMA if $\omega_a < -1$. And prefer to be located into PS if $\omega_a > 1$. Moreover, the CB is located at the interface between PalkylMA and PS if $-1 < \omega_a < 1$.

The surface energies include a polar part γ^p and a disperse part γ^d: $\gamma=\gamma^d+\gamma^p$, the interfacial tension between PalkylMA and PS can be obtained through the Wu's harmonic-mean average equation [108]:

$$\gamma_{12} = \gamma_1 + \gamma_2 - 4\left(\frac{\gamma_1^d \gamma_2^d}{\gamma_1^d + \gamma_2^d} + \frac{\gamma_1^p \gamma_2^p}{\gamma_1^p + \gamma_2^p}\right) \quad (5.2)$$

And the geometric-mean equation:

$$\gamma_{12} = \gamma_1 + \gamma_2 - 2\left(\sqrt{\gamma_1^d\ \gamma_2^d} + \sqrt{\gamma_1^p\ \gamma_2^p}\right) \quad (5.3)$$

where γ_1 and γ_2 are the surface energies of PalkylMA and PS in this work, respectively; γ_1^d and γ_2^d are the dispersive parts, γ_1^p, γ_2^p are the polar parts of the surface energies of PalkylMA and PS, respectively [97, 108].

Through calculating the ω_a as given by Eq. 5.2 and 5.3, the location of CB particles in PalkylMA/PS blends and PChMA/PS blend were predicted.

The surface energies of PMMA, PBMA, PEMA, PS and CB are taken from the literature [66, 109, 110]. The surface energies of PChMA is obtained from contact angle measurement. And

they all are presented in Table 5.1.

Table 5.1 Surface energies of PalkylMA, PS and CB.

Components	mN m^{-1}		
	γ	γ^d	γ^p
PMMA	41.1	29.6	11.5
PEMA	35.9	26.9	9.0
PBMA	31.2	26.2	5.0
PChMA	41.2	37.1	4.1
PS	40.7	34.5	6.1
CB	98.1	94.5	3.6

The interfacial tensions between PalkylMA (PChMA) and PS were calculated according to Eq. 5.2 and Eq. 5.3, and the results are shown in Table 5.2.

Table 5.2 Interfacial tensions and wetting coefficient (Harmonic-mean equation).

Components	$\gamma_{CB/PalkylMA}$ (mN m^{-1})	$\gamma_{CB/PS}$ (mN m^{-1})	$\gamma_{PalkylMA/PS}$ (mN m^{-1})	ω_a (Eq. 5.2)	ω_a(Eq.5.3)
PMMA	38.08	28.56	2.12	4.49	4.77
PEMA	39.96	28.56	1.60	7.13	7.63
PBMA	38.90	28.56	1.34	7.72	8.22
PChMA	25.06	28.56	0.58	-6.03	-1.31

As shown in Table 5.2, CB particles were predicted located in PS at PMMA/PS, PEMA/PS and PBMA/PS blends. In contrast, CB would be located in the PChMA phase at PChMA/PS blends.

5.3 Miscibility of polymer blends

The Flory-Huggins interaction parameter, in a binary polymer blends system, is broadly used in predicting the miscibility between two polymers [111-113]. The equation as follows:

$$\chi_{12,cr} = \frac{1}{2}\left(\frac{1}{\sqrt{N_1}} + \frac{1}{\sqrt{N_2}}\right)^2 \quad (5.4)$$

where $\chi_{12,\,cr}$ is the critical Flory-Huggins interaction parameter, N_1 and N_2 are the chain length of polymer 1 and polymer 2, respectively. The two polymers are immiscible with each other if the $\chi_{12\,cr}$ is smaller than χ_{12} between the two polymers [113].

In this work, the chain length was estimated roughly by both average M_n and M_w, respectively, yielding a range for the corresponding $\chi_{12,cr}$.

Table 5.3 Critical interaction parameters for M_n and M_w, for benchmarking literature are given.

System	$\chi_{12,\,cr}$ for M_n	$\chi_{12,\,cr}$ for M_w	$\chi_{literature}$ [54]
PMMA/PS	0.0032	0.0015	0.0326
PEMA/PS	0.0011	0.0005	0.0020
PBMA/PS	0.0024	0.0009	0.0100
PChMA/PS	0.0038	0.0014	/

As shown in Table 5.3, the PEMA/PS blend is a weak incompatible system in this work because of the interaction parameter $\chi_{PEMA/PS}$ in the same order of magnitude as the critical $\chi_{12,\,cr}$, while PMMA/PS is remarkably more incompatible [114, 115]. With increasing immiscibility between PalkylMA/PS blend, PChMA has already miscibility with PS [55].

5.4 Electrical conductivity of ternary composite films

5.4.1 PMMA/PS/CB

5.4.1.1 Percolation threshold investigation

The logarithm value of the electrical conductivity of PMMA/PS/CB versus CB volume fraction is shown in Figure 5.1. Different polymer blend ratios in the PMMA/PS/CB are presented by different symbols. Each data point is obtained from an average of 10 experimental measurements, and vertical error bars represent standard deviations. All curves show a steep increase in electrical conductivity on reaching a critical concentration, which is corresponding to ϕ_c. The fitting ϕ_c results are shown in Table 5.1.

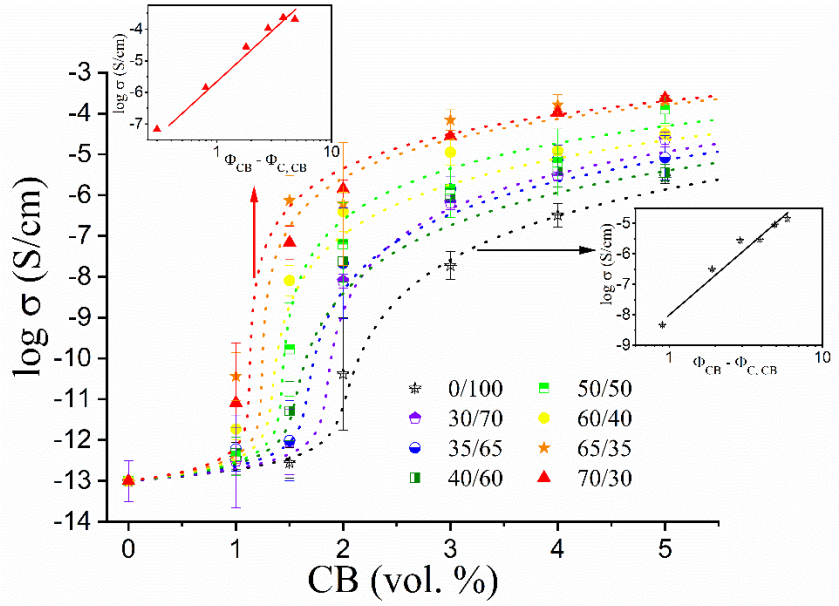

Figure 5.1 The logarithm value of the electrical conductivity versus CB concentration for ternary PMMA/PS/CB composite films prepared from the solution casting method with a different polymer blend ratio of PMMA/PS. The dashed lines show the best fit utilizing the McLachlan Eq. 2.2, the percolation volume fraction ϕ_c. The two insets illustrate the linear fit using Eq. 2.1 for pure PS (PMMA/PS=0/100) and PMMA/ PS= 70/30, respectively.

Table 5.4 Fitting results of experimental data utilizing the McLachlan theory

PMMA/ PS	0/100	30/70	35/65	40/60	50/50	60/40	65/35	70/30
ϕ_c (%)	2.03 ±0.09	1.75 ±0.12	1.67 ±0.08	1.56 ±0.09	1.45 ±0.08	1.33 ±0.14	1.24 ±0.12	1.12 ±0.11

The ϕ_c obtained from the GEM theory was further checked utilizing the classical percolation theory (Eq. 2.1). The linear relationship between log σ and log (ϕ - ϕ_c) is satisfying, and two of them are shown in Figure 5.1. The ϕ_c towards a lower concentration with increasing PMMA content in PMMA/PS polymer blends.

5.4.1.2 Compared with melt blending

The ternary PMMA/PS/CB composites produced from the melt blending were investigated by Pan et al. [116]. The ϕ_c of the composites was also fitted through McLachlan's theory. As shown in Figure 5.2, the same tendency can be observed for the ϕ_c of CPCs with different PMMA/PS ratios obtained from both melt blending and solution casting. The ϕ_c of binary PMMA/CB, as well as PS/CB composites (PMMA content at 100 and 0 %) obtained from melt blending, are higher than solution casting. In contrast, the ϕ_c of PMMA/PS/CB composites obtained from melt blending are all lower than that from the solution casting. As shown in Figure 3.5, firstly, PMMA, PS, CB and THF can be formed as a homogenous solution (Figure 3.5(a)). And then, the system would come to a critical point with THF evaporating (Figure 3.5(b)) where the phase separation between PMMA and PS begins to happen. Therefore, the CB towards the PS phase because of the thermodynamic factor after a critical point. The migration ability of CB particles would be decreased with THF evaporating. Therefore, there is a point that CB particles cannot move towards the PS phase anymore when THF content low enough. During this process, not all the CB particles migrated into the PS phase. In this case, the actual CB concentration in the PS phase is lower than that of samples obtained from the

melt blending. This is the reason that the ϕ_c of ternary PMMA/PS/CB composites prepared from melt blending are all lower than that from the solution casting.

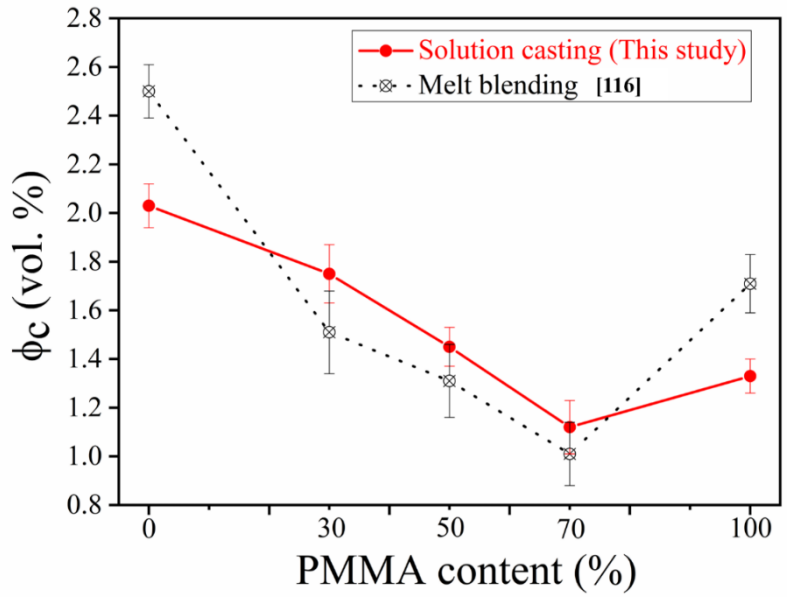

Figure 5.2 The percolation thresholds of PMMA/PS/CB composites prepared from the solution casting method and melt blending as a function of different polymer blend ratios [116].

5.4.2 PalkylA/PS/CB

5.4.2.1 percolation threshold investigation

For others ternary PalkylMA/PS/CB and PChMA/PS/CB composite films are investigated as well. The conductivity after thermal annealing is investigated as well. As typical examples, the logarithm value of electrical conductivity PBMA/PS/CB versus CB concentration is presented in Figure 5.3. The fitting information is the same as when fitting in PMMA/PS/CB composite films. All the ϕ_c of PalkylMA/PS/CB and PChMA/PS/CB films before and after thermal annealing are obtained through this fitting method and are shown in Figure 5.4. The green arrow in Fig. 5.4(d) shows ϕ_c of ternary PChMA/PS/CB (after annealing) composite film changing tendency with PChMA content increasing.

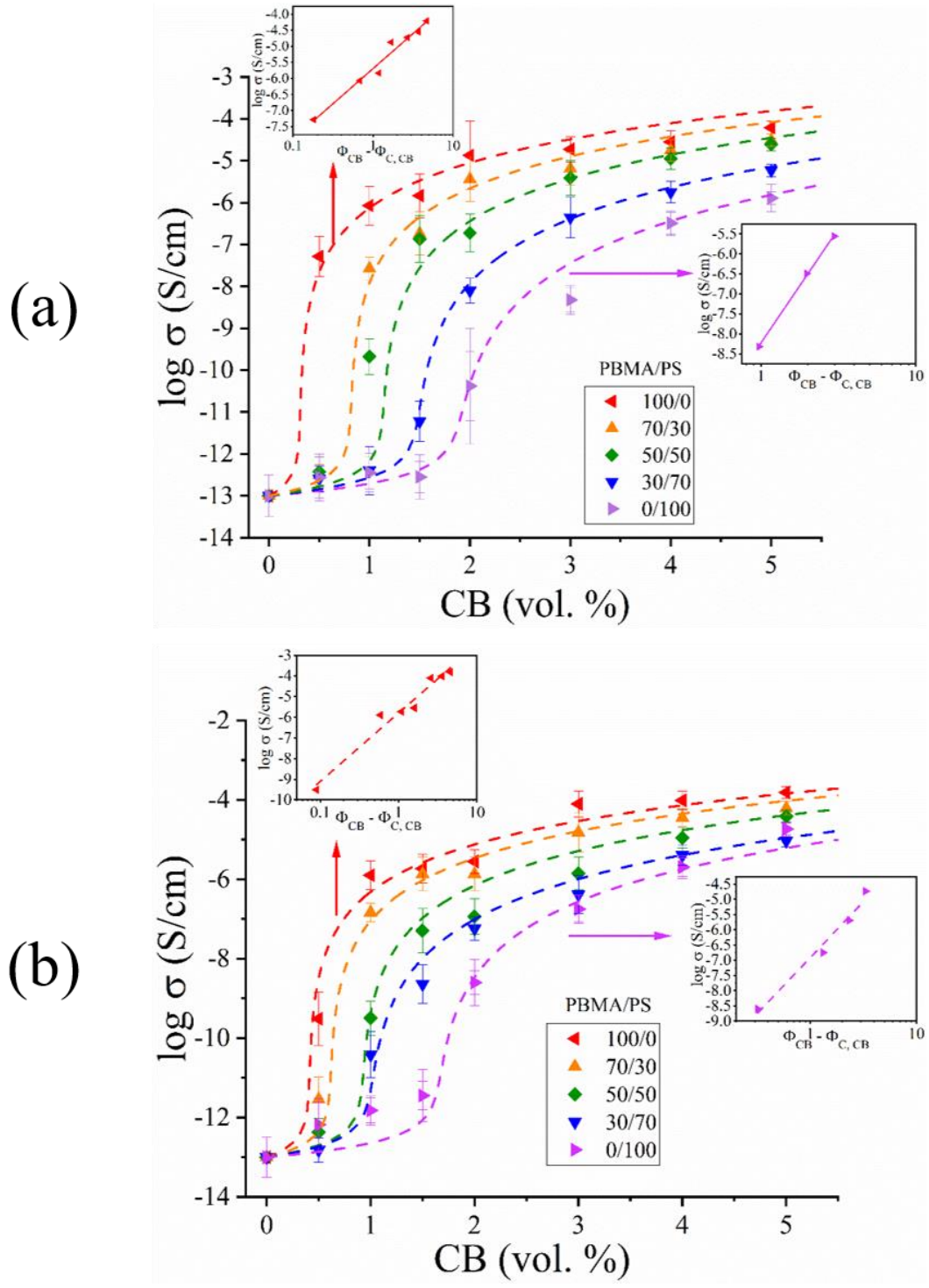

Figure 5.3 The logarithm value of the electrical conductivity as a function of CB concentration for PBMA/PS/CB films before (a) and after (b) annealing with different PBMA/PS ratios. The dashed lines show the best fit utilizing the McLachlan theory. The two insets illustrate the linear fit using Eq. 2.1 for PBMA and PS, respectively.

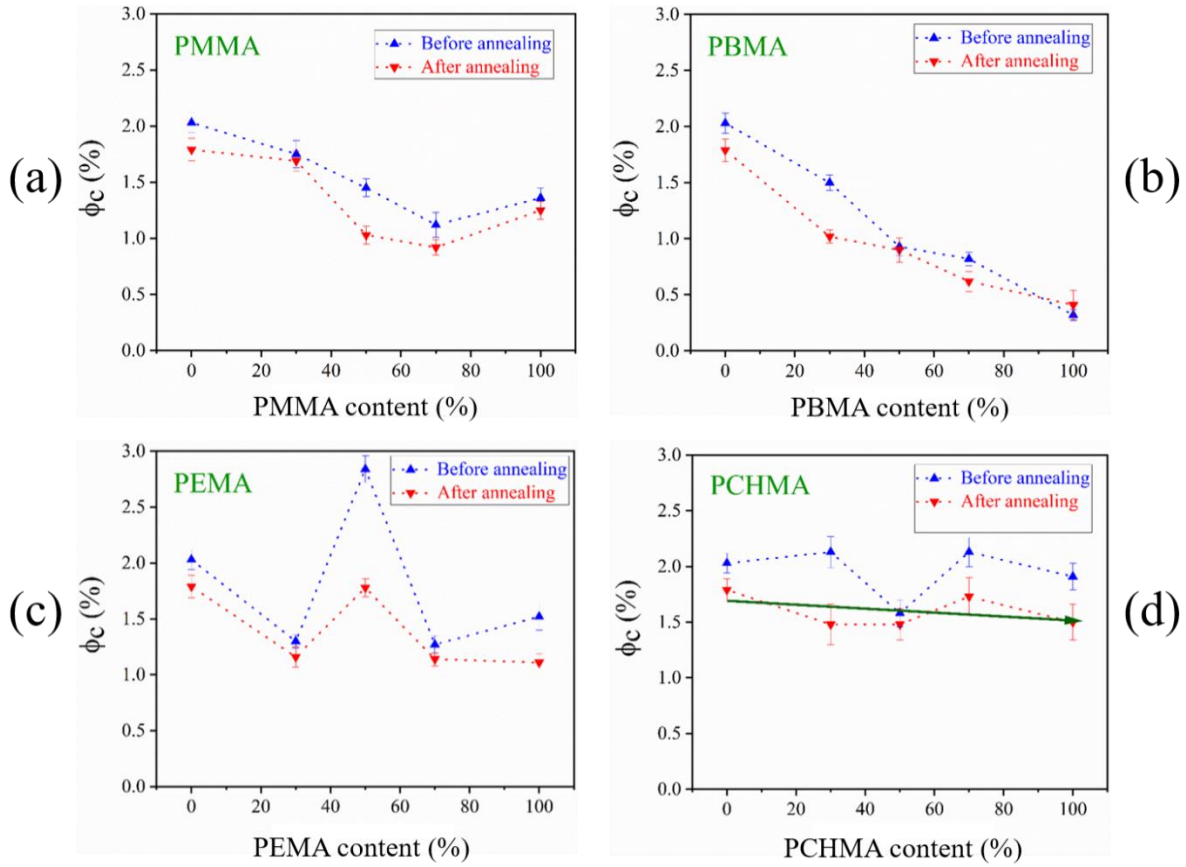

Figure 5.4 The fitting percolation thresholds of PalkylMA/PS/CB films as a function of different PalkylMA content in PalkylMA/PS blends. From a-d, the PalkylMA represents PMMA, PBMA, PEMA and PChMA, respectively. Moreover, the immiscibility between PalkylMA with PS is one-way decreasing. The green arrow in (d) shows ϕ_c of PChMA/PS/CB system after annealing changing tendency with PChMA content increasing.

5.4.2.2 Contour plots of conductivity

Figure 5.5 presents four conductivity contour plots diagram according to all experimental data before and after thermal annealing of (a) PMMA/PS, (b) PBMA/PS, (c) PEMA/PS and (d) PChMA blends with different polymer blend ratios and CB volume fractions, respectively. The actual experimental data are presented by black dots on the contour plot. The colors in the contour plot represent the logarithm value of conductivity.

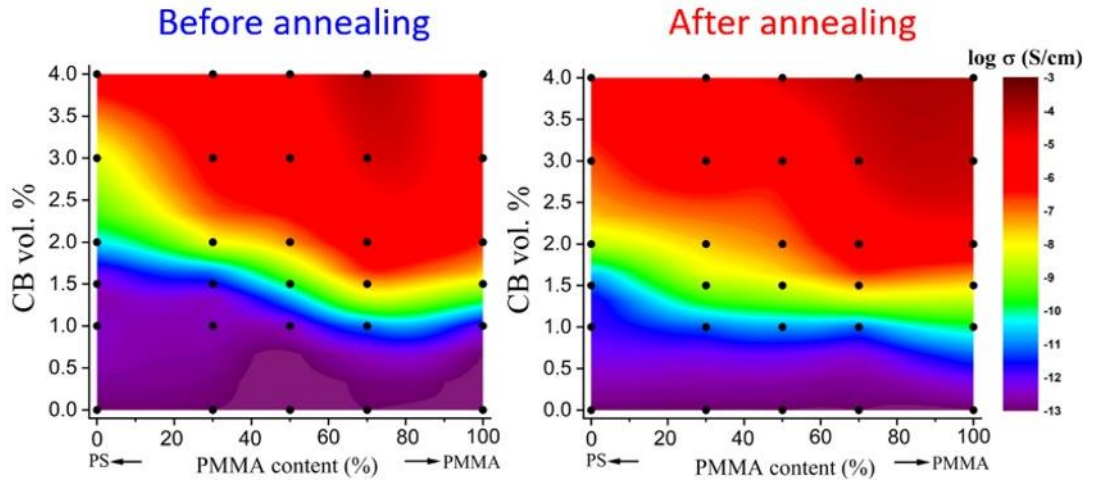
Before annealing
After annealing
log σ (S/cm)
CB vol. %
PS
PMMA content (%)
PMMA

(a)

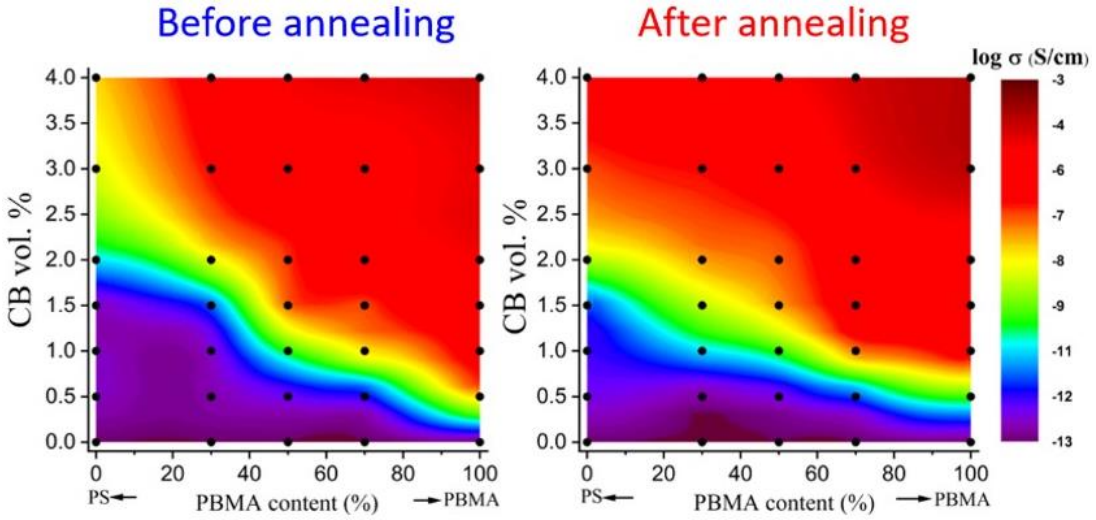
Before annealing
After annealing
log σ (S/cm)
CB vol. %
PS
PBMA content (%)
PBMA

(b)

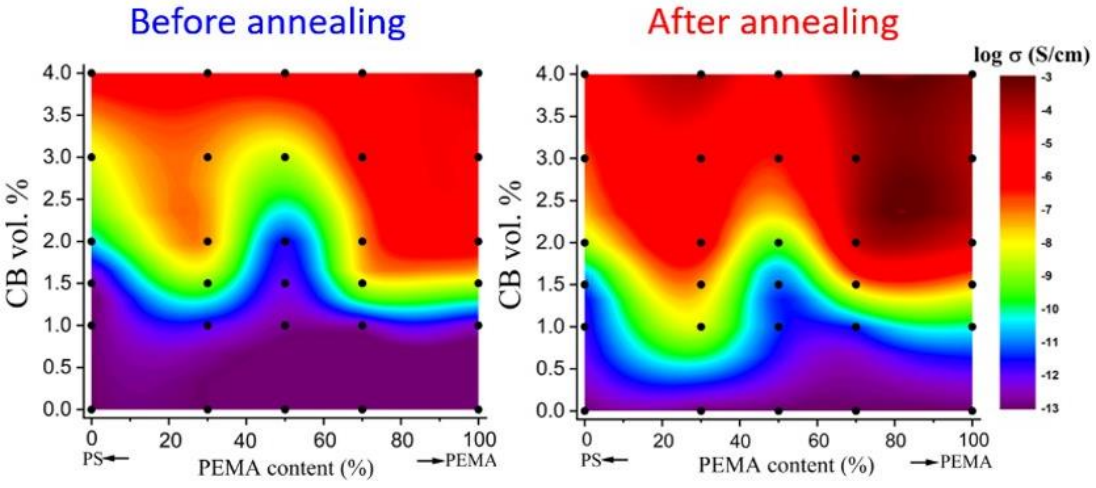
Before annealing
After annealing
log σ (S/cm)
CB vol. %
PS
PEMA content (%)
PEMA

(c)

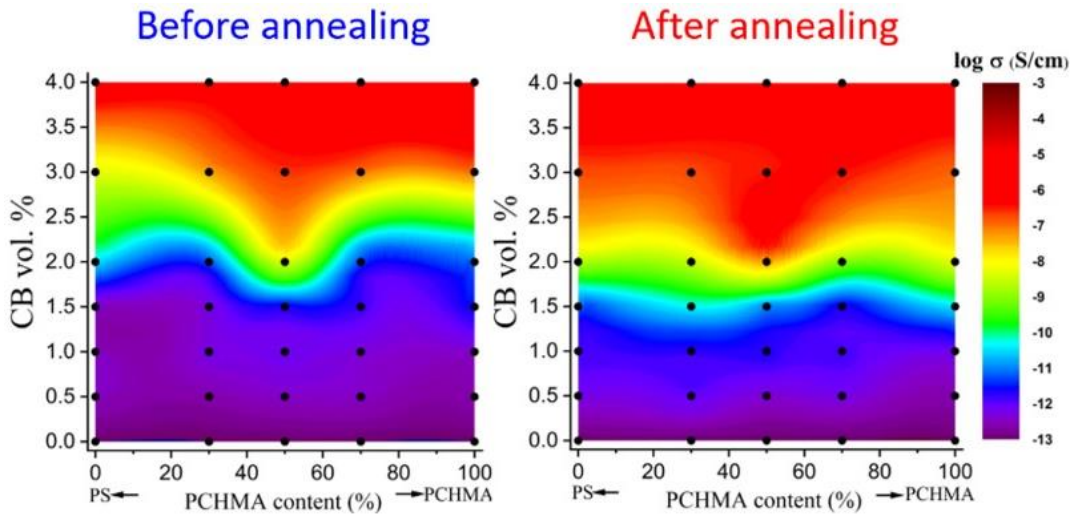

(d)

Figure 5.5 The logarithm value of conductivity of PalkylMA/PS/CB [117] ternary composite films before and after annealing versus PalkylMA content in PalkylMA/PS blends and CB volume fraction. From a-d, the PalkylMA represents PMMA, PBMA, PEMA and PChMA, respectively.

The electrical conductivity increases with a CB concentration (along the Y-axis). In addition, Fig. 5.4 clearly shows that the PalkylMA contents influence all the ϕ_c of ternary PalkylMA/PS/CB composite films (along with all the X-axis). However, four different kinds of PalkylMA with PS show different conductive behaviors when the PalkylMA content increasing in PalkylMA/PS blends.

For ternary PMMA/PS/CB composite films, the ϕ_c area typically corresponds to the green area in contour plot starts with lower CB volume fraction, this means the ϕ_c towards a lower concentration with PMMA content increasing. All the ϕ_c of ternary PMMA/PS/CB films after annealing are lower than the corresponding system before annealing [117]. This is because of the CB particles re-aggregate during the thermal annealing process and forms a more conductive network in the PS phase at relatively lower concentrations [18].

For PBMA/PS/CB system, though the immiscibility between PBMA and PS is lower than that between PMMA and PS, PBMA/PS/CB films show the double percolation effect as well, which the ϕ_c of ternary composites decreasing with the second phase (PBMA) increasing.

However, in the PBMA/PS/CB system, the PBMA/CB binary composite film shows an extremely low ϕ_c and even lower than all of the investigated PBMA/PS/CB ternary composite films. This is probably because the T_g of PBMA in this work is 20℃ which is lower than room temperature. Therefore, the rubbery PBMA matrix helps CB particles contacting with each other and forming a conductive network easily.

Similar to PMMA/PS/CB films, the PEMA content in PEMA/PS blend influences the ϕ_c of ternary PEMA/PS/CB composite films as well. The ϕ_c area shifted to lower CB concentration with PEMA content in polymer blends increasing (0-40 %). However, with still growing PEMA concentration, the ϕ_c of ternary PEMA/PS/CB films is different from PMMA/PS/CB. In particular, when PEMA concentration at 50 % and 60 %, an extremely high ϕ_c can be observed in comparison with other polymer blend ratios.

In terms of the PChMA/PS/CB system, the CB particles prefer to locate only at the PChMA phase according to thermodynamic theory as well. While Figure 5.4 shows that only polymer blend ratio at 50/50, the ϕ_c of PChMA/PS/CB film before annealing lower than binary composite films. However, a double percolation effect on all the other ternary PChMA/PS/CB composite films cannot be observed. With increasing miscibility between PalkylMA/PS blend, PChMA has already miscible with PS. Thus, the CB particles cannot be determined in PChMA or PS phase under the microscope. In addition, with thermal annealing, the distribution of CB particles is more uniform than without annealing in PChMA/PS blends. Consequently, the ϕ_c of PChMA/PS/CB films are linear and towards from ϕ_c of PS/CB binary composite films to ϕ_c of PChMA/CB binary composite films with PChMA content increasing. Therefore, as shown in Figure 5.4(d), if both ϕ_c of both binary systems (polymer A/filler and polymer B/filler) is determined, then a linear relationship between the ϕ_c of the ternary composites (A+B+fillers) with the ratio of two polymers can be revealed when polymer A and B are miscible.

5.5 Morphological investigation

5.5.1 PMMA/PS/CB

Figure 5.6 shows SEM graphs of PMMA/PS/CB films with CB volume fraction at 2 vol. % and different polymer blend ratios: (a) 30/70, (b) 40/60, (c) 50/50, (d) 60/40, (e) 70/30 and (f) 70/30. The PS phase was etched by cyclohexane in Fig. 5.6(f). The CB particles are preferentially located in the PS phase as shown in Fig. 5.6, which is in accordance with the theoretical calculation.

Due to the CB particles are preferred to the PS phase, with increasing PMMA content (from Fig. 5.6(a) to (e)), the relative CB volume fraction in the PS phase is increasing, which leads to the ϕ_c of CPC films to a lower CB volume fraction. Moreover, when CB concentration at 2 vol. %, with PMMA increasing from 30 to 70 in PMMA/PS polymer blend, the phase transitions of polymer blends from the sea-island structure (a, b, c) to co-continuous structure(d) and then return to sea-island (e).

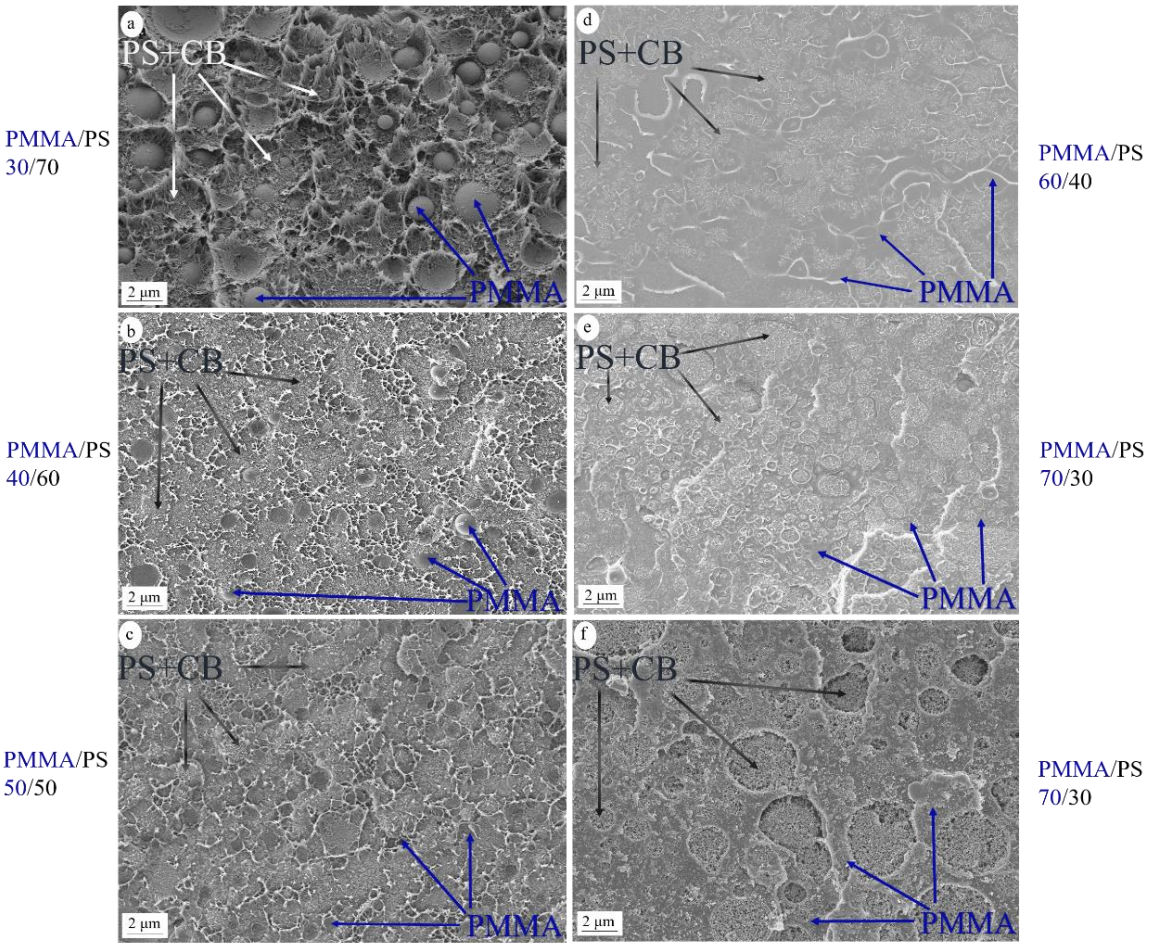

Figure 5.6 SEM graphs of the ternary PMMA/PS/CB films with 2 vol. % of CB, PMMA/PS ratios are: (a) 30/70; (b) 40/60; (c) 50/50; (d) 60/40; (e) 70/30 and (f) 70/30, respectively. The PS phase was etched by cyclohexane in (f).

5.5.2 Pure PMMA/PS and PEMA/PS blends

The phase morphologies of pure polymer blends were investigated as well to reveal the different conductive behaviors between PEMA/PS/CB films and PMMA/PS/CB films with different polymer blend ratios.

Figure 5.7 shows SEM micrographs of the pure PEMA/PS (a, b, c) and PMMA/PS (d, e, f) blends with polymer blend ratios at 30/70 (a, d), 50/50 (b, e) and 70/30 (c, f), respectively. Immiscible polymer blends system would form different phase morphologies like co-continuous, fiber, sea-island as well as laminar (Figure 2.3) based on the processing conditions and blend compositions [105,118]. As shown in Figure 5.7, the phase morphologies of both

PMMA/PS and PEMA/PS blends changing with PEMA and PMMA content growing. Moreover, it can be observed that the PMMA/PS blend shows the sea-island structure (Fig. 5.7 (e)) while PEMA/PS blend forms double emulsion structure when PEMA/PS=50/50 where PS phase was isolated by PEMA phase (Fig. 5.7 (b)).

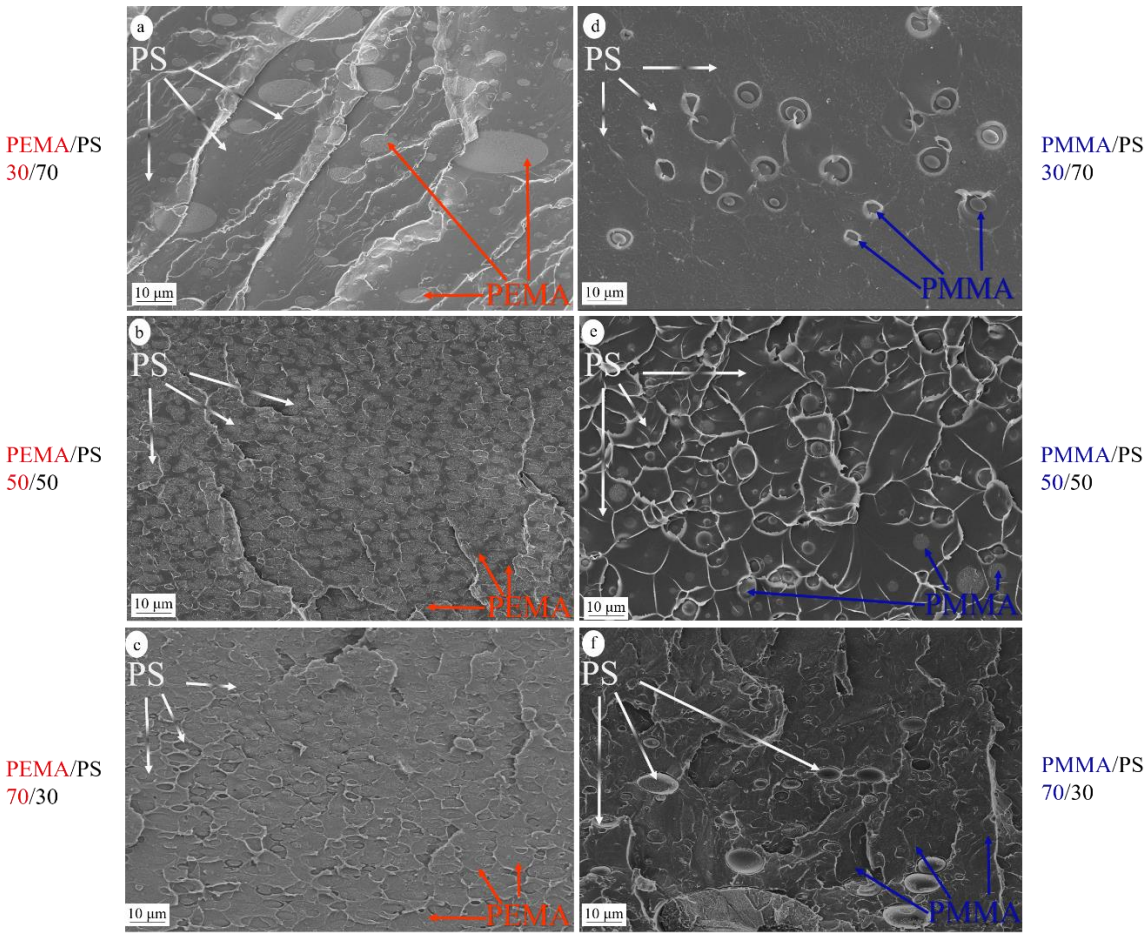

Figure 5.7. SEM graphs of the pure PEMA/PS (a, b, c) and PMMA/PS (d, e, f) blends with ratios are 30/70 (a, d), 50/50 (b, e) and 70/30 (c, f), respectively.

5.5.3 PEMA/PS/CB and PMMA/PS/CB films with different CB concentration

A double emulsion structure was formed at PEMA/PS blend when the ratio of PEMA/PS is 50/50. The filler might change the morphology of immiscible polymer blends [119-121] and as reported by Harrats et al., the double emulsion morphology is harmful to electrical conductivity [105]. Thus, both phase morphologies of PMMA/PS=50/50 and PEMA/PS=50/50 with

different CB concentration in this work were investigated. Figure 5.8 shows SEM graphs of the PEMA/PS/CB (a-d) and PMMA/PS/CB (e-h) films at both PEMA/PS=50/50 and PMMA/PS=50/50 with different CB volume fractions (a, e) 1 vol. %, (b, f) 2 vol. %, (c, g) 3 vol. %, and (d, h) 4 vol. %, respectively.

As shown in Figure 5.8, for PEMA/PS/CB films, CB particles were selectively located into the PS phase (disperse phase) at a lower CB concentration and were isolated by the PEMA phase (continuous phase) ((a), (b)). PEMA/PS/CB films are not conductive to this morphology structure. The PS phase comes into contact with each other with still increasing CB concentration. Which leads to CB contact with each other, and thus forms the filler conductive pathway [(c), (d)].

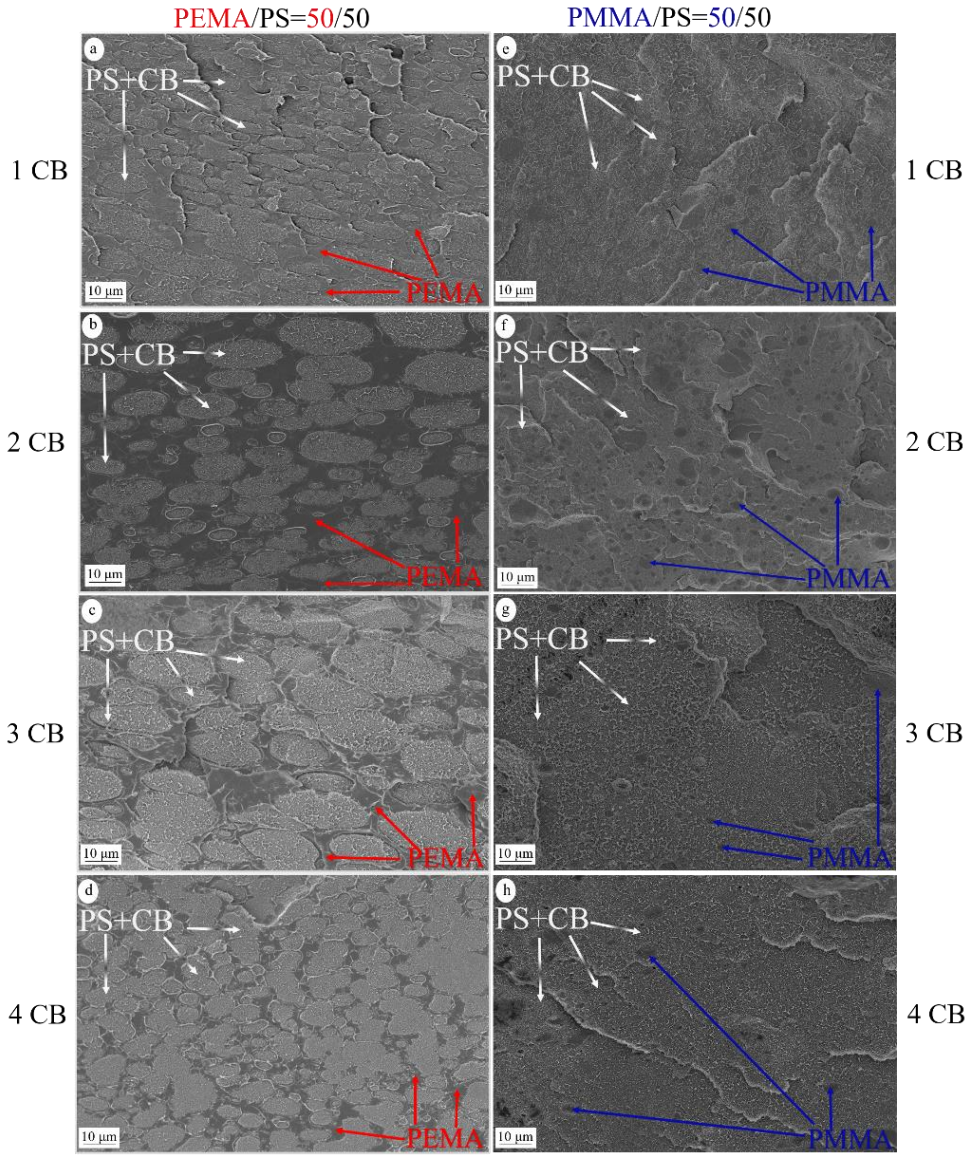

Figure 5.8 SEM graphs of the PEMA/PS/CB (a-d) and PMMA/PS/CB (e-h) films at PEMA/PS=50/50 and PMMA/PS=50/50 with different CB concentration (a, e) 1 vol. %; (b, f) 2 vol. %; (c, g) 3 vol. % and (d, h) 4 vol. %, respectively.

5.5.4 A schematic illustration for PEMA/PS/CB morphologies

To make it clearer, a schematic diagram of the phase morphology structure in PEMA/PS/CB (a-c) and PMMA/PS/CB (d-f) films is shown in Figure 5.9. Light yellow and orange area represents the PEMA and PMMA phase, respectively. The PS phase is represented in the dark teal area and CB particles are represented in black dots, respectively.

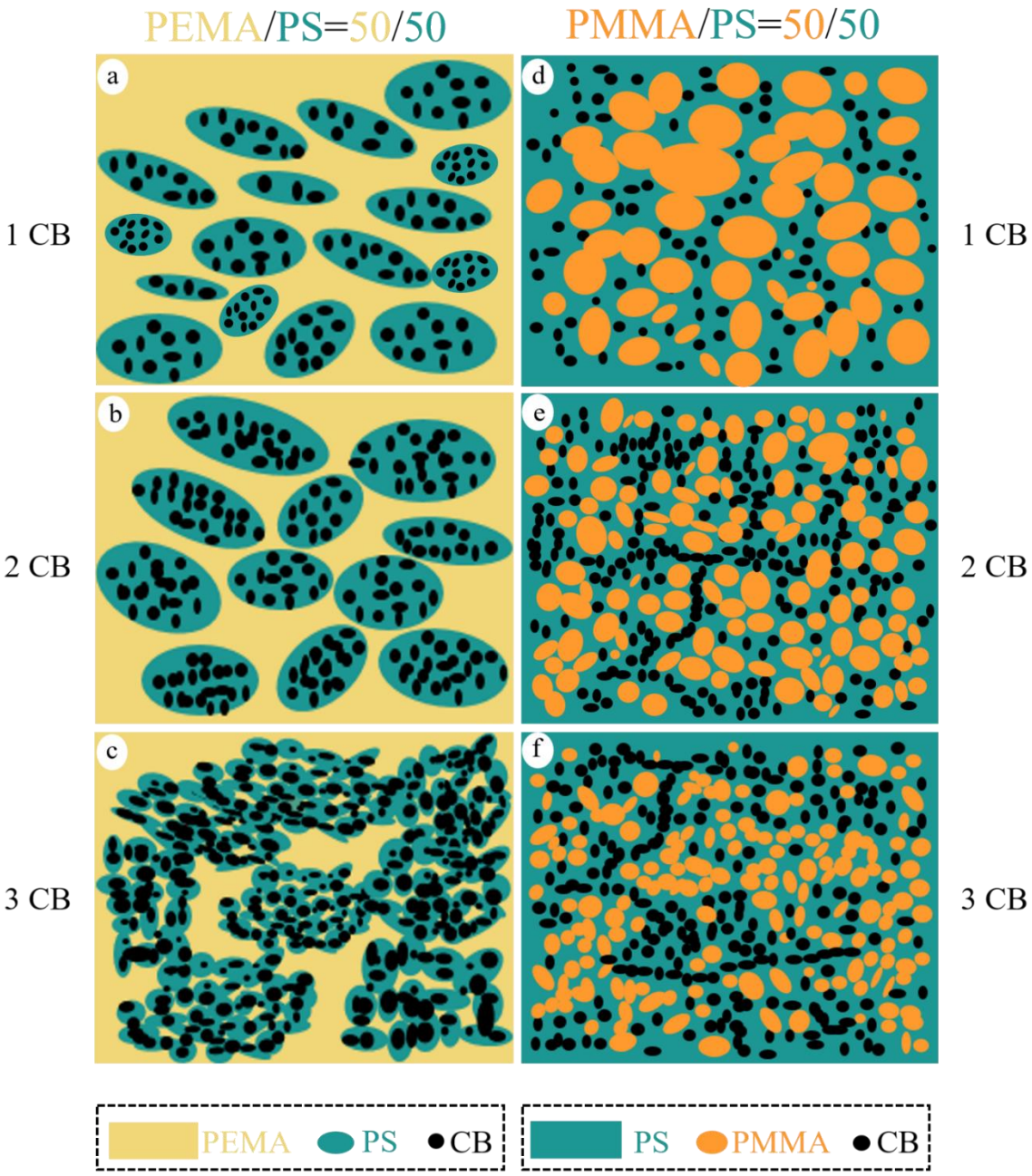

Figure 5.9 Schematic diagram of the phase morphology structure in PEMA/PS/CB (a-c) and PMMA/PS/CB (d-f) films when PEMA/PS=50/50 and PMMA/PS=50/50 with different CB concentration (a, d) 1 vol. %; (b, e) 2 vol. %; (c, f) 3 vol. %, respectively.

5.5.5 Morphology of PalkylMA/PS/CB films after thermal annealing

To investigate the phase morphology, PalkylMA/PS/CB films with different ratios of PalkylMA and PS as well as different CB concentration before and after annealing were studied by SEM, respectively. As typical examples, the polymer blend ratio at PalkylMA/PS=50/50 and

CB concentration at 2 vol. % were presented in this thesis. Figure 5.10 shows the SEM graphs of ternary PalkylMA/PS/CB films. From a-c (before annealing) and A-C (after annealing), PalkylMA represents PMMA, PBMA, PEMA and PChMA (d, D) (immiscibility with PS is one-way decreasing), respectively. It can be seen that all the PalkylMA/PS/CB show different phase morphologies (the PEMA/PS forms double emulsion structure when the ratio of PEMA and PS at 50/50 which is not good for the conductivity of composites [117]) when polymer blend ratio was at 50/50 with a CB concentration of 2 vol. %.

PBMA/PS/CB, as well as PMMA/PS/CB forms the sea-island structure and CB agglomerates were selectively located in the PS phase as well. However, phase separation between PChMA and PS cannot be observed. From Figure 5.10 (d, D) and Figure 5.11, PChMA/PS/CB forms a homogenous system where CB particles are probably located in both PChMA and PS phases. This contrasts the predicted result by the thermodynamic theory which predicts CB located at only the PChMA phase. This can be explained by that the PChMA and PS are a miscible system. Thus, they would not undergo phase separation [55].

Schubert et al. [54] revealed that the neutron reflectivity curve at the PalkylMA/PS blends would be shifted after thermal annealing. In other words, the interface between PalkylMA and PS would be changed during the annealing process. Altstädt and Cai [122,123] et al. reported that an increase in the size of the phase domains and a reduction in the interfacial area would occur during further processing. The coarsening often takes place by the coalescence of dispersed polymer droplets if the phase morphology is a sea-island structure, which would lead to an increase in dispersed particle size. This can be observed in both PMMA/PS/CB and PBMA/PS/CB systems which phase morphology is sea-island structures (Fig.5.10 (A) and (B)).

In addition, Böhm et al. [124] reported that thermal treatment at elevated temperatures can accelerate the formation of the conductive network. This means the filler at temperatures above T_g prefers to aggregate. Thus, the CB particles located in the PS phase which was covered by

the PEMA phase at PEMA/PS/CB (Fig. 5.10(c)) system would tend to re-aggregate during the annealing process. Therefore, phase morphology is changing from a double emulsion structure (Fig. 5.10 (c)) to a co-continuous (Fig. 5.10 (C)) structure.

Similarly, the CB particles re-aggregate would happen in PChMA/PS/CB system as well. However, PChMA and PS are miscible with each other. Therefore, the different phase morphology before and after annealing at PChMA/PS/CB system cannot be observed.

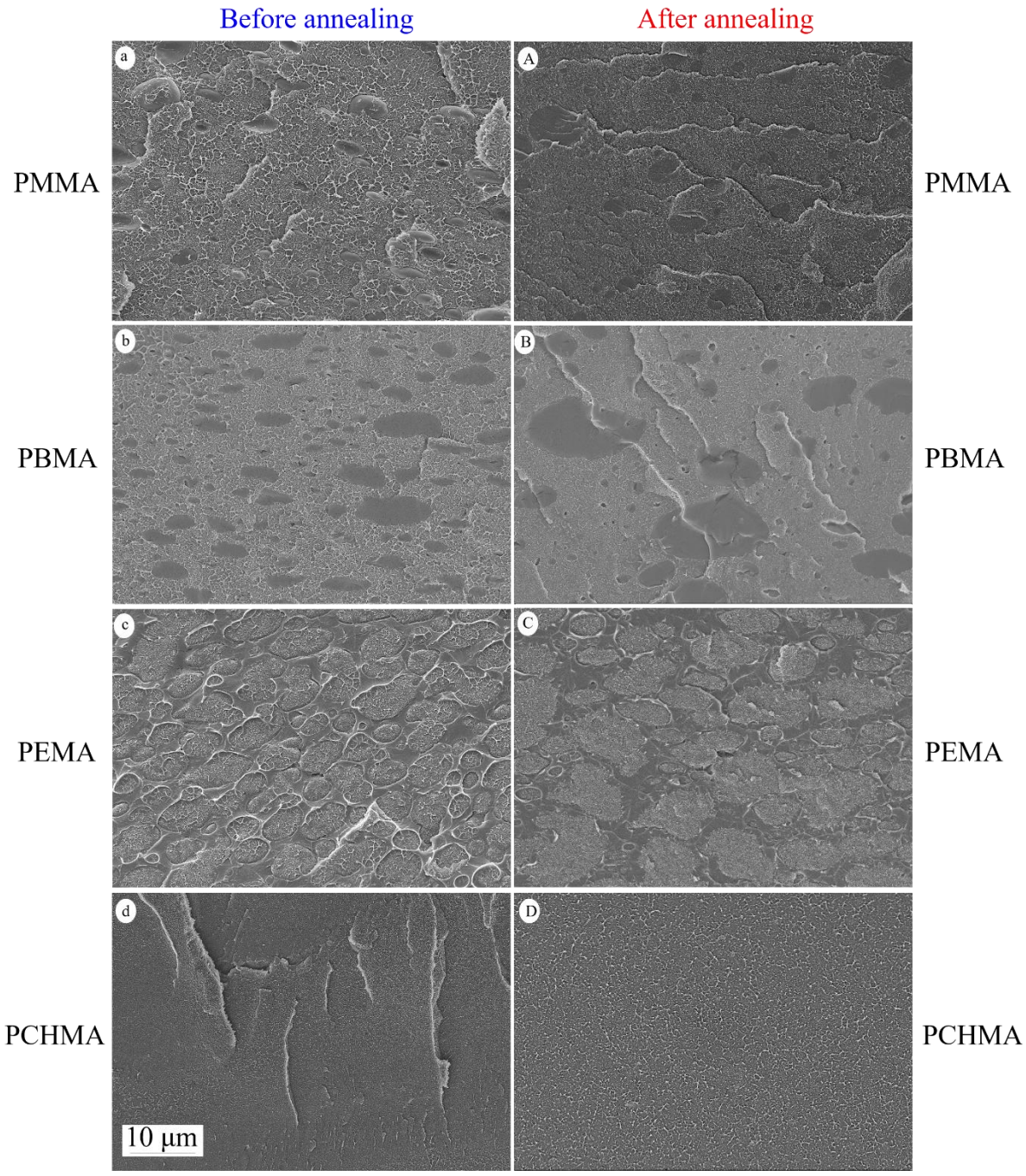

Figure 5.10 SEM images (cross-section) of PalkylMA/PS/CB and PChMA/PS/CB ternary composite films before (a-d) and after (A-D) annealing for polymer blend ratios at 50/50 with CB concentration at 2 vol. %: (a, A) PMMA, (b, B) PBMA, (c, C) PEMA, (d, D) PChMA, respectively. All images have the same scale bar of 10 µm. From a-d and A-D, the immiscibility between PalkylMA with PS is one-way decreasing.

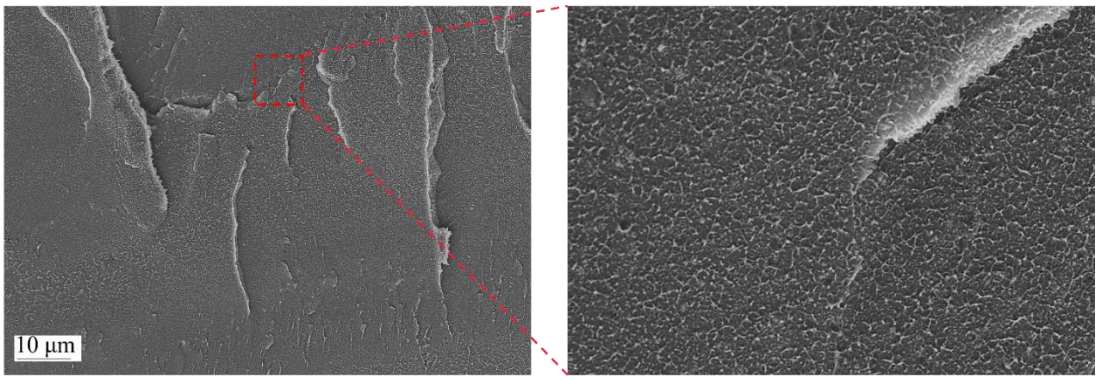

Figure 5.11 SEM images of PChMA/PS=50/50 with CB volume fraction at 2 vol. %.

5.6 Conclusions

In this work, the conductivity of ternary poly (alkyl methacrylate) (PalkylMA)/Polystyrene (PS)/carbon black (CB) and poly (cyclohexyl methacrylate) (PChMA)/PS/CB composite films prepared from solution casting. The ϕ_c of all the films before and after annealing have been investigated. The conductivity of all four different kinds of composite films was presented in four contour plots versus CB concentration and polymer blend ratios, respectively. The CB particles was preferentially located into the PS phase for PMMA/PS, PBMA/PS, PEMA/PS blends, and into the PChMA phase for PChMA/PS blend, respectively. The ϕ_c of both PMMA/PS/CB and PBMA/PS/CB ternary composite films were decreased when PMMA and PBMA were added into the PS phase, this may be the reason that the double percolation effect. However, even if the CB particles are only located in the PS phase as well, the PEMA/PS/CB films (PEMA/PS = 50/50) show a higher ϕ_c due to the double emulsion structure of PEMA/PS blends. The ϕ_c of PMMA/PS/CB composites obtained from melt blending are all lower than that from the solution casting even they show the same changing tendency with polymer blend ratio changing.

As typical examples, the SEM images with PalkylMA/PS of 50/50 and CB volume fraction at 2 vol. % before and after annealing were presented. In PMMA/PS/CB and PBMA/PS/CB

composite films, thermal annealing leads to an increase in the size of the dispersed particle and lower ϕ_c. Phase morphology of PEMA/PS/CB is changing from a double emulsion structure to a co-continuous structure. In PChMA/PS/CB system, the phase separation cannot be observed under SEM. After thermal annealing, all the ϕ_c of ternary PChMA/PS/CB composite films with different PChMA/PS ratios show a linear behavior with PChMA content increasing. If both ϕ_c of both binary systems (polymer A/filler and polymer B/filler) is determined, then a linear relationship between the ϕ_c of the ternary composites (A+B+fillers) and the ratio of two polymers can be revealed when polymer A and B are miscible. Compared with the typical double percolation effect generally using an immiscible polymer blend system, this can provide a new idea to design ternary conductive polymer composites with good mechanical properties.

6

PalkylMA/PS/CNTs ternary system

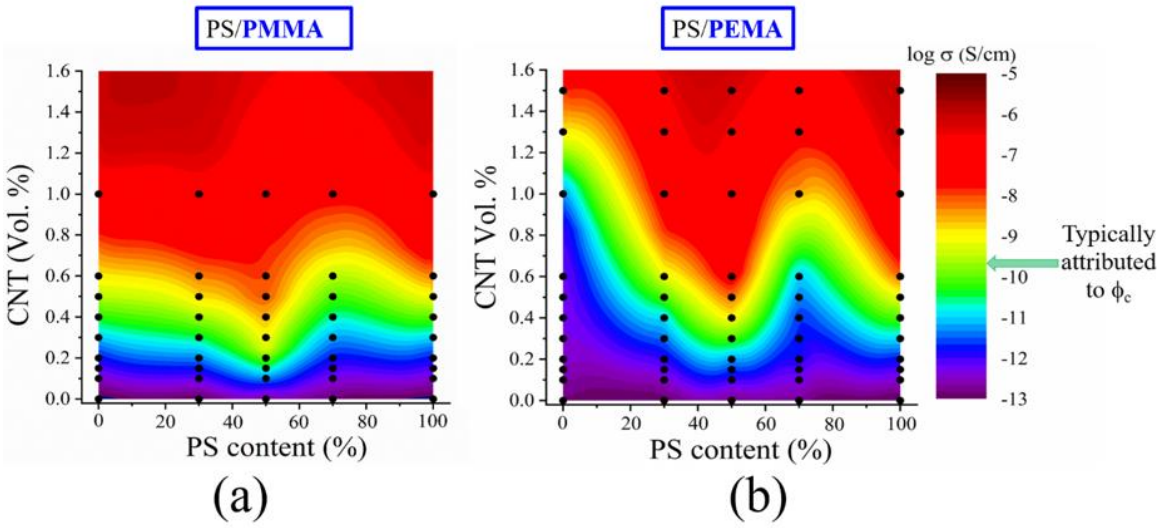

6.1 Introduction

Conductive polymer composite (CPC) films are widely used in electromagnetic interference and photovoltaic conversion [125,126]. Owing to unique mechanical properties, electronics and the high aspect ratio (AR), Carbon nanotubes (CNT) are considered to be ideal fillers for CPCs. The CNT can form a conductive pathway in polymer composites, even at a very low amount [127-130].

In addition, it is known different fillers show different surface tensions. Thus, the location of CNT in PalkylMA and PS blends would be different from CB. Moreover, CNT with a large aspect ratio is easy to entangle with each other. Consequently, the influence of PalkylMA content in the electrical conductivity of PalkylMA/PS/CNT ternary composite films would be different from corresponding PalkylMA/PS/CB ternary composite films.

In chapter 5, PMMA/PS/CB and PEMA/PS/CB systems show a significantly different conductive behavior with PMMA or PEMA content increasing in polymer blends. To further research how the different kinds of PalkylMA content in PalkylMA/PS blends influence conductivity of PalkylMA/PS/filler ternary composites; PMMA/PS/CNT, as well as PEMA/PS/CNT films, were investigated.

6.2 CNT location predicting

Through calculating the ω_a as given by Eq. 5.2 and 5.3, the location of CNT in PalkylMA/PS blends was predicted. The surface energies of CNT, PS, PMMA as well as PEMA are taken from the literature [131, 132] and listed in Table 6.1.

Table 6.1. Surface energies of PMMA, PEMA, PS and CNT at 20 °C.

Components	20 °C (mN m^{-1})		
	γ	γ^d	γ^p
PMMA	41.1	29.6	11.5
PEMA	35.9	26.9	9.0
PS	40.7	34.5	6.1
CNT	45.3	18.4	26.9

Table 6.2 and Table 6.3 show the results of the interfacial tension. The ω_a from both Eq. 5.2 and Eq. 5.3 are lower than -1, which indicates that CNT prefers to be located in PalkylMA (PMMA, PEMA) phase based on the thermodynamic factor. This is the opposite of CB particles, which is preferred to be located in the PS phase in PalkylMA/PS blends.

Table 6.2. Interfacial tensions and wetting coefficient (Harmonic-mean equation).

Components	$\gamma_{CNT/PalkylMA}$ (mN m^{-1})	$\gamma_{CNT/PS}$ (mN m^{-1})	$\gamma_{PalkylMA/PS}$ (mN m^{-1})	ω_a
PMMA	8.76	18.12	2.12	-4.42
PEMA	10.52	18.12	1.60	-4.75

Table 6.3. Interfacial tensions and wetting coefficient (Geometric-mean equation).

Components	$\gamma_{CNT/PalkylMA}$ (mN m^{-1})	$\gamma_{CNT/PS}$ (mN m^{-1})	$\gamma_{PalkylMA/PS}$ (mN m^{-1})	ω_a
PMMA	4.54	9.98	1.12	-4.86
PEMA	5.58	9.98	0.86	-5.12

6.3 Electrical conductivity of ternary composite films

6.3.1 Percolation threshold investigation

The logarithm of electrical conductivities vs CNT concentration is shown in Figure 6.1 and Figure 6.2. Different polymer blend ratios in the PalkylMA/PS/CNT are presented by different symbols. Each data point is obtained from an average of 10 experimental measurements, and vertical error bars represent standard deviations. All curves show a steep increase in electrical conductivity on reaching a critical concentration, which is corresponding to ϕ_c. The fitting ϕ_c results are shown in Fig. 6.3. The dashed lines represent the fits according to Eq. 2.2, results are shown in Figure 6.1 and Figure 6.2.

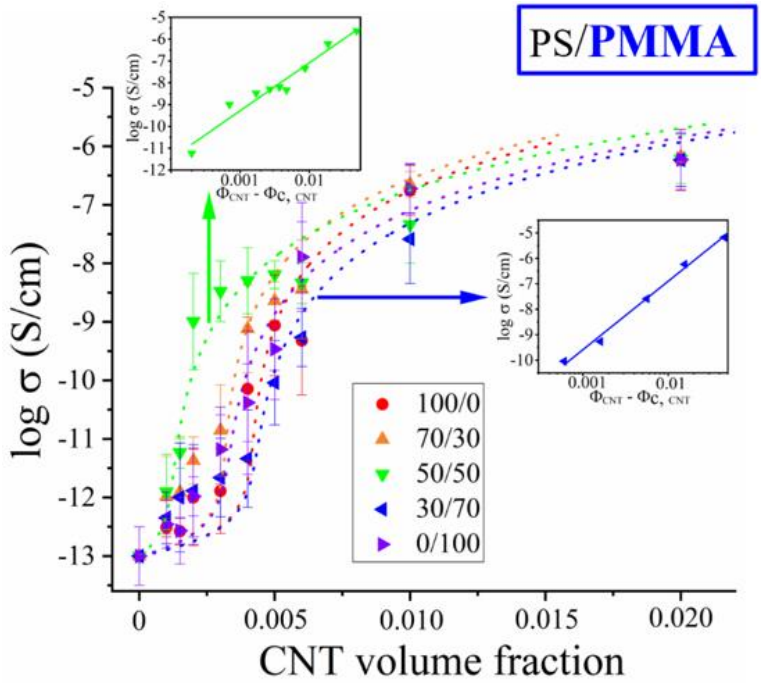

Figure 6.1 The logarithm value of electrical conductivity versus CNT concentration for PMMA/PS/CNT films obtained from solution casting. For the Eq. 2.2, the best fit is presented by the dashed lines. The two insets illustrate the linear fit using Eq. 2.1 of polymer blend ratios at PMMA/PS=50/50 and PMMA/ PS= 30/70, respectively.

The ϕ_c obtained from the GEM theory was further checked utilizing the classical percolation theory (Eq. 2.1). The linear relationship between log σ and log (ϕ - ϕ_c) is satisfying, and two of them are shown in Figure 6.1 and Figure 6.2.

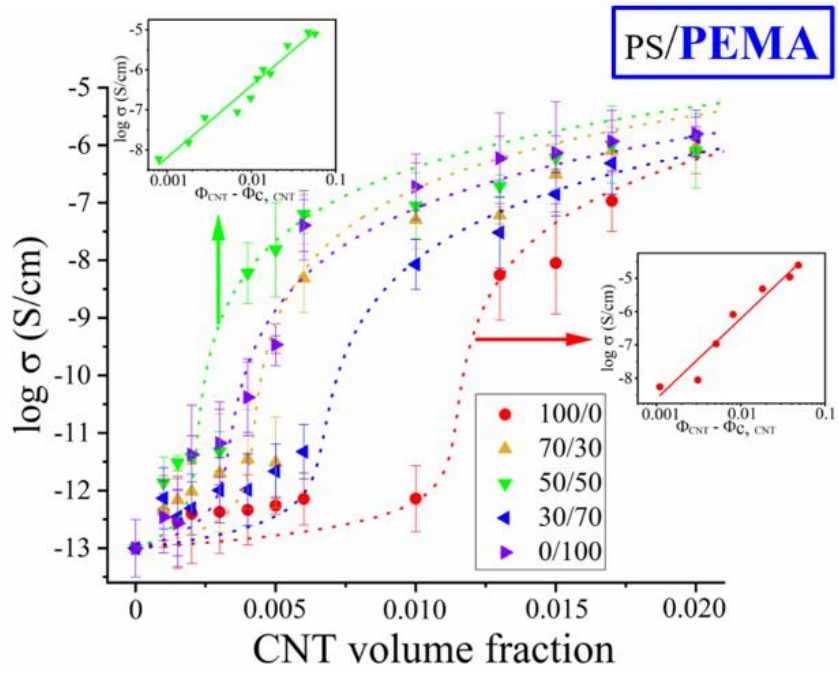

Figure 6.2 The logarithm electrical conductivity versus CNT concentration for PEMA/PS/CNT films (The other information is the same as Fig. 6.1).

Figure 6.3 shows the fitting ϕ_c of PalkylMA/PS/CNT films with different polymer blend ratios. When PS content is 0%, as shown in Fig. 6.3, which corresponding to binary PMMA/CNT and PEMA/CNT composite films, the ϕ_c of PMMA/CNT is much lower than that of PEMA/CNT, it might be a consequence of high viscosity of PEMA. And accordingly, all the ϕ_c of ternary PMMA/PS/CNT are lower than that of PEMA/PS/CNT. Different from that PEMA/PS/CB and PMMA/PS/CB, all the ϕ_c of PEMA/PS/CNT shows the same tendency with PMMA/PS/CNT. With PS content from 0 % to 50% in polymer blends, a typical double percolation effect is presented [133-135]. The ϕ_c of ternary composite films at PMMA/PS=50/50 and PEMA/PS=50/50 decreased by 69.0% and 73.1% in comparison to that pure PMMA/CNT and PEMA/CNT, respectively. The formation of the CNT conductive pathway would be transversely restricted once the PS content exceeds a certain concentration, where it is PS rather than PalkylMA forms a continuous phase in polymer blends, which corresponding to a high ϕ_c (70%) of CPCs.

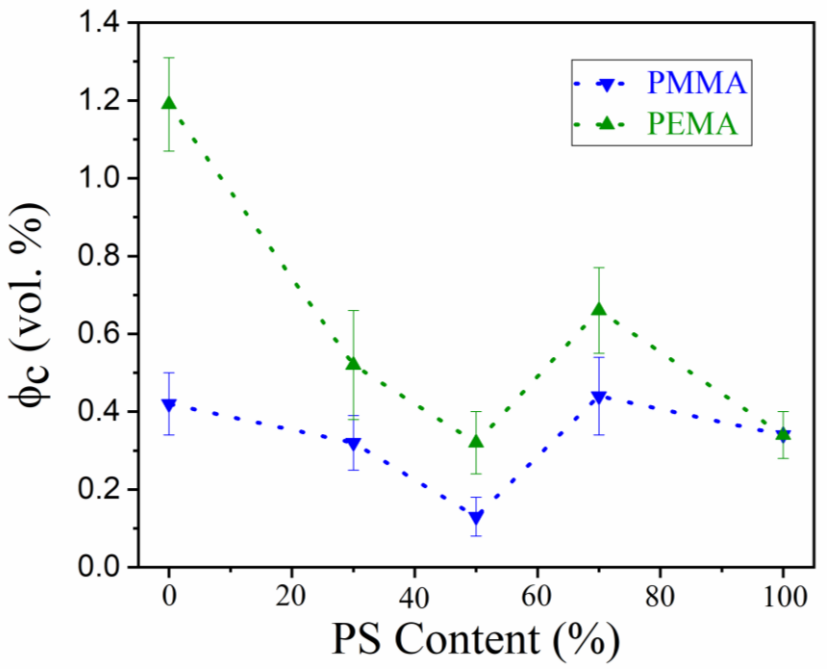

Figure 6.3 The percolation thresholds of PMMA/PS/CNT, PEMA/PS/CNT ternary composite films versus different PS content in polymer blends.

6.3.2 Contour plot of conductivity

Figure 6.4 presents a conductivity contour plot diagram according to all experimental data. The actual experimental data are presented by black dots on the contour plot. The colors in the contour plot represent the logarithm value of conductivity.

The electrical conductivity increases with CNT volume fraction (along the Y-axis). In addition, Fig. 6.4 clearly shows that the PS content influences the ϕ_c of PalkylMA/PS/CNT ternary composite films (along all the X-axis). The ϕ_c area corresponds to the green area in the contour plot at a lower volume fraction (50%) with PS content was introduced to the PalkylMA matrix. This kind of contour plot considering both filler concentration and polymer blend ratio provides a convenient way to determine filler volume fraction and polymer blend ratio when design CPCs.

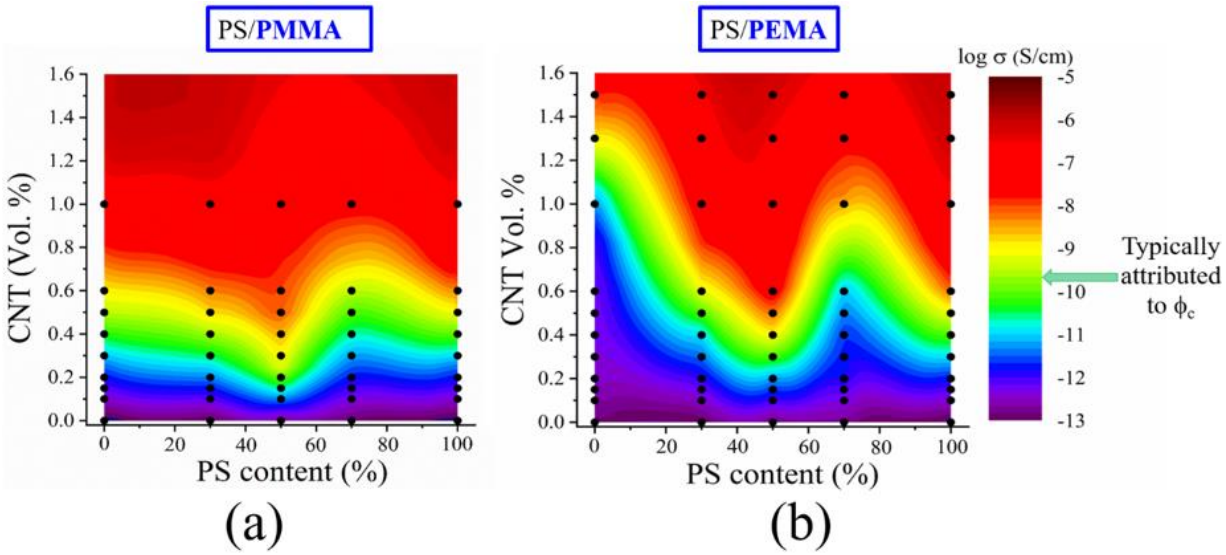

Figure 6.4 The logarithm value electrical conductivity of PMMA/PS/CNT as well as PEMA/PS/CNT as a function of PS content and CNT concentration.

6.4 Morphological investigation

6.4.1 PalkylMA/PS/CNT with a different polymer blend ratio

The distribution of CNT in both PEMA/PS/CNT and PMMA/PS/CNT films with CNT volume fraction at 0.5 vol. % is shown in Figure 6.5. The PalkylMA/PS ratios are (a) PMMA/PS=70/30; (b) PMMA/PS=50/50; (c) PMMA/PS=30/70; (d) PEMA/PS=70/30; (e) PEMA/PS=50/50; (f) PEMA/PS=30/70, respectively. The phase separation between both PS and PMMA, PS and PEMA have been observed in different PalkylMA/PS ratios. The phase morphology of composites went through from sea-island structure (a, d) to co-continuous structure (b, e) and then return to sea-island structure (c, f) with PS concentration increasing. However, the continuous phase is changed from PalkylMA to the PS phase with PS concentration from 30% to 70%. From Fig. 6.5, it can be also observed that the interface between PEMA and PS is blurred than PMMA and PS, which can be explained by the fact that incompatibility between PEMA and PS is different from PMMA and PS [54,55].

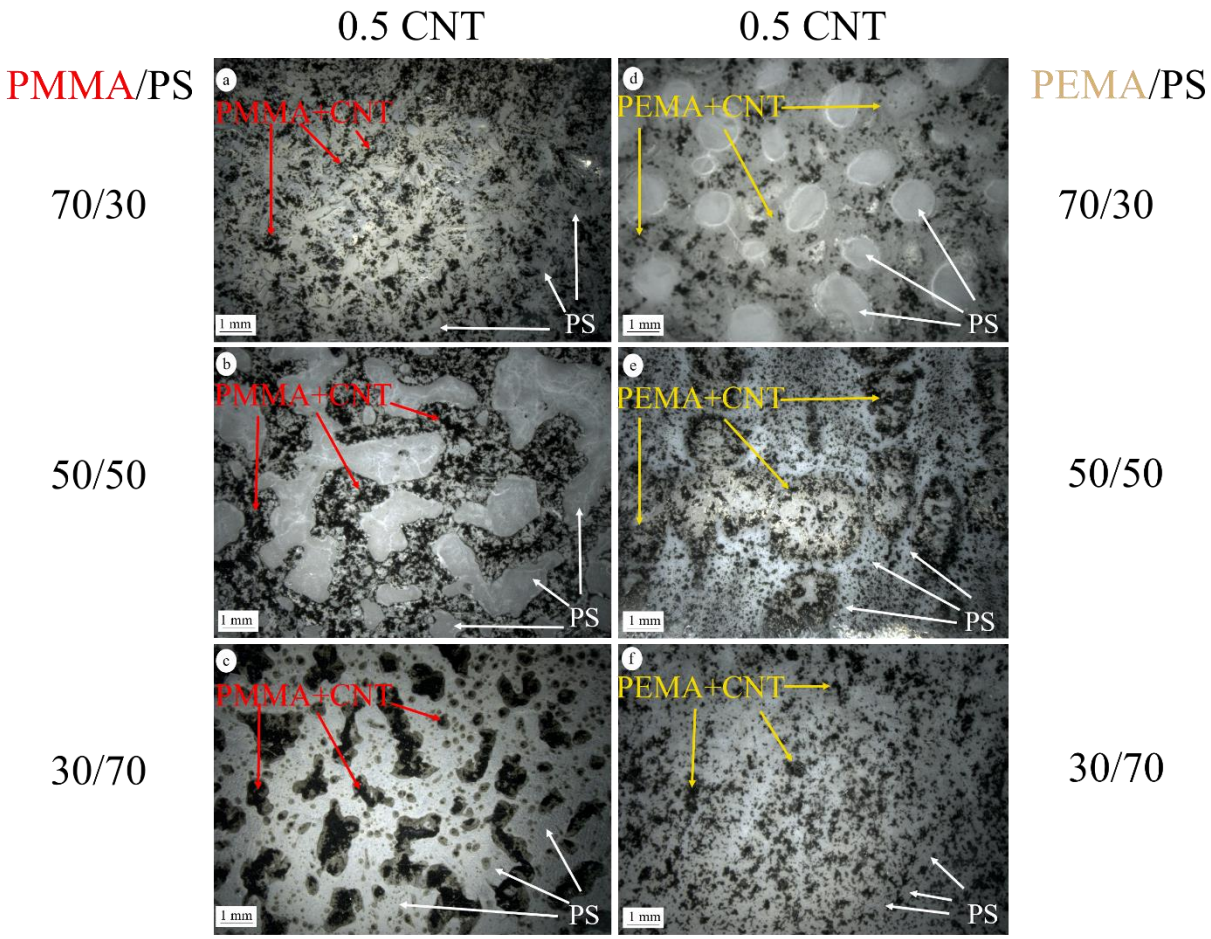

Figure 6.5 CNT distribution in the PalkylMA/PS/CNT films with 0.5 vol. % CNT and PalkylMA/PS ratios are (a) PMMA/PS=70/30; (b) PMMA/PS=50/50; (c) PMMA/PS=30/70; (d) PEMA/PS=70/30; (e) PEMA/PS=50/50; (f) PEMA/PS=30/70, respectively.

To investigate the phase morphology which perpendicular direction to the composite films, the cross-section of composite films was observed by SEM. As shown in Fig. 6.6, SEM graphs of films with CNT concentration at 0.5 vol. % and PalkylMA/PS ratios are (a) PMMA/PS=70/30; (b) PMMA/PS=50/50; (c) PMMA/PS=30/70 (d) PEMA/PS=70/30; (e) PEMA/PS=50/50; (f) PEMA/PS=30/70, respectively. Similar to that PalkylMA/PS/CB films prepared from the solution casting method, even CNT show affinity with only PalkylMA and prefer to be located into this phase, while still not all CNT located in PalkylMA. This is explained in the corresponding part of the PalkylMA/PS/CB system.

From Figure 6.5(c, f) and Figure 6.6(c, f), it can be observed that in both PMMA/PS=30/70

and PEMA/PS=30/70 situation, the CNT located in the disperse phase and thus isolated by PS continuous phase, that is not good for conductive pathway forming. Therefore, in this case, the ternary composite films would show a higher ϕ_c.

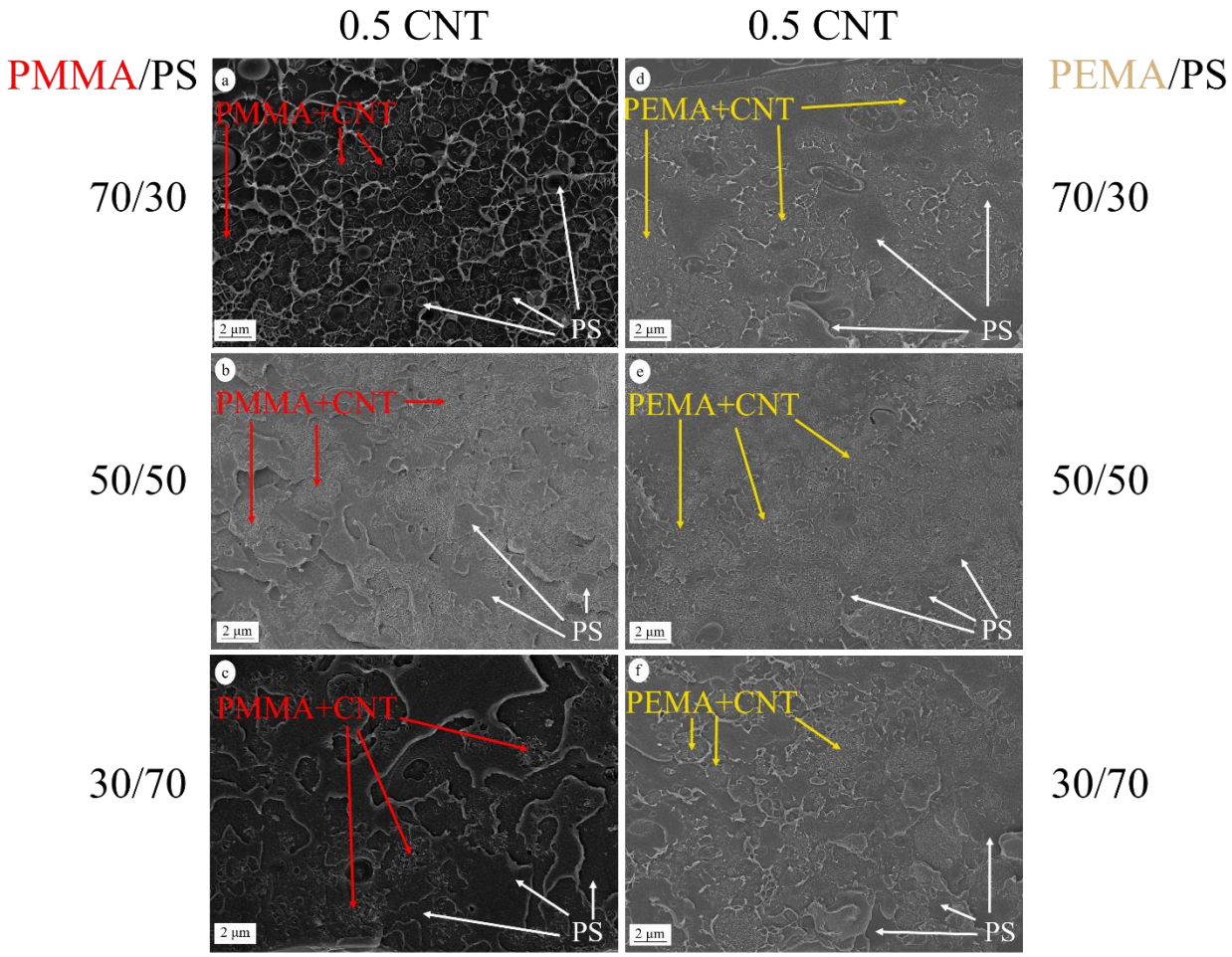

Figure 6.6 SEM graphs of PalkylMA/PS/CNT films with CNT volume fraction at 0.5 vol. % and PalkylMA/PS ratio are (a) PMMA/PS=70/30; (b) PMMA/PS=50/50; (c) PMMA/PS=30/70; (d) PEMA/PS=70/30; (e) PEMA/PS=50/50; (f) PEMA/PS=30/70, respectively.

6.4.2 PalkylMA/PS/CNT with different CNT concentration

From both Figure 6.3 (ϕ_c) and Figure 6.4 (contour plot), it can be observed that PalkylMA/PS/CNT films show lower ϕ_c when PalkylMA/PS ratio at 50/50. Therefore, the phase morphology of PalkylMA/PS=50/50 with different CNT concentrations were presented. As shown in Figure 6.7, light microscopy images of the PalkylMA/PS/CNT films when

polymer blend ratio at PalkylMA/PS=50/50 and with different CNT volume fractions (a, d) 0.1 vol. %; (b, e) 0.5 vol. %; (c, f) 1.0 vol. %, respectively. It can be observed that both PMMA/PS and PEMA/PS form co-continuous structures when the polymer blend ratio at 50/50 even the incompatibility between PMMA, PEMA and PS is different. While the interface between the PEMA phase and PS phase is not clear as that PMMA with PS. This kind of phase morphology is good for CNT filler form conductive pathway [136-139].

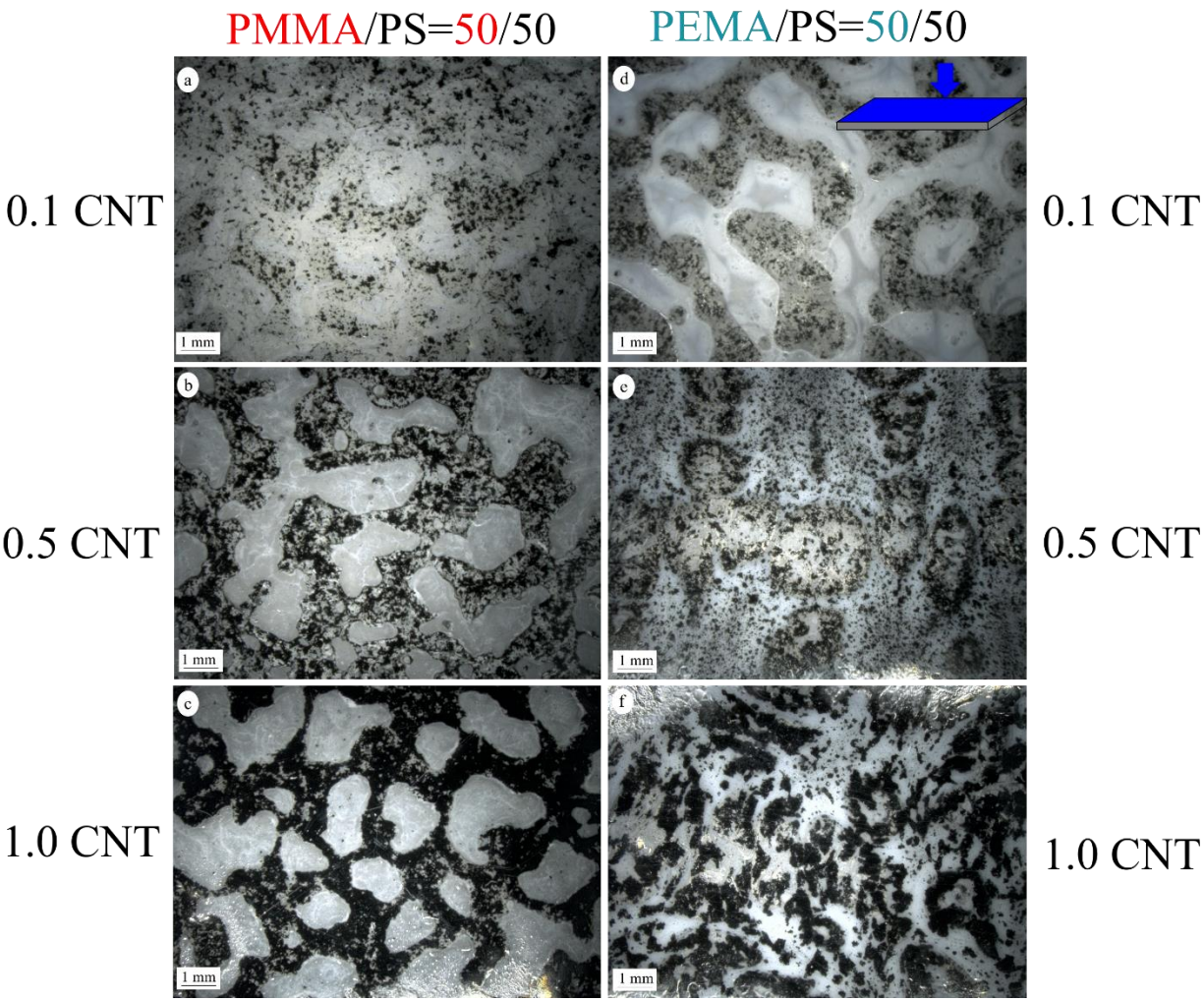

Figure 6.7 Light microscopy graphs of the PalkylMA/PS/CNT films when PalkylMA/PS=50/50 with different CNT concentration (a, d) 0.1 vol. %; (b, e) 0.5 vol. %; (c, f) 1.0 vol. %, respectively. The direction of blue shows the observation direction under the microscope.

Figure 6.8 shows SEM graphs of the PalkylMA/PS/CNT films when PalkylMA/PS=50/50 without CNT (a, d) and with (b, e) 0.5 vol. %; (c, f) 1.0 vol. % CNT, respectively. The blends

of PMMA/PS show different phase behavior than that of PEMA/PS. The PMMA/PS forms co-continuous structure (Fig.6.8 (a)) while PEMA with PS forms double emulsion structure (Fig.6.8 (d)) [105]. As shown in Fig. 6.8(e) and (f), with CNT volume fraction increasing, the PEMA/PS blend forms a co-continuous structure as well.

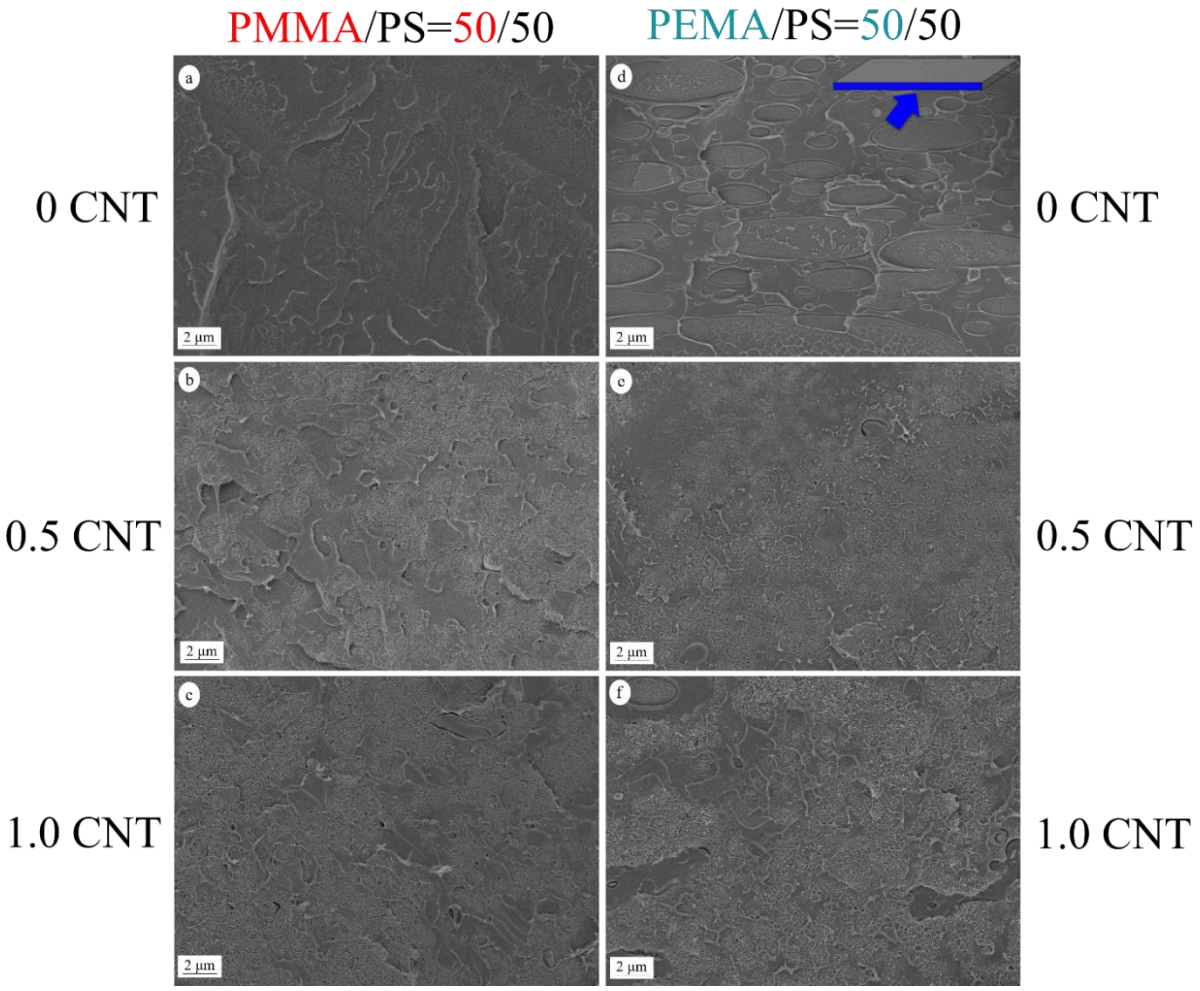

Figure 6.8 SEM graphs of the PalkylMA/PS/CNT films when PalkylMA/PS=50/50 without CNT (a, d) and with (b, e) 0.5 vol. %; (c, f) 1.0 vol. % CNT, respectively. The direction of blue shows the observation direction under the microscope.

6.5 Conclusions:

Ternary PalkylMA/PS/CNT composite films with different polymer blend ratios and CNT volume fractions were prepared using the solution casting method. CNT was preferentially located in the PalkylMA phase which is different from PalkylMA/PS/CB films. All the ϕ_c of ternary PalkylMA/PS/CNT composite films were systemically revealed and the experimental

data were fitted utilizing McLachlan's theory. An obvious double percolation effect was observed when PalkylMA/PS ratio is 50/50. The ϕ_c of ternary PalkylMA/PS/CNT composite films at PMMA/PS=50/50 and PEMA/PS=50/50 decreased by 69.0% and 73.1% in comparison to that pure PMMA/CNT and PEMA/CNT, respectively. A conductivity contour plot diagram according to all experimental data was presented to show the conductivity versus CNT volume fractions and polymer blend ratio. Different from PalkylMA/PS/CB, the conductivity of both PMMA/PS/CNT and PEMA/PS/CNT films show a similar tendency with PS content increasing.

7

Relationship between percolation threshold and exponent t

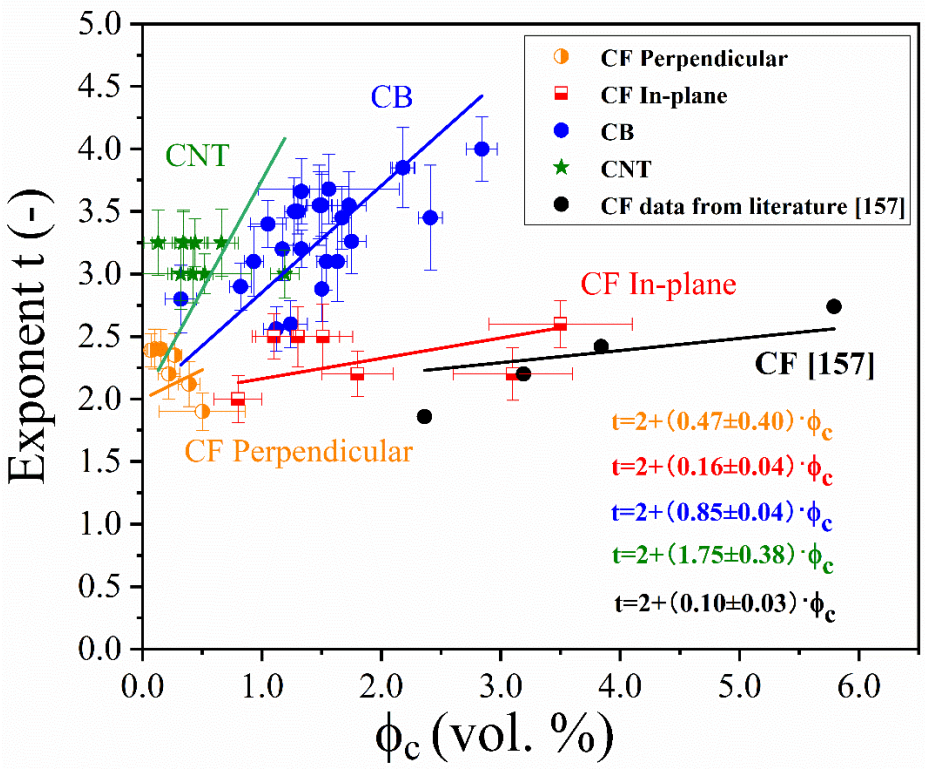

McLachlan GEM equation describes the relationship between the conductivity of a composite depending on the filler and matrix conductivity. There are two exponents s and t in the McLachlan equation. At first, it was believed that simulations based on conductive networks, lattice and continuum media belong to the same universal class and that s and t only depend on the dimension of the system. In three dimensions the most widely accepted universal exponents for DC conductivity are $s_{un} = 0.87$ and $t_{un} = 2.0$ [140]. In most cases the values obtained for s are close to the universal value, however, the exponent t is often larger than the universal value [141]. It was even found that very high values of t tend to occur when the conducting particles have extreme geometries like fibers [142-144].

Some previous researches have attempted to explain the non-universality of exponent t. Kogut and Straley [145] considered an infinite resistor lattice network, whose bonds have conductivities σ chosen randomly from the distribution as follows:

$$g(\sigma)=(1-p)\cdot\delta(\sigma)+p\cdot h(\sigma) \tag{7.1}$$

corresponding to a lattice with a fraction 1-p of insulators and a fraction p of conductors distributed via the normalized function h(σ). There is a critical concentration p=p*, called the percolation threshold, above which infinite chains of bonds whose conductivities are chosen from h(σ) span the lattice. For well-behaved h(σ), the specific conductivity ∑ shows a power law behavior for p just above p*:

$$\sum \sim (p-p^*)^{t} \tag{7.2}$$

Where t is the universal conductivity exponent. They imagined a normalized function h(σ) which contains a large number of poor conductors (e.g. $h(\sigma) \sim \sigma^{-\alpha}$ for small σ, with $0<\alpha<1$) and which causes the critical conductivity exponent t to depart from its universal value and to depend on the conductivity distribution function. In their study, they examined the exponent t conduction problems in several model systems and found identical distribution-induced non-universality. For distribution Eq. (7.1), with $h(\sigma) \sim \sigma^{-\alpha}$ for small σ, the usually universal

exponent t must be replaced by:

$$t=t_{un}+\alpha/(1-\alpha),\ 0<\alpha<1 \tag{7.3}$$

Note that this model does not allow t to be lower than the accepted universal values of t_{un}.

Balberg [146] derived an expression for a non-universal t value as follows:

$$t= t_{un}+(\mu+\omega-1)/(1-\omega) \tag{7.4}$$

In this model, Balberg assumed that the resistance distribution function h(ϵ), where ϵ is the proximity parameter, has the form $\epsilon^{-\omega}$ as $\epsilon\rightarrow 0$ ($-\infty<\omega<1$). The parameter μ is related to the dimensionality d of the system and is such that μ=d-3/2 for the Swiss-cheese model [147], and μ=d/2-1 for the inverse-Swiss-cheese model [148]. Different combinations of μ and ω will give various values of the exponent t in the Balberg model. A large number of experimental systems, some specifically designed to test the theory, show exponent t values greater than 2.0 indicating that the exponent t could be larger than 2.0 [149].

A huge amount of effort has been made to investigate the physical background behind exponent t. It has been suggested that exponent t is related to the size and shape of the filler. The McLachlan equation parameters, like ϕ_c and exponent t, are directly related to the geometry of the filler and matrix in the composite and the microstructure of the composite itself [150]. In the McLachlan GEM equation, the percolation step is more smeared out as t increases (as shown in Figure 7.1) [150]. Even though often mentioned, there is no specific description of the relationship between the parameters ϕ_c, exponent t and the conducting filler shapes. Even McLachlan himself suggested that more experimental data is needed to test these relationships in composite systems [28].

Runyan, J. et al. and Kovacik, J. postulated that exponent t is sensitive to the filler geometry, in this work s is kept constant and the changes in exponent t by different fillers geometries are investigated [150-151].

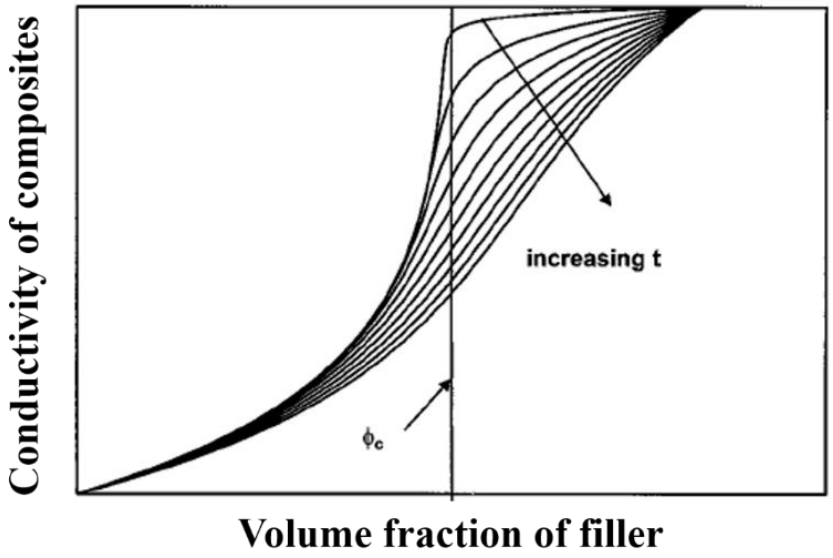

Figure 7.1. Conductivity calculated from McLachlan equation shown for changing exponent t, while s and ϕ_c are kept constant [150].

To the best of our knowledge, there are few public literatures [28,140,150,153-159] that discussed the relationship between ϕ_c and exponent t in the McLachlan GEM equation. The public literature giving values for exponent t different from the "universal" value are listed in Table 7.1 and Figure 7.2. It should be mentioned that the data from the source [152] is not derived from experiments but simulations and theoretical calculations based on a "universal" 3D system.

Table 7.1. Values for ϕ_c and exponent t in public literature with measuring orientation at 0° (along the x-y plane) and 90° (along the x-z plane). The samples can be considered as 3D regarding McLachlan's height-criterion.

. Matrix	Filler	ϕ_c (%)	Exponent t (-)	Orientation (°)	AR (-)	Reference
Talc-wax powder	Ground carbon black	1.20±0.10	2.06±0.10	90	1	[140]
Talc-wax powder	Raw carbon black	1.30±0.10	2.26±0.11	90	1	[140]
Talc-wax powder	Graphite/boron nitride	3.30±0.10	2.51±0.12	90	1	[140]
Talc-wax powder	Fe_3O_4	2.50±0.30	4.12±0.23	90	1	[140]

Talc-wax powder	Niobium carbide	6.50±0.30	5.25±0.67	90	1	[140]
BN	B_4C Parallel	39.20	2.88	0[1)]	2000	[150]
BN	B_4C Perpendicular	33.80	3.88	90[1)]	2000	[150]
Epoxy	Graphite	12.40	4.80	90	111	[28]
“Universal” 3D system	/	16.00	2.00	90	1	[152]
Epoxy	Graphite	42.10	3.00	/	/	[152]
Epoxy	Carbon	7.40	4.49	/	/	[152]
Epoxy	CB (9.6 nm)[2)]	3.60	3.40	90	1	[153]
Epoxy	CB (9.0 nm) [2)]	2.75	2.50	90	1	[153]
PA6	Flake graphite	0.74±0.05	2.32±0.07	0°	235	[154]
ABS	MWCNT	0.05	1.93	90	60-1000	[155]
ABS	MWCNT	0.49	2.10	90	158	[156]
Polyimide	SWCNT	0.05	2.22	90	2500-3300	[158]
PMMA	CF	13.13±4.67	4.40±0.72	0 (X)	9.2	[159]
PMMA	CF	13.25±4.35	3.50±0.52	0 (Y)	9.2	[159]
PMMA	CF	14.28±4.23	2.65±0.45	90	9.2	[159]

1) Measurement direction parallel and perpendicular to BN platelet faces
2) Epoxy/CB (9.6 nm) and (9.0 nm) means that the average carbon black size is 9.6 nm and 9.0 nm

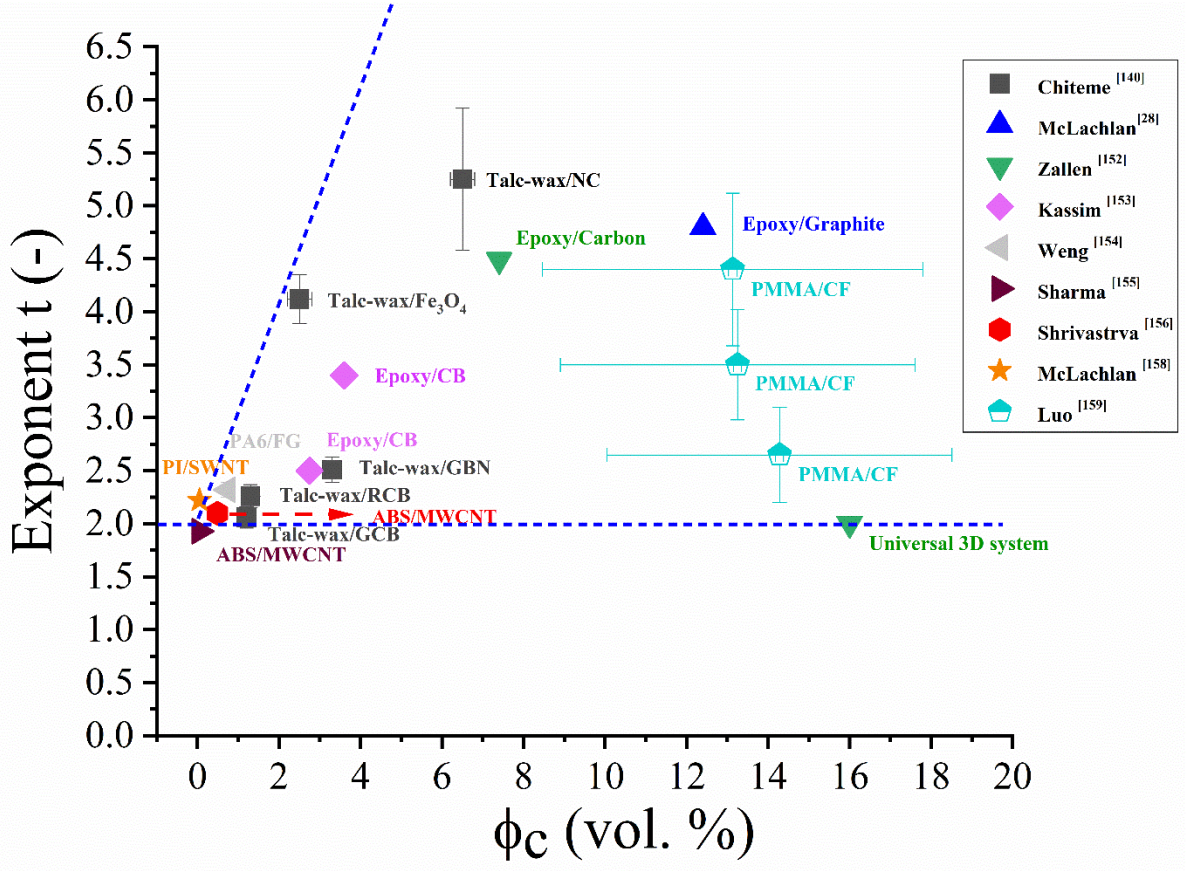

Figure 7.2. Exponent t in the McLachlan equation as a function of ϕ_c for conductive composites from the literature [28, 140, 152-159]. Different symbols represent the data from different sources and different colors represent different matrix/filler combinations. The blue dash lines are the range of exponent t. Only the ϕ_c data from 0-20 vol. % are shown in the Figure.

As shown in Figure 7.2, the exponent t in the McLachlan equation from different conductive composite systems are all in a range between two blue dash lines. From the figure, it can be roughly estimated that the exponent t increases with increasing ϕ_c of the composites.

In this work, all the ϕ_c were obtained from fitting experimental data with the GEM equation. In terms of the fitting parameter in this equation, the exponent s is fixed at a universal value of 0.87 and exponent t as an adjustable parameter to obtain the best fit. Thus, there is a corresponding exponent t for each ϕ_c obtained in this work. Three different classes of carbon-based fillers with different shapes and structures were included. Thus, they would yield different exponent t in the McLachlan GEM equation.

In addition, various ϕ_c values are obtained for each kind of filler. In particular, for CF, ϕ_c values with seven different ARs were investigated along in-plane and perpendicular direction of the film. For CB and CNT, the ϕ_c values are shown for four polymer blends with different compatibility and at different compositions. Thereby, the relationship between ϕ_c and exponent t can be revealed by a large number of ϕ_c and corresponding exponent t data.

From the fitting result for exponent t as shown in Fig. 7.3, it can be easily found that the exponent t value of all the three fillers is non-universal. As the ϕ_c of the composite films increases, the exponent t also increases as derived from Figure 7.2. Additionally, for all of the three different kinds of filler, it is remarkable that the relationship between ϕ_c and exponent t shows a linear behavior as follows:

$$t = 2.0 + a \cdot \phi_c \tag{7.5}$$

Where a is an adjustable parameter and the value 2.0 corresponds to the universal value for exponent t in the McLachlan equation.

As shown in Figure 7.3, exponent t as a function of ϕ_c for CF, CB and CNT is presented, respectively. It can be seen that Eq. 7.5 describes all the experimental data within the experimental error. Thus, from the fitting result, the parameter a for different classes of carbon-based filler can be obtained for solution cast films. For CF perpendicular, CF in-plane, CB and CNT, the parameter a is revealed as 0.47, 0.16, 0.85 and 1.75, respectively.

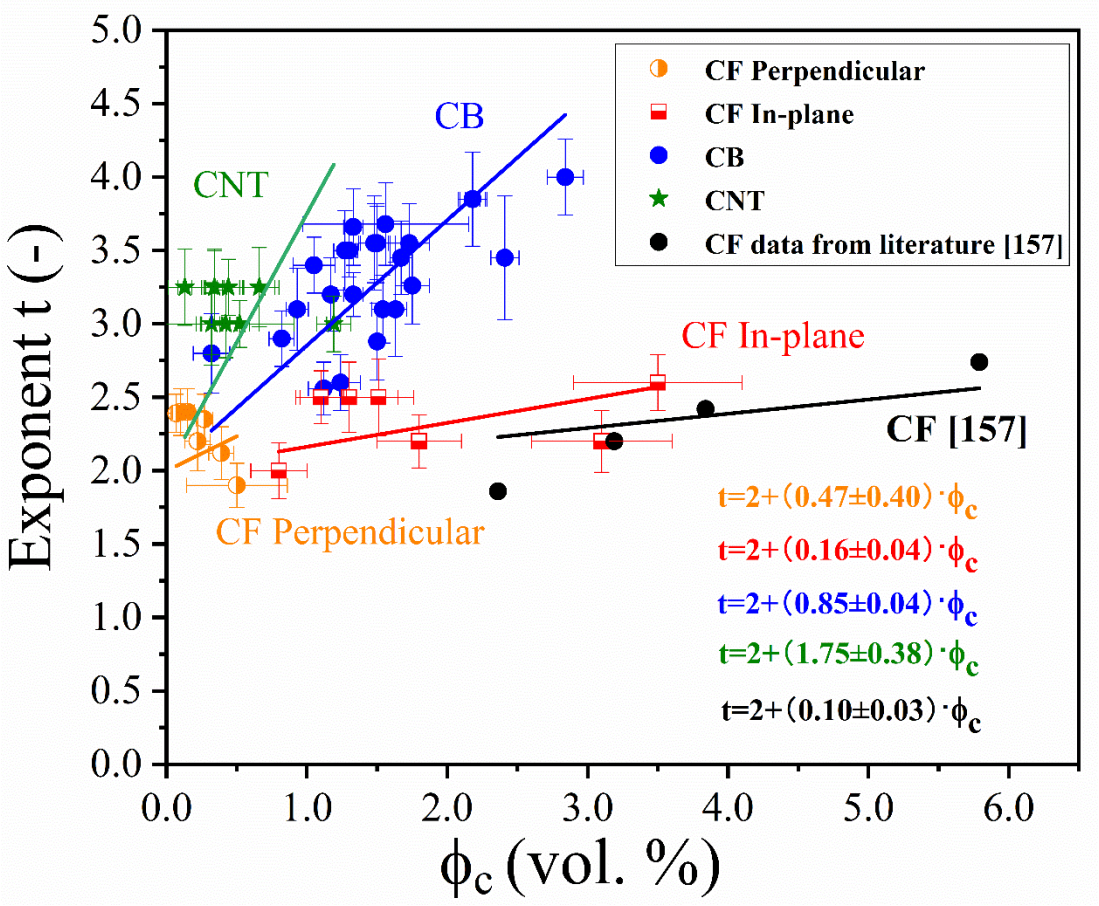

Figure 7.3. Relationship between exponent t and ϕ_c of the composite films with CF, CB and CNT as fillers. Black circles are data from the literature for CF [157]. Solid lines are the best fits to the data utilizing Eq. 7.5 indicating a common intersection point with the t-axis at 2.0 when extrapolating to ϕ_c=0.

The only available data in the public literature which gives different ϕ_c and exponent t pairs for the same CF but with different AR is from Yi J. et al. based on hot-pressed samples [157]. This data can also be fitted with Eq. 7.5 as indicated in Figure 7.3.

In particular, the data shown in Figure 7.3 also hints at a common intersection on the t-axis. Thus, this work suggests that t=2.0 is a general behavior when ϕ_c approaches zero.

For the public data in Table 7.1, the samples with CB and MWCNT fillers only have two data points, so it cannot be fitted by Eq. 7.5. However, the exponent t increases with increasing ϕ_c.

Conclusions:

For the solution cast films in this work, a series of ϕ_c and exponent t pairs could be obtained from the percolation curves of different carbon-based fillers utilizing the McLachlan equation. In particular, pairs derived perpendicular and in-plane to the films for binary composite films with CF of different AR as well as pairs derived perpendicular for ternary composite films with different polymer blends and different polymer blend ratios for both CB and CNT filler were investigated. In these systems, the exponent t for all three fillers is different from the value of 2.0 often referred to as “universal”. For the first time a relationship between ϕ_c and exponent t following a linear behavior $t = 2.0 + a \cdot \phi_c$ is proposed, indicating there is an intersection with the t-axis at t=2.0 when ϕ_c approaches 0.

8

Summary (English)

In this work, binary PMMA/CB, PMMA/CF and PMMA/CNT composite films, as well as ternary PalkylMA/PS/CB and PalkylMA/PS/CNT composite films were fabricated and the electrical behavior of the composite films were investigated.

(a) PMMA/CF binary composite films with seven ARs of CF from 49 to 616 and different CF volume fractions from 0.1 to 5.0 vol. % were prepared utilizing the solution casting method. As both AR of CFs and CF volume fraction increases, in-plane and perpendicular directions conductivities of composite films increase. Two different pre-factors $K_{\parallel}=6.05$ and $K_{\perp}=0.80$ for Balberg excluded volume theory is revealed considering measurement directions for the in-plane and perpendicular direction of the film. A proportionality was revealed for $\phi_{c,\parallel}$ and $\phi_{c,\perp}$: $\phi_{c,\parallel} \approx 7.65 \times \phi_{c,\perp}$. Moreover, binary PMMA/CB and PMMA/CNT composite films were obtained from solution casting as well. An obvious difference between the CB distribution at the bottom and the top of the PMMA/CB composite film was observed when CB volume fraction at 0.5 vol. %. The in-plane $\phi_{c,\parallel}$ and perpendicular $\phi_{c,\perp}$ with different carbon fillers (CB, CF and CNT)

show totally different behaviors. The $\phi_{c,\parallel}$ is much smaller than $\phi_{c,\perp}$ for binary PMMA/CB composite films. The $\phi_{c,\parallel}$ is much higher than $\phi_{c,\perp}$ for PMMA/CF and finally the $\phi_{c,\parallel}$ and $\phi_{c,\perp}$ do not show a tremendous difference for PMMA/CNT. For different filler types (CB, CF, CNT), a power-law behavior was revealed as $t_{perpendicular}/t_{in\text{-}plane} = (1.08\pm0.03)\times(\phi_{c,\,perpendicular}/\phi_{c,\,in\text{-}plane})^{1/4}$ correlating the ϕ_c and corresponding exponent t in McLachlan theory for perpendicular and in-plane directions.

(b) In this work, the conductivity of poly(alkyl methacrylate) (PalkylMA)/Polystyrene (PS)/carbon black (CB) and poly (cyclohexyl methacrylate) (PChMA)/PS/CB ternary composite films were prepared from the solution casting. The ϕ_c of all the films before and after annealing have been investigated. The conductivity of all four different kinds of composite films was presented in four contour plots versus CB concentration and polymer blend ratios, respectively. The location of CB particles was preferentially located into the PS phase for PMMA/PS, PBMA/PS, PEMA/PS blends, and into the PChMA phase for PChMA/PS blend, respectively. The ϕ_c of both PMMA/PS/CB and PBMA/PS/CB ternary composite films decreased when PMMA and PBMA were added into the PS phase, this can be explained by the double percolation effect. However, even if the CB particles were only located in the PS phase as well, the PEMA/PS/CB films (PEMA/PS = 50/50) showed a higher ϕ_c due to the double emulsion structure of PEMA/PS blends. The ϕ_c of PMMA/PS/CB composites obtained from melt blending are all lower than that from the solution casting even they show the same changing tendency with polymer blend ratio changing.

As typical examples, the SEM images with PalkylMA/PS of 50/50 and CB concentration at 2 vol. % before and after annealing were presented. In PMMA/PS/CB and PBMA/PS/CB composite films, thermal annealing lead to an increase in the dispersed particle size and lower ϕ_c. Phase morphology of PEMA/PS/CB was changing from a double emulsion structure to a

co-continuous structure. In PChMA/PS/CB system, the phase separation cannot be observed under SEM. After thermal annealing, all the ϕ_c of PChMA/PS/CB ternary composite films with different PChMA/PS ratios showed a linear behavior with PChMA content increasing. If ϕ_c of both binary systems (polymer A/filler and polymer B/filler) is determined, then a linear relationship between the ϕ_c of the ternary composites (A+B+fillers) and the ratio of two polymers can be revealed when polymer A and B are miscible. Compared with the typical double percolation effect generally using an immiscible polymer blend system, this can provide a new idea to design ternary conductive polymer composites with good mechanical properties.

(c) Ternary PalkylMA/PS/CNT composite films with different PalkylMA/PS ratios and CNT concentrations were prepared using solution casting. CNT was preferentially in the PalkylMA phase which is different from PalkylMA/PS/CB films. All the ϕ_c of PalkylMA/PS/CNT composite films were systemically investigated and the experimental data were fitted utilizing McLachlan's theory. An obvious double percolation effect was observed when PalkylMA/PS ratio is 50/50. The ϕ_c of ternary composite films at PMMA/PS=50/50 and PEMA/PS=50/50 decreased by 69.0% and 73.1% in comparison to that pure PMMA/CNT and PEMA/CNT, respectively. A conductivity contour plot diagram according to all experimental data was presented to show the conductivity versus CNT volume fraction and polymer blend ratio. Different from PalkylMA/PS/CB, the conductivity of both PMMA/PS/CNT and PEMA/PS/CNT films showed a similar tendency with PS content increasing.

(d) For the solution cast films in this work, a series of ϕ_c and exponent t pairs could be obtained from the percolation curves of different carbon-based fillers utilizing the McLachlan equation. In particular, pairs derived perpendicular and in-plane to the films for binary composite films with CF of different AR as well as pairs derived perpendicular for ternary composite films with different polymer blends and different polymer blend ratios for both CB and CNT filler were investigated. In these systems, the exponent t for all three fillers is different

from the value of 2.0 often referred to as “universal”. For the first time a relationship between ϕ_c and exponent t following a linear behavior $t = 2.0 + a \cdot \phi_c$ is proposed, indicating there is an intersection with the t-axis at t=2.0 when ϕ_c approaches 0.

9

9. Zusammenfassung (German)

In dieser Arbeit wurden binäre Verbundfolien aus Polymethylmethacrylat (PMMA)/Kohlefaser (CF), PMMA/Kohlenschwarz (CB), PMMA/Kohlenstoff-Nanoröhren (CNT), sowie ternäre Verbundfolien aus Polyalkylmethacrylat (PalkylMA)/ Polystyrol (PS)/CB und PalkylMA/PS/CNT hergestellt. Diese produzierten, leitfähigen Polymerverbundwerkstoffe wurden bezüglich ihres elektrischen Verhaltens analysiert.

(a) Unter Verwendung des Filmgießprozesses wurden Folien aus PMMA/CF mit verschiedenen CF Konzentrationen von 0,1 bis 5,0 Vol .-%. und sieben Aspektverhältnissen von CF von 49 bis 616 hergestellt. Die Analyse der Leitfähigkeit dieser Verbundfolien zeigte sowohl senkrecht als auch parallel zur Filmebene eine Zunahme ebendieser Kenngröße, wenn sowohl das Aspektverhältnis der CF als auch die Konzentration zunehmen. Weiterhin wurde gezeigt, dass für die „excluded volume theory“ nach Balberg die Vorfaktoren $K_{\perp} = 0{,}80$ und $K_{/\!/} = 6{,}05$, unter Berücksichtigung der Messrichtung entlang und senkrecht der Ebene, gelten. Hierbei wurde eine

Proportionalität zwischen $\phi_{c,\perp}$ und $\phi_{c,//}$ festgestellt: $\phi_{c,//} \approx 7{,}65 \times \phi_{c,\perp}$. Zusätzlich wurden leitfähige Verbundfolien mit unterschiedlichen Füllstoffkonzentrationen mithilfe des selben Verfahrens aus PMMA/CB und PMMA/CNT hergestellt. REM-Aufnahmen der PMMA/CB Verbundfilme zeigen, dass der obere und untere Randbereich dieser Proben einen offensichtlichen Konzentrationsunterschied von 0,5 Vol .-% zum Rest der Probe aufweist. Die kritischen Perkolationsfüllgrade senkrecht $\phi_{c,\perp}$ und parallel zur Messebene $\phi_{c,//}$ zeigen für die unterschiedlichen Füllstoffe extrem unterschiedliche Verhaltensweisen. Für PMMA / CB-Verbundfolien ist $\phi_{c,\perp}$ viel höher als $\phi_{c,//}$, für PMMA/CF wiederum ist $\phi_{c,\perp}$ viel niedriger als $\phi_{c,//}$ und für PMMA/CNT konnte zwischen $\phi_{c,\perp}$ und $\phi_{c,//}$ kein signifikanter Unterschied festgestellt werden. Für die verschiedenen Füllstoffe (CB, CF, CNT) wurde ein Potenzgesetz $t_{\text{senkrecht}} / t_{\text{in der Ebene}} = (1{,}08 \pm 0{,}03) \times (\phi_{c,\text{ senkrecht}} / \phi_{c,\text{ in der Ebene}})$ ^ 1/4 ermittelt, indem der Exponent t aus der McLachlan-Gleichung mit dem senkrechten und parallel zur Ebene liegenden ϕ_c korreliert wurde.

(b) In dieser Arbeit wurde die elektrische Leitfähigkeit und im Besonderen ϕ_c von ternären Verbundfilmen aus filmgegossenen PalkylMA/PS/CB und PchMA/PS/CB Folien vor und nach dem Tempern untersucht. Die Leitfähigkeit der vier verschiedenen PalklyMA/PS Folien wurde in vier Konturplots über die CB Konzentration und Polymermischungsverhältnisse aufgetragen. Die Analyse der Filme ergab, dass die CB-Partikel sich bevorzugt in der PS Phase für PMMA/PS, Polybutylmethacrylat (PBMA)/PS, Polyethylmethacrylat (PEMA)/PS Blends bzw. in der Polycyclohexylmethacrylat (PchMA) Phase für PChMA/PS Blends befanden. Die

Perkolationsschwellen ϕ_c der ternären Verbundfilme PMMA/PS/CB und PBMA/PS/CB nehmen mit der Zugabe von PMMA oder PBMA in die PS Phase ab. Dies kann durch das Auftreten eines doppelten Perkolationseffekts erklärt werden. Unter der Annahme, dass das CB hier ebenfalls nur im PS gelöst ist, zeigen die PEMA/PS/CB Filme (PEMA/PS=50/50) eine höhere Perkolationsschwelle aufgrund der Mischungsstruktur des PEMA/PS Blends. Die Perkolationsschwellen der PMMA/PS/CB Mischungen, die über eine Mischung der Polymerschmelzen hergestellt wurden, liegen, im Vergleich zu den filmgegossenen Proben, alle bei kleineren Werten. Eine Änderung der Mischungszusammensetzungen der Proben, die mit dieser Herstellungsmethode erzeugt wurden, zeigen vergleichbare Trends zu denen der filmgegossenen Proben. REM Aufnahmen von PalkylMA/PS mit dem Mischungsverhältnis 50/50 und CB Konzentrationen von 2 vol.% vor und nach dem Tempern wurden als typische Beispiele dargestellt. In PMMA/PS/CB und PBMA/PS/CB Verbundfolien führt das Tempern zu einer Erhöhung der Partikelgröße und einer niedrigeren Perkolationsschwelle. Die Phasenmorphologie von PEMA/PS/CB ändert sich von einer Doppelemulsionsstruktur zu einer co-kontinuierlichen Struktur. Im PChMA/PS/CB System kann unter dem REM keine Phasenseparation beobachtet werden. Nach dem Tempern zeigen alle ϕ_c von ternären PChMA/PS/CB-Verbundfilmen mit unterschiedlichen PChMA/PS Verhältnissen ein lineares Verhalten mit zunehmendem PChMA-Gehalt. Wenn die beiden ϕ_c beider binären Systeme (Polymer A / Füllstoff und Polymer B / Füllstoff) bestimmt werden, kann eine lineare Beziehung zwischen dem ϕ_c der ternären Verbundstoffe (A + B + Füllstoffe) und dem Verhältnis zweier Polymere beobachtet werden, wenn Polymer A und B mischbar sind. Verglichen mit dem typischen Doppelperkolationseffekt, der im

Allgemeinen unter Verwendung eines nicht mischbaren Polymermischungssystems verwendet wird, kann dies einen neuen Ansatz liefern, ternär leitende Polymerverbundstoffe mit guten mechanischen Eigenschaften zu entwerfen.

(c) In diesem Teil wurden ternäre PalkylMA/PS/CNT-Verbundfilme mit unterschiedlichen Polymermischungsverhältnissen und CNT-Konzentrationen unter Verwendung eines Lösungsgießverfahrens hergestellt. CNT befand sich bevorzugt in der PalkylMA-Phase, was diese von den PalkylMA/PS/CB-Filmen unterscheidet, bei denen sich CB bevorzugt im PS löst. Alle ϕ_c von ternären PalkylMA/PS/CNT-Verbundfilmen wurden systematisch untersucht und die experimentellen Daten wurden unter Verwendung der McLachlan-Theorie angepasst. Ein offensichtlicher doppelter Perkolationseffekt wurde beobachtet, wenn das PalkylMA/PS-Verhältnis 50/50 beträgt. Der ϕ_c von ternären Verbundfilmen bei PMMA/PS = 50/50 und PEMA/PS = 50/50 nahm im Vergleich zu reinem PMMA/CNT bzw. PEMA/CNT um 69,0% bzw. 73,1% ab. Ein Diagramm der Leitfähigkeitskontur gemäß allen experimentellen Daten wurde präsentiert, um die Leitfähigkeit gegenüber dem CNT-Volumenanteil und dem Polymermischungsverhältnis zu zeigen. Anders als bei PalkylMA/PS/CB zeigt die Leitfähigkeit sowohl von PMMA/PS/CNT- als auch von PEMA/PS/CNT-Filmen eine ähnliche Tendenz mit zunehmendem PS-Gehalt.

(d) Für die in dieser Arbeit lösungsgegossenen Filme konnte eine Reihe von ϕ_c- und Exponenten-t-Paaren aus den Perkolationskurven verschiedener Füllstoffe auf Kohlenstoffbasis unter Verwendung der McLachlan-Gleichung erhalten werden. Insbesondere wurden Paare untersucht, die senkrecht und in der Ebene zu den Filmen für binäre Verbundfilme mit CF unterschiedlicher AR abgeleitet wurden, sowie Paare, die senkrecht zu ternären Verbundfilmen mit unterschiedlichen Polymermischungen und

unterschiedlichen Polymermischungsverhältnissen sowohl für CB- als auch CNT-Füllstoffe abgeleitet wurden. In diesen Systemen unterscheidet sich der Exponent t für alle drei Füllstoffe von dem Wert von 2,0, der häufig als "universell" bezeichnet wird. Zum ersten Mal wird eine Beziehung zwischen ϕ_c und Exponent t nach einem linearen Verhalten $t = 2{,}0 + a \cdot \phi_c$ vorgeschlagen, was darauf hinweist, dass es einen Schnittpunkt mit der t-Achse bei t = 2,0 gibt, wenn sich ϕ_c 0 nähert.

10

10. Appendix

10.1 Original GPC results for PBMA and PChMA

The original GPC result is presented in Figure 10.1. The molecular weight and disperse for PBMA and PChMA cannot be found on the supplier's website. Therefore, PBMA and PChMA used in this work are determined by GPC and the results are presented.

AUSWERTUNG MIT RI-DETEKTOR										LS-Detektor	
Verzweigung	Probe	Lsgm	Messfile	Datum	Einwaage	inj. Menge	gef. Menge	gef/inj	Mw	Mn	Mw/Mn
			AstraV\Messungen THF/WW5/Eder PS THF		mg	mg/ml	mg	%	kg/mol	kg/mol	
			[PS_Eder_PEMA_Xu]								
	PBMA	THF	PBMA(001)[PS_Eder_PEMA_Xu]	19/11/2019	2	2.00	1.92	96.0	227.3	94.0	2.4
			PBMA(002)[PS_Eder_PEMA_Xu]				1.88	94.0	227.0	100.5	2.3
	Mittelwert							**95.0**	**227.2**	**97.3**	**2.3**
	Stdev.							***1.0***	***0.2***	***3.3***	***0.1***
	PCHMA	THF	PCHMA(001)[PS_Eder_PEMA_Xu]	19/11/2019	2	2.00	1.94	97.0	147.6	51.7	2.9
			PCHMA(002)[PS_Eder_PEMA_Xu]				1.92	96.0	146.0	53.3	2.7
	Mittelwert							**96.5**	**146.8**	**52.5**	**2.8**
	Stdev.							***0.5***	***0.8***	***0.8***	***0.1***

Figure 10.1 Original GPC results for PBMA and PChMA.

10.2 Surface tension of PChMA

The surface tension of PChMA cannot be found through the internet and public literature. Therefore, it was obtained from contact angle measurement. The original results are presented

in Table 10.1.

Table 10.1. The test results of surface tension for PChMA

	Sample 1	Sample 2	Sample 3	**Average**
γ	41.56	41.5	40.54	41.2
γ^d	36.04	38.06	37.2	37.1
γ^p	5.52	3.44	3.34	4.1

10.3 Thermogravimetric analysis (TGA) of pure PalkylMA

The thermal decomposition of pure PalkylMA was investigated as a function of temperature under N_2 atmosphere. As shown in Figure 2, the onset degradation temperature for PEMA and PBMA is lower than 150℃. However, the processing temperature for PS is higher than 150℃. Therefore, the PalkylMA/PS blends cannot be mixed by the melting method. This is the reason that the processing method in this study is solution casting.

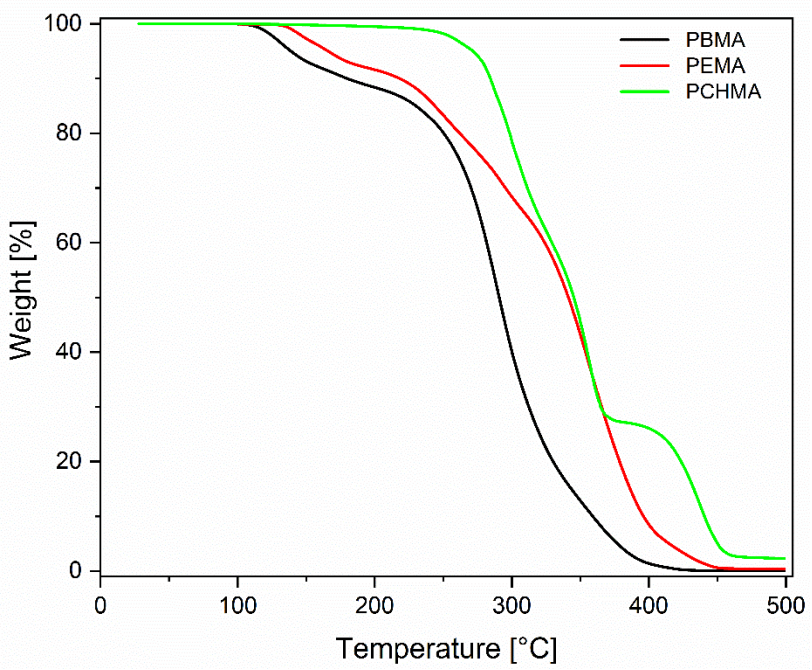

Figure 10.2 TGA scans of PalkylMA. The samples were heated at 10°C/min from 25°C to 500°C under an N_2 atmosphere.

10.4 Dynamic mechanical thermal analysis (DMTA)

The dynamic storage modulus as a function of temperature for PMMA, PEMA, PMMA/PS/CB and PEMA/PS/CB is shown in Figure 10.3, 10.4, 10.5 respectively. All the storage modulus curves show the same pattern, which can be divided into glass-rubber transition and rubbery. As shown in Figures, the T_g of PEMA is much smaller than PMMA. Therefore, the storage modulus of PEMA/PS/CB ternary composites reduces earlier than that of PMMA/PS/CB ternary composites.

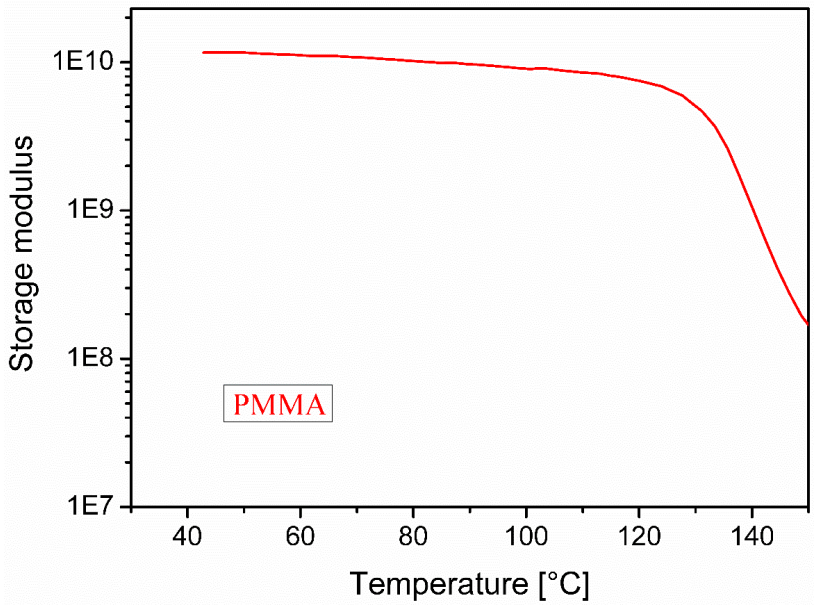

Figure 10.3 Storage modulus as a function of the temperature of PMMA in DMTA.

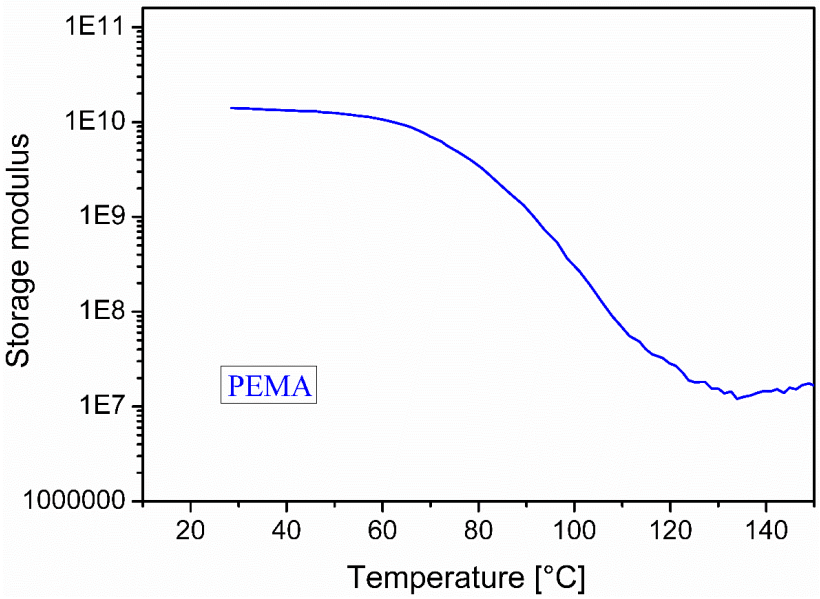

Figure 10.4 Storage modulus as a function of the temperature of PEMA in DMTA.

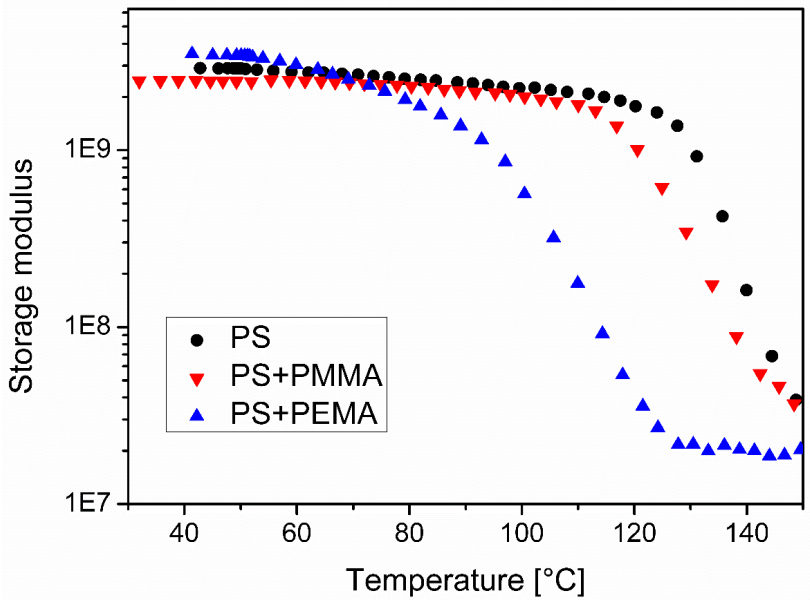

Figure 10.5 Storage modulus as a function of the temperature of PS, PMMA/PS/CB and PEMA/PS/CB in DMTA.

10.4 Rheological properties of composites

When long measuring time and high temperatures are applied, a precondition for reliable rheological measurements is the thermal stability of the material. As shown in Figure 10.6, the PEMA/PS/CB composites cannot be stable for a long time during 200℃.

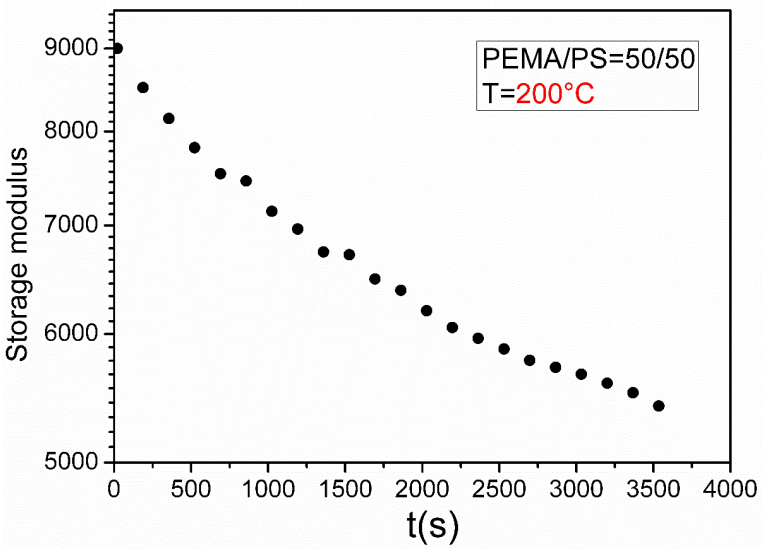

Figure 10.6 Storage modulus as a function of the residence time at 200°C for PEMA/PS blend with CB concentration at 2 vol.%.

10.5 Differential scanning calorimetry (DSC)

Figure 10.7 and 10.8 shows the DSC results of PMMA/PS/CB and PEMA/PS/CB ternary composites, respectively. The ratio of PMMA and PEMA with PS are both 50 to 50. As shown in Figures, there is only one T_g can be observed in PMMA/PS/CB and two Tg can be observed in PEMA/PS/CB. This is the Tg between PMMA and PS is close to each other and cannot be distinguished by DSC. However, the Tg of PEMA and PS are hugely different and can be distinguished by DSC.

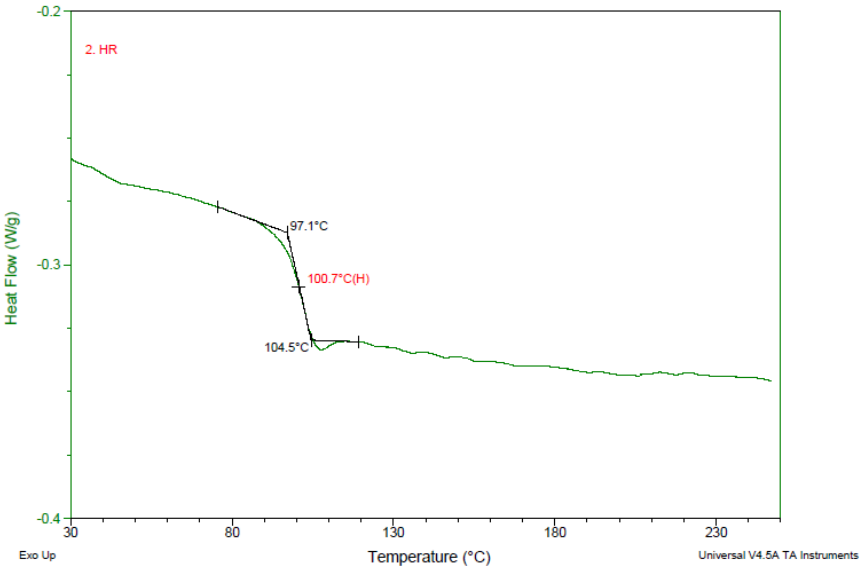

Figure 10.7 DSC reheating curves of the PMMA/PS/CB composites.

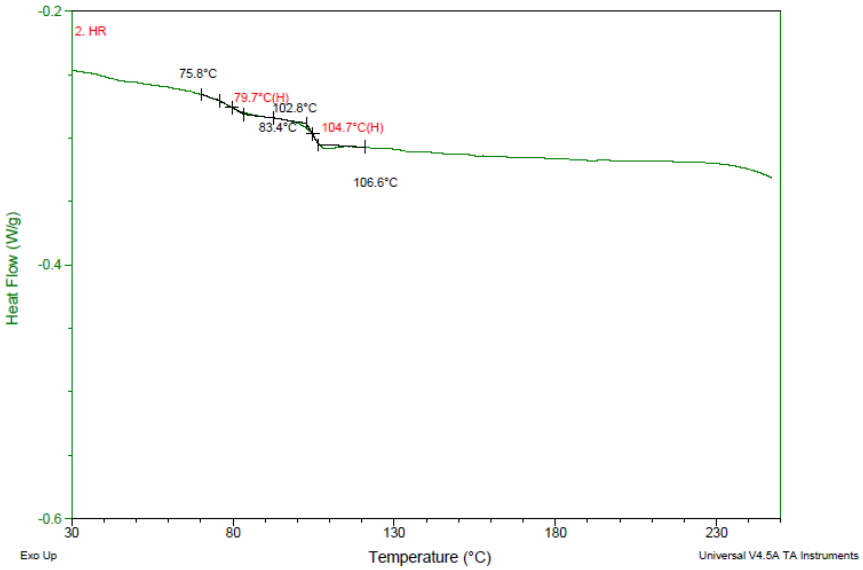

Figure 10.8 DSC reheating curves of the PEMA/PS/CB composites.

10.6 SEM images for PChMA/PS/CB composites

Figure 10.9 shows the SEM images for PChMA/PS/CB with different PChMA/PS ratios and different CB concentration. It can be seen that PChMA/PS blends did not undergo phase separation in different PChMA/PS ratios.

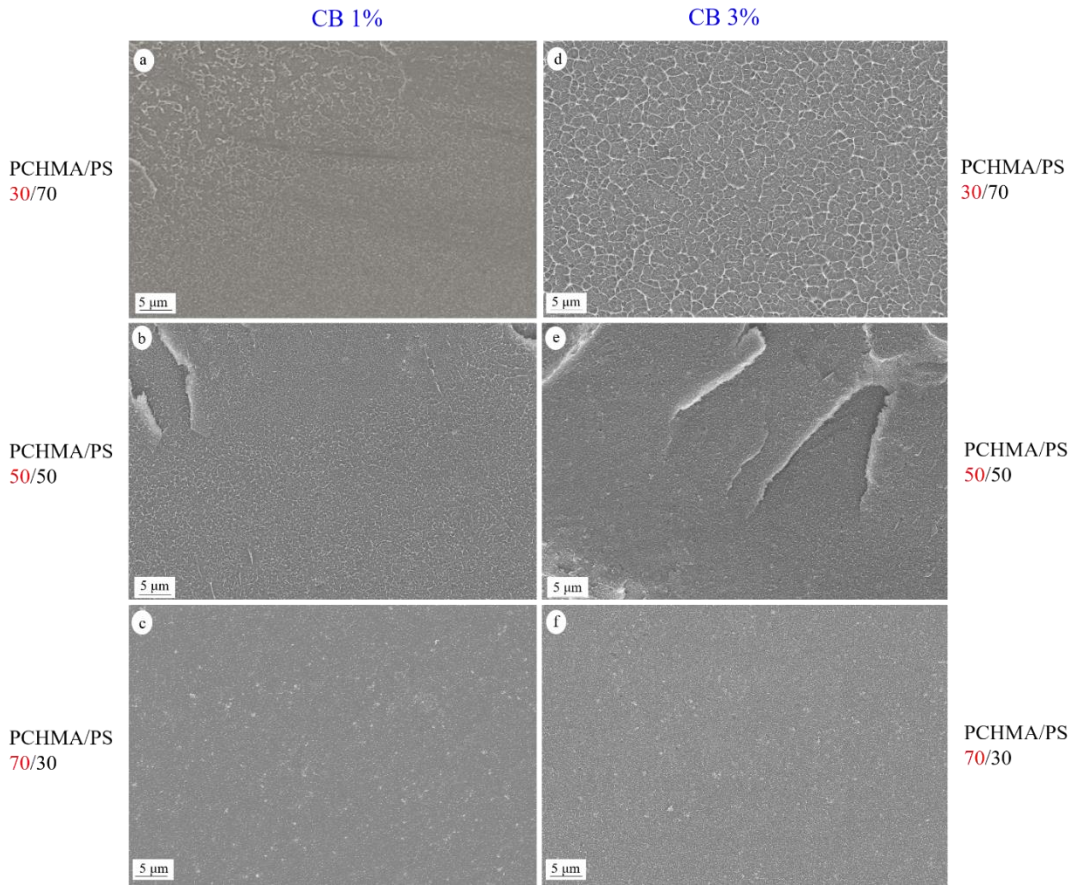

Figure 10.9 SEM images of the PChMA/PS/CB composites with different CB concentration and different PChMA/PS ratios. (a, b, c) CB at 1 vol. %, (d, e, f) CB at 3 vol.%

10.7 Sedimentation of CB particles

Figure 10.10 shows that the SEM images were divided into eight areas along the perpendicular direction of the film. (a)CB 0.5 vol. % (b) 1.5 vol. %. The analyzing results were represented in Figure 10.11.

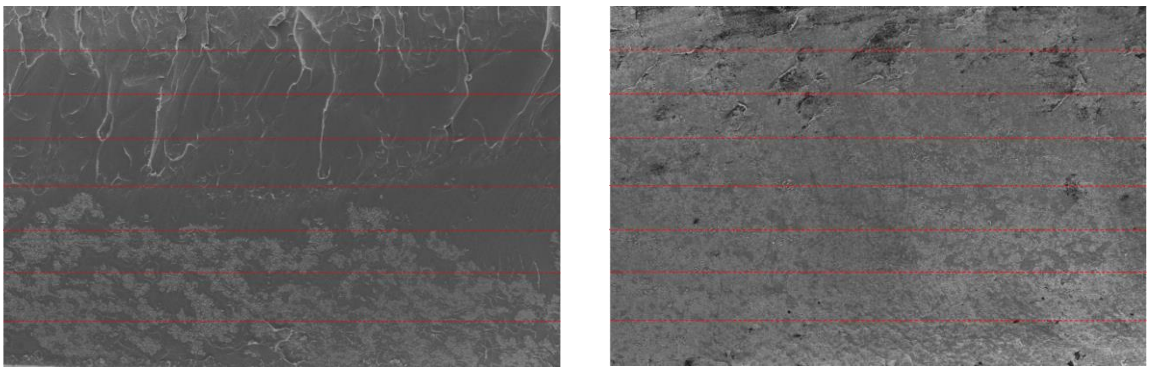

(a) **(b)**

Figure 10.10 CB concentration analyzing, the CB concentration at (a) 0.56 vol.%; (b)1.5 vol. %. The SEM imagines were divided into eight areas.

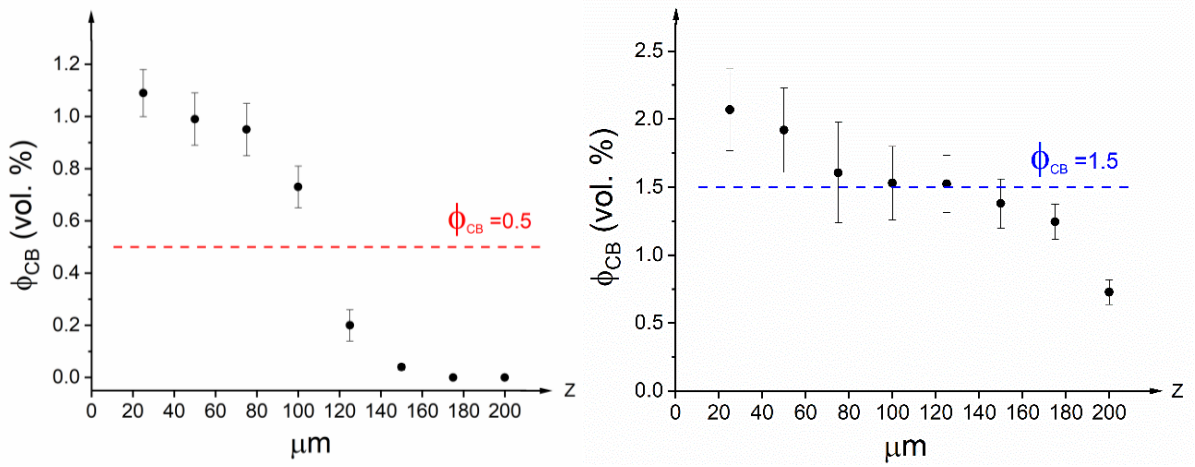

Figure 10.11 CB distribution results align the perpendicular direction of the film.

10.8 McLachlan equation parameter used in Origin software

y=100*(((1*10^ (-13))^(1/0.87)- (10^x)^(1/0.87))/((1*10^ (-13))^(1/0.87)+ ((1-C)/C)*(10^x)^(1/0.87))/(((1*10^ (-13))^(1/0.87)- (10^x)^(1/0.87))/((1*10^ (-13))^(1/0.87)+ ((1-C)/C)*(10^x)^(1/0.87))-((0.8)^(1/2)- (10^x)^(1/2))/((0.8)^(1/2)+ ((1-C)/C)*(10^x)^(1/2))))

10.9 All the ϕ_c and exponent t in this work

Perpendicular and In-plane represent measurement direction to the films

Matrix + Filler	ϕ_c (%)	Exponent t	Dimension	AR
PS/CB Perpendicular	2.18±0.10	3.85±0.32	3	1
PMMA/PS/CB Perpendicular	1.67±0.08	3.45±0.25	3	1
	1.75±0.12	3.26±0.26	3	1
	1.56±0.59	3.68±0.28	3	1
	1.54±0.08	3.10±0.23	3	1
	1.33±0.07	3.20±0.15	3	1
	1.24±0.14	2.60±0.19	3	1

	1.12±0.11	2.56±0.18	3	1
PMMA/CB Perpendicular	1.33±0.10	3.55±0.30	3	1
PMMA/CB In-plane	0.40±0.07	2.40±0.20	3	1
PEMA/PS/CB Perpendicular	1.17±0.04	3.20±0.25	3	1
	1.30±0.06	3.50±0.18	3	1
	1.05±0.15	3.40±0.19	3	1
	2.84±0.13	4.00±0.26	3	1
	2.41±0.10	3.45±0.42	3	1
	1.63±0.08	3.10±0.32	3	1
	1.27±0.08	3.50±0.27	3	1
PEMA/CB Perpendicular	1.50±0.03	2.88±0.26	3	1
PBMA/PS/CB Perpendicular	1.50±0.06	3.55±0.25	3	1
	0.93±0.08	3.10±0.28	3	1
	0.82±0.09	2.90±0.19	3	1
PBMA/CB Perpendicular	0.32±0.13	2.80±0.27	3	1
PCHMA/PS/CB Perpendicular	1.48±0.11	3.55±0.32	3	1
	1.48±0.10	3.54±0.27	3	1
	1.73±0.14	3.56±0.27	3	1
PCHMA/CB Perpendicular	1.50±0.13	3.55±0.27	3	1
PMMA/CF Perpendicular	0.50±0.36	1.90±0.15	2	49
	0.39±0.09	2.12±0.18	2	105
	0.27±0.06	2.35±0.17	2	227
	0.22±0.09	2.20±0.20	2	312
	0.15±0.05	2.40±0.16	2	417
	0.10±0.06	2.40±0.19	2	527
	0.07±0.04	2.39±0.13	2	616
	3.50±0.60	2.60±0.19	2	49
	3.10±0.50	2.20±0.21	2	105

PMMA/CF In-plane	1.80±0.30	2.20±0.18	2	227
	1.51±0.25	2.50±0.26	2	312
	1.30±0.35	2.50±0.24	2	417
	1.10±0.18	2.50±0.18	2	527
	0.80±0.20	2.00±0.19	2	616
PS/CNT Perpendicular	0.34±0.06	3.25±0.25	2	>77
PMMA/PS/CNT Perpendicular	0.44±0.10	3.25±0.19	2	>77
	0.13±0.05	3.21±0.26	2	>77
	0.32±0.07	2.97±0.28	2	>77
PMMA/CNT Perpendicular	0.42±0.08	3.21±0.23	2	>77
PMMA/CNT In-plane	0.37±0.06	3.00±0.15	2	>77
PEMA/PS/CNT Perpendicular	0.66±0.11	3.25±0.27	2	>77
	0.32±0.08	3.00±0.21	2	>77
	0.52±0.14	3.10±0.16	2	>77
PEMA/CNT Perpendicular	1.19±0.12	3.20±0.19	2	>77

Abbreviations and symbols

Abbreviations

ABS	Acrylonitrile Butadiene Styrene
AR	Aspect Ratios
CB	Carbon Black
CF	Carbon Fibers
CNT	Carbon Nanotubes
CPCs	Conductive Polymer Composites
DSC	Differential Scanning Calorimetry
FTIR	Fourier Transform infrared spectrometer
GEM	General Effective Medium
LCST	Lower Critical Solution Temperature
MWCNT	Multi-Wall Carbon Nanotubes
NMR	Nuclear Magnetic Resonance
NR	Natural Rubber
PalkylMA	Poly(alkyl MethAcrylate)
PBMA	Poly(Butyl Methacrylate)
PC	PolyCarbonate
PCHMA	Poly(CycloHexyl Methacrylate)
PCL	Poly-ε-CaproLactone
PEMA	Poly(Ethyl Methacrylate)

PiPrMA	Poly(iso-Propyl Methacrylate)
PLA	Poly(Lactic Acid)
PMMA	Poly(Methyl-MethAcrylate)
PP	PolyPropylene
PS	Polystyrene
PtBMA	Poly(tert-Butyl Methacrylate)
SEC	Size exclusion chromatography
SEM	Scanning Electron Microscopy
THF	Tetrahydrofuran

Greek letters

$\gamma_{1/2}$	interfacial tensions between 1 and 2
γ^d	disperse part of the surface tension
γ^p	polar part of the surface tension
Φ	the volume fraction of the filler
ϕ_c	the critical percolation threshold
ϕ_{γ_i}	volume fraction of component i in equation 2.18
$\phi_{c,\perp}$	perpendicular percolation threshold of the CPC films
$\phi_{c,\parallel}$	in-plane percolation threshold of the CPC films
σ	electrical conductivity of composites
σ_0	electrical conductivity of filler
σ_c	electrical conductivity of composites
σ_F	the conductivity of composites when $\phi = F$ in equation 2.6
σ_m	electrical conductivity of polymer matrix

$\sigma_{\perp}$	perpendicular conductivity of the film
$\sigma_{\parallel}$	In-plane conductivity of the film
γ	the angle between two cylinders in Balberg theory
γ_{pf}	surface tension in equation 2.8
$\rho_{c,long}$	the longitudinal electrical resistivity in equation 2.11
ρ_f	the fiber electrical resistivity in equation 2.12
ρ_m	resistivity of a bulk sample of metal in equation 2.10
θ	angle of orientation in equation 2.12
η_{γ_i}	melt viscosity of component i in equation 2.18
ω	wetting coefficient
$\chi_{12,cr}$	critical Flory-Huggins interaction parameter

Latin letters

A	constant parameter in equation 2.8
AR	aspect Ratio of fillers
B	constant parameter in equation 2.8
d	the thickness of the sample
d_c	diameter of the circle of contact in equation 2.18
F	the maximum volume fraction in equation 2.6
K	the coefficient in Balberg theory
$K_{\parallel}$	in-plane Pre-factor of Balberg equation
$K_{\perp}$	fitting parameter in equation 2.2
l	fiber length in equation 2.12

L	the length of cylinder in Balberg theory
m	number of contact in equation 2.12
M_n	number average molar mass
M_w	weight average molar mass
N	chain length
$R_\perp$	perpendicular electrical resistance of the film
$R_\parallel$	in-plane electrical resistance of the film
s	fitting parameter in equation 2.2
S	reference factor in equation 2.15
t	fitting parameter in equation 2.2
T_g	glass transition temperature
V_A	a monolayer volume percent in equation 2.9
V_B	a double layer volume percent in equation 2.10
V_{ex}	the excluded volume of filler in Balberg theory
V_f	the volume of filler in Balberg theory
W	the width of cylinder in Balberg theory
X	function of the number of contacts in equation 2.12

References

1. Zhang, W., Dehghani-Sanij, A. A., & Blackburn, R. S. (2007). Carbon based conductive polymer composites. *Journal of materials science*, *42*(10), 3408-3418.

2. Al-Saleh, M. H., & Sundararaj, U. (2009). A review of vapor grown carbon nanofiber/polymer conductive composites. *Carbon*, *47*(1), 2-22.

3. Lanticse, L. J., Tanabe, Y., Matsui, K., Kaburagi, Y., Suda, K., Hoteida, M., ... & Yasuda, E. (2006). Shear-induced preferential alignment of carbon nanotubes resulted in anisotropic electrical conductivity of polymer composites. *Carbon*, *44*(14), 3078-3086.

4. Jian, M., Wang, C., Wang, Q., Wang, H., Xia, K., Yin, Z., ... & Zhang, Y. (2017). Advanced carbon materials for flexible and wearable sensors. *Science China Materials*, *60*(11), 1026-1062.

5. Calberg, C., Blacher, S., Gubbels, F., Brouers, F., Deltour, R., & Jérôme, R. (1999). Electrical and dielectric properties of carbon black filled co-continuous two-phase polymer blends. Journal of Physics D: Applied Physics, 32(13), 1517.

6. Bokobza, L., Rahmani, M., Belin, C., Bruneel, J. L., & El Bounia, N. E. (2008). Blends of carbon blacks and multiwall carbon nanotubes as reinforcing fillers for hydrocarbon rubbers. Journal of Polymer Science Part B: Polymer Physics, 46(18), 1939-1951.

7. Thongruang, W., Spontak, R. J., & Balik, C. M. (2002). Bridged double percolation in conductive polymer composites: an electrical conductivity, morphology and mechanical property study. Polymer, 43(13), 3717-3725.

8. Vilčáková, J., Sáha, P., & Quadrat, O. (2002). Electrical conductivity of carbon fibres/polyester resin composites in the percolation threshold region. European Polymer Journal, 38(12), 2343-2347.

9. Tijing, L. D., Park, C. H., Choi, W. L., Ruelo, M. T. G., Amarjargal, A., Pant, H. R., ... & Kim, C. S. (2013). Characterization and mechanical performance comparison of multiwalled carbon nanotube/polyurethane composites fabricated by electrospinning and solution casting. *Composites Part B: Engineering*, *44*(1), 613-619.

10. Aguilar, J. O., Bautista-Quijano, J. R., & Avilés, F. (2010). Influence of carbon nanotube clustering on the electrical conductivity of polymer composite films. *Express Polym. Lett*, *4*(5), 292-299.

11. Yoshio, M., Kagata, T., Hoshino, K., Mukai, T., Ohno, H., & Kato, T. (2006). One-dimensional ion-conductive polymer films: alignment and fixation of ionic channels formed by self-organization of polymerizable columnar liquid crystals. *Journal of the American Chemical Society*, *128*(16), 5570-5577.

12. Lu, X., Zhang, W., Wang, C., Wen, T. C., & Wei, Y. (2011). One-dimensional conducting polymer nanocomposites: synthesis, properties and applications. *Progress in Polymer Science*, *36*(5), 671-712.

13. Behnam, A., Guo, J., & Ural, A. (2007). Effects of nanotube alignment and measurement direction on percolation resistivity in single-walled carbon nanotube films. *Journal of Applied Physics*, *102*(4), 044313.

14. Ram, R., Rahaman, M., Aldalbahi, A., & Khastgir, D. (2017). Determination of percolation threshold and electrical conductivity of polyvinylidene fluoride (PVDF)/short carbon fiber (SCF) composites: effect of SCF aspect ratio. *Polymer International*, *66*(4), 573-582.

15. Huang, J. C. (2002). Carbon black filled conducting polymers and polymer blends. Advances in Polymer Technology: Journal of the Polymer Processing Institute, 21(4), 299-313.

16. Chen, J., Cui, X., Sui, K., Zhu, Y., & Jiang, W. (2017). Balance the electrical properties and mechanical properties of carbon black filled immiscible polymer blends with a double percolation structure. Composites Science and Technology, 140, 99-105.

17. Sumita, M., Sakata, K., Asai, S., Miyasaka, K., & Nakagawa, H. (1991). Dispersion of fillers and the electrical conductivity of polymer blends filled with carbon black. Polymer bulletin, 25(2), 265-271.

18. Cao, Q., Song, Y., Tan, Y., & Zheng, Q. (2010). Conductive and viscoelastic behaviors of carbon black filled polystyrene during annealing. Carbon, 48(15), 4268-4275.

19. Ravindren, R., Mondal, S., Nath, K., & Das, N. C. (2019). Prediction of electrical conductivity, double percolation limit and electromagnetic interference shielding effectiveness of copper nanowire filled flexible polymer blend nanocomposites. Composites Part B: Engineering, 164, 559-569.

20. Liu, Y., Zhang, H., Porwal, H., Busfield, J. J., Peijs, T., & Bilotti, E. (2019). Pyroresistivity in conductive polymer composites: a perspective on recent advances and new applications. Polymer International, 68(3), 299-305.

21. Gao, J., Wang, L., Guo, Z., Li, B., Wang, H., Luo, J., ... & Xue, H. (2020). Flexible, superhydrophobic, and electrically conductive polymer nanofiber composite for multifunctional sensing applications. Chemical Engineering Journal, 381, 122778.

22. Narongthong, J., Le, H. H., Das, A., Sirisinha, C., & Wießner, S. (2019). Ionic liquid enabled electrical-strain tuning capability of carbon black based conductive polymer composites for small-strain sensors and stretchable conductors. Composites Science and Technology, 174, 202-211.

23. Song, B., Wang, T., Wang, L., Liu, H., Mai, X., Wang, X., ... & Wujcik, E. K. (2019). Interfacially reinforced carbon fiber/epoxy composite laminates via in-situ synthesized graphitic carbon nitride (g-C3N4). Composites Part B: Engineering, 158, 259-268.

24. Shi, Y. D., Li, J., Tan, Y. J., Chen, Y. F., & Wang, M. (2019). Percolation behavior of electromagnetic interference shielding in polymer/multi-walled carbon nanotube nanocomposites. Composites Science and Technology, 170, 70-76.

25. Taherian, R. (2016). Experimental and analytical model for the electrical conductivity of polymer-based nanocomposites. Composites Science and Technology, 123, 17-31.

26. Radzuan, N. A. M., Sulong, A. B., & Sahari, J. (2017). A review of electrical conductivity models for conductive polymer composite. International Journal of Hydrogen Energy, 42(14), 9262-9273.

27. Sahimi, M. Applications of Percolation Theory; CRC Press: Boca Raton, FL, USA, 1994.

28. McLachlan, D. S., Blaszkiewicz, M., & Newnham, R. E. (1990). Electrical resistivity of composites. Journal of the American Ceramic Society, 73(8), 2187-2203.

29. Balberg, I., Binenbaum, N., & Wagner, N. (1984). Percolation thresholds in the three-dimensional sticks system. Physical Review Letters, 52(17), 1465.

30. Balberg, I., Anderson, C. H., Alexander, S., & Wagner, N. (1984). Excluded volume and its relation to the onset of percolation. Physical review B, 30(7), 3933.

31. Mamunya, Y. P., Davydenko, V. V., Pissis, P., & Lebedev, E. V. (2002). Electrical and thermal conductivity of polymers filled with metal powders. European polymer journal, 38(9), 1887-1897.

32. Mamunya, E. P., Davidenko, V. V., & Lebedev, E. V. (1996). Effect of polymer-filler interface interactions on percolation conductivity of thermoplastics filled with carbon black. Composite Interfaces, 4(4), 169-176.

33. Malliaris, A., & Turner, D. T. (1971). Influence of particle size on the electrical resistivity of compacted mixtures of polymeric and metallic powders. Journal of Applied Physics, 42(2), 614-618.

34. Weber, M., & Kamal, M. R. (1997). Estimation of the volume resistivity of electrically conductive composites. Polymer composites, 18(6), 711-725.

35. McCullough, R. L. (1985). Generalized combining rules for predicting transport properties of composite materials. Composites Science and Technology, 22(1), 3-21.

36. Barton, R. L., Keith, J. M., & King, J. A. (2007). Development and modeling of electrically conductive carbon filled liquid crystal polymer composites for fuel cell bipolar plate applications. Journal of New Materials for Electrochemical Systems, 10(4), 225.

37. Shakir, M. F., Rashid, I. A., Tariq, A., Nawab, Y., Afzal, A., Nabeel, M., ... & Hamid, U. (2020). EMI shielding characteristics of electrically conductive polymer blends of PS/PANI in microwave and IR region. Journal of Electronic Materials, 49(3), 1660-1665.

38. Prapainainar, P., Du, Z., Theampetch, A., Prapainainar, C., Kongkachuichay, P., & Holmes, S. M. (2020). Properties and DMFC performance of nafion/mordenite composite membrane fabricated by solution-casting method with different solvent ratio. Energy, 190, 116451.

39. Suresha, S., Avinash, B. S., Harish, B. M., Chaturmukha, V. S., Jayanna, H. S., & Lamani, A. R. (2020). AC Conductivity and Dielectric Studies of Lithium Perchlorate Doped/(PVA/CMC) Composite Polymer Films. Sensor Letters, 18(1), 26-30.

40. Li, L., Sun, Q., Chen, X., Xu, Y., & Jiang, Z. (2020). Crystallization and Dielectric Properties of MWCNT/Poly (1-Butene) Composite Films by a Solution Casting Method. Materials, 13(3), 755.

41. Behnam, A., Guo, J., & Ural, A. (2007). Effects of nanotube alignment and measurement direction on percolation resistivity in single-walled carbon nanotube films. Journal of Applied Physics, 102(4), 044313.

42. Ram, R., Rahaman, M., Aldalbahi, A., & Khastgir, D. (2017). Determination of percolation threshold and electrical conductivity of polyvinylidene fluoride (PVDF)/short carbon fiber (SCF) composites: effect of SCF aspect ratio. Polymer International, 66(4), 573-582.

43. Gao, J. F., Yan, D. X., Yuan, B., Huang, H. D., & Li, Z. M. (2010). Large-scale fabrication and electrical properties of an anisotropic conductive polymer composite utilizing preferable location of carbon nanotubes in a polymer blend. Composites Science and Technology, 70(13), 1973-1979.

44. Lu, C., & Mai, Y. W. (2008). Anomalous electrical conductivity and percolation in carbon nanotube composites. Journal of Materials Science, 43(17), 6012-6015.

45. Qu, M., & Schubert, D. W. (2016). Conductivity of melt spun PMMA composites with aligned carbon fibers. Composites Science and Technology, 136, 111-118.

46. Kocabas, C., Pimparkar, N., Yesilyurt, O., Kang, S. J., Alam, M. A., & Rogers, A. J. (2007). Experimental and theoretical studies of transport through large scale, partially aligned arrays of single-walled carbon nanotubes in thin film type transistors. Nano letters, 7(5), 1195-1202.

47. Bertolotti, M., Ferrari, A., Liakhou, G. L., Li Voti, R., Marras, A., Ezquerra, T. A., & Balta-Calleja, F. J. (1995). Thermal anisotropy of polymer carbon fiber composites as revealed by photodeflection methods. Journal of applied physics, 78(9), 5706-5712.

48. Stankovich, S., Dikin, D. A., Dommett, G. H., Kohlhaas, K. M., Zimney, E. J., Stach, E. A., ... & Ruoff, R. S. (2006). Graphene-based composite materials. nature, 442(7100), 282.

49. Ding, P., Zhang, J., Song, N., Tang, S., Liu, Y., & Shi, L. (2015). Anisotropic thermal conductive properties of hot-pressed polystyrene/graphene composites in the through-plane and in-plane directions. Composites Science and Technology, 109, 25-31.

50. Suherman, H., Sahari, J., & Sulong, A. B. (2013). Effect of small-sized conductive filler on the properties of an epoxy composite for a bipolar plate in a PEMFC. Ceramics International, 39(6), 7159-7166.

51. Paul, D. R., & Newman, S. (1978). Polymer Blends, Vol. 1 and Vol. 2.

52. Olabis, O. (2012). Polymer-polymer miscibility. Elsevier.

53. Xavier, P., Rao, P., & Bose, S. (2016). Nanoparticle induced miscibility in LCST polymer blends: critically assessing the enthalpic and entropic effects. Physical Chemistry Chemical Physics, 18(1), 47-64.

54. Schubert, D. W., Stamm, M., & Müller, A. H. E. (1999). Neutron reflectometry studies on the interfacial width between polystyrene and various poly (alkylmethacrylates). Polymer Engineering & Science, 39(8), 1501-1507.

55. Kim, J. H., Park, D. S., & Kim, C. K. (2000). Characterization of the interaction energies for polystyrene blends with various methacrylate polymers. Journal of Polymer Science Part B: Polymer Physics, 38(20), 2666-2677.

56. Voulgaris, D., & Petridis, D. (2002). Emulsifying effect of dimethyldioctadecylammonium-hectorite in polystyrene/poly (ethyl methacrylate) blends. Polymer, 43(8), 2213-2218.

57. Friedrich, C., Schwarzwaelder, C., & Riemann, R. E. (1996). Rheological and thermodynamic study of the miscible blend polystyrene/poly (cyclohexyl methacrylate). Polymer, 37(12), 2499-2507.

58. Chang, L. L., & Woo, E. M. (2003). Thermal, morphology, and NMR characterizations on phase behavior and miscibility in blends of isotactic polystyrene with poly (cyclohexyl methacrylate). Journal of Polymer Science Part B: Polymer Physics, 41(8), 772-784.

59. Jang, F. H., & Woo, E. M. (1999). Composition dependence of phase instability and cloud point in solution-blended mixtures of polystyrene with poly (cyclohexyl methacrylate). Polymer, 40(9), 2231-2237.]

60. Voulgaris, D., & Petridis, D. (2002). Emulsifying effect of dimethyldioctadecylammonium-hectorite in polystyrene/poly (ethyl methacrylate) blends. Polymer, 43(8), 2213-2218.

61. Affrossman, S., Jérôme, R., O'neill, S. A., Schmitt, T., & Stamm, M. (2000). Surface structure of thin film blends of polystyrene and poly (n-butyl methacrylate). Colloid and Polymer Science, 278(10), 993-999.

62. Wen, B., & Zheng, X. (2019). Effect of the selective distribution of graphite nanoplatelets on the electrical and thermal conductivities of a polybutylene terephthalate/polycarbonate blend. Composites Science and Technology, 174, 68-75.

63. Gubbels, F., Jérôme, R., Teyssie, P., Vanlathem, E., Deltour, R., Calderone, A., ... & Brédas, J. L. (1994). Selective localization of carbon black in immiscible polymer blends: a useful tool to design electrical conductive composites. Macromolecules, 27(7), 1972-1974.

64. Foulger, S. H. (1998, October). Reduced percolation thresholds of immiscible conductive blends of poly (ethylene-co-vinyl acetate) and high density polyethylene. In Electrical Insulation and Dielectric Phenomena, 1998. Annual Report. Conference on (Vol. 1, pp. 282-287). IEEE.

65. Xu, Z., Zhao, C., Gu, A., Fang, Z., & Tong, L. (2007). Effect of morphology on the electric conductivity of binary polymer blends filled with carbon black. Journal of applied polymer science, 106(3), 2008-2017.

66. Cheah, K., Forsyth, M., & Simon, G. P. (2000). Processing and morphological development of carbon black filled conducting blends using a binary host of poly (styrene co-acrylonitrile) and poly (styrene). Journal of Polymer Science Part B: Polymer Physics, 38(23), 3106-3119.

67. Nair, S. T., Vijayan, P. P., Xavier, P., Bose, S., George, S. C., & Thomas, S. (2015). Selective localisation of multi walled carbon nanotubes in polypropylene/natural rubber blends to reduce the percolation threshold. Composites Science and Technology, 116, 9-17.

68. Mamunya, Y., Levchenko, V., Boiteux, G., Seytre, G., Zanoaga, M., Tanasa, F., & Lebedev, E. (2016). Controlling morphology, electrical, and mechanical properties of polymer blends by heterogeneous distribution of carbon nanotubes. Polymer Composites, 37(8), 2467-2477.

69. Nasti, G., Gentile, G., Cerruti, P., Carfagna, C., & Ambrogi, V. (2016). Double percolation of multiwalled carbon nanotubes in polystyrene/polylactic acid blends. Polymer, 99, 193-203.

70. Chen, Y., Yang, Q., Huang, Y., Liao, X., & Niu, Y. (2015). Influence of phase coarsening and filler agglomeration on electrical and rheological properties of MWNTs-filled PP/PMMA composites under annealing. Polymer, 79, 159-170.

71. Dil, E. J., & Favis, B. D. (2015). Localization of micro and nano-silica particles in a high interfacial tension poly (lactic acid)/low density polyethylene system. Polymer, 77, 156-166.

72. Hwang, T. Y., Yoo, Y., & Lee, J. W. (2012). Electrical conductivity, phase behavior, and rheology of polypropylene/polystyrene blends with multi-walled carbon nanotube. Rheologica acta, 51(7), 623-636.

73. Cipriano, B. H., Kota, A. K., Gershon, A. L., Laskowski, C. J., Kashiwagi, T., Bruck, H. A., & Raghavan, S. R. (2008). Conductivity enhancement of carbon nanotube and nanofiber-based polymer nanocomposites by melt annealing. Polymer, 49(22), 4846-4851.

74. Deng, H., Bilotti, E., Zhang, R., Loos, J., & Peijs, T. (2010). Effect of thermal annealing on the electrical conductivity of high-strength bicomponent polymer tapes containing carbon nanofillers. Synthetic Metals, 160(5-6), 337-344.

75. Liu, X., & Schubert, D. W. (2016). Influence of the pressure-dependent contact area between electrode and composite surface on the electrical conductivity. Composite Structures, 136, 414-418.

76. Kandare, E., Khatibi, A. A., Yoo, S., Wang, R., Ma, J., Olivier, P., ... & Wang, C. H. (2015). Improving the through-thickness thermal and electrical conductivity of carbon fibre/epoxy

laminates by exploiting synergy between graphene and silver nano-inclusions. Composites Part A: Applied Science and Manufacturing, 69, 72-82.

77. Liang, J. Z., & Yang, Q. Q. (2017). Effects of carbon fiber content and size on electric conductive properties of reinforced high density polyethylene composites. Composites Part B: Engineering, 114, 457-466.

78. Nomura, T., Tabuchi, K., Zhu, C., Sheng, N., Wang, S., & Akiyama, T. (2015). High thermal conductivity phase change composite with percolating carbon fiber network. Applied energy, 154, 678-685.

79. Yu, G. C., Wu, L. Z., & Feng, L. J. (2015). Enhancing the thermal conductivity of carbon fiber reinforced polymer composite laminates by coating highly oriented graphite films. Materials & Design, 88, 1063-1070.

80. Lee, S. H., Kim, J. Y., Koo, C. M., & Kim, W. N. (2017). Effects of processing methods on the electrical conductivity, electromagnetic parameters, and EMI shielding effectiveness of polypropylene/nickel-coated carbon fiber composites. Macromolecular Research, 25(9), 936-943.

81. Jang, J. U., Park, H. C., Lee, H. S., Khil, M. S., & Kim, S. Y. (2018). Electrically and thermally conductive carbon fibre fabric reinforced polymer composites based on Nanocarbons and an in-situ Polymerizable cyclic Oligoester. Scientific reports, 8(1), 7659.

82. Nicoletto, G., Riva, E., & Stocchi, A. (2016). Mechanical characterization of advanced random discontinuous carbon/epoxy composites. Materials Today: Proceedings, 3(4), 1079-1084.

83. Jiang, X., Bin, Y., Kikyotani, N., & Matsuo, M. (2006). Thermal, electrical and mechanical properties of ultra-high molecular weight polypropylene and carbon filler composites. Polymer journal, 38(5), 419.

84. Schubert, D. W. (2018). Novel Theoretical Self-Consistent Mean-Field Approach to Describe the Conductivity of Carbon Fiber Filled Thermoplastics—PART I—Theory. Macromolecular Theory and Simulations, 27(4), 1700104.

85.Chekanov, Y., Ohnogi, R., Asai, S., & Sumita, M. (1998). Positive temperature coefficient effect of epoxy resin filled with short carbon fibers. Polymer journal, 30(5), 381.

86. Qu, M., Nilsson, F., & Schubert, D. W. (2018). Effect of Filler Orientation on the Electrical Conductivity of Carbon Fiber/PMMA Composites. Fibers, 6(1), 3.

87. De Vivo, B., Lamberti, P., Spinelli, G., Tucci, V., Guadagno, L., & Raimondo, M. (2015). The effect of filler aspect ratio on the electromagnetic properties of carbon-nanofibers reinforced composites. Journal of Applied Physics, 118(6), 064302.

88. Fei, J., Luo, W., Huang, J., Ouyang, H., Wang, H., & Cao, L. (2015). Effect of hydrothermal modified carbon fiber through Diels–Alder reaction and its reinforced phenolic composites. RSC Advances, 5(79), 64450-64455.

89. Ribeiro, R. F., Pardini, L. C., Alves, N. P., Júnior, B., & Rios, C. A. (2015). Thermal Stabilization study of polyacrylonitrile fiber obtained by extrusion. Polimeros, 25(6), 523-530.

90. Li, J., Ma, P. C., Chow, W. S., To, C. K., Tang, B. Z., & Kim, J. K. (2007). Correlations between percolation threshold, dispersion state, and aspect ratio of carbon nanotubes. Advanced Functional Materials, 17(16), 3207-3215.

91. Bigg, D. M. (1979). Mechanical, thermal, and electrical properties of metal fiber-filled polymer composites. Polymer Engineering & Science, 19(16), 1188-1192.

92. Grujicic, M., Cao, G., & Roy, W. N. (2004). A computational analysis of the percolation threshold and the electrical conductivity of carbon nanotubes filled polymeric materials. Journal of materials science, 39(14), 4441-4449.

93. Ram, R., Rahaman, M., Aldalbahi, A., & Khastgir, D. (2017). Determination of percolation threshold and electrical conductivity of polyvinylidene fluoride (PVDF)/short carbon fiber (SCF) composites: effect of SCF aspect ratio. Polymer International, 66(4), 573-582.

94. Carmona, F., Prudhon, P., & Barreau, F. (1984). Percolation in short fibres epoxy resin composites: conductivity behavior and finite size effects near threshold. Solid state communications, 51, 255-257.

95. McLachlan, D. S., & Sauti, G. (2007). The AC and DC conductivity of nanocomposites. Journal of Nanomaterials, 2007.

96. Starý, Z., Krückel, J., Weck, C., & Schubert, D. W. (2013). Rheology and conductivity of carbon fibre composites with defined fibre lengths. Composites Science and Technology, 85, 58-64.

97. Deng, H., Lin, L., Ji, M., Zhang, S., Yang, M., & Fu, Q. (2014). Progress on the morphological control of conductive network in conductive polymer composites and the use as electroactive multifunctional materials. *Progress in Polymer Science*, *39*(4), 627-655.

98. Mathieu, B., Anthony, C., Arnaud, A., & Lionel, F. (2015). CNT aggregation mechanisms probed by electrical and dielectric measurements. *Journal of Materials Chemistry C*, *3*(22), 5769-5774.

99. Kim, S. (2018). Effect of Particle Size on Carbon Nanotube Aggregates Behavior in Dilute Phase of a Fluidized Bed. *Processes*, *6*(8), 121.

100. Huang, J., Mao, C., Zhu, Y., Jiang, W., & Yang, X. (2014). Control of carbon nanotubes at the interface of a co-continuous immiscible polymer blend to fabricate conductive composites with ultralow percolation thresholds. Carbon, 73, 267-274.

101. Cohen, E., Zonder, L., Ophir, A., Kenig, S., McCarthy, S., Barry, C., & Mead, J. (2013). Hierarchical structures composed of confined carbon nanotubes in cocontinuous ternary polymer blends. Macromolecules, 46(5), 1851-1859.

102. Mondal, R. K., Dubey, K. A., Bhardwaj, Y. K., Panicker, L., & Varshney, L. (2016). Acronitrile butadiene styrene/polycaprolactam/nano carbon black composites: Selective percolation, glass transition and temperature dependence of electrical conductivity. Polymer Composites, 37(2), 481-487.

103. Reich, S., & Cohen, Y. (1981). Phase separation of polymer blends in thin films. Journal of Polymer Science: Polymer Physics Edition, 19(8), 1255-1267.

104. Yan, D., Zhang, H. B., Jia, Y., Hu, J., Qi, X. Y., Zhang, Z., & Yu, Z. Z. (2012). Improved electrical conductivity of polyamide 12/graphene nanocomposites with maleated polyethylene-octene rubber prepared by melt compounding. ACS applied materials & interfaces, 4(9), 4740-4745.

105. Harrats, C., Groeninckx, G., & Thomas, S. (2005). Micro-and nanostructured multiphase polymer blend systems: phase morphology and interfaces. CRC press.

106. Utrachi, L. A. (1990). Polymer Alloys and Blends, Chapter 3.

107. Paul, D. R., & Barlow, J. W. (1980). Polymer blends. Journal of Macromolecular Science—Reviews in Macromolecular Chemistry, 18(1), 109-168.

108. Baudouin, A. C., Devaux, J., & Bailly, C. (2010). Localization of carbon nanotubes at the interface in blends of polyamide and ethylene–acrylate copolymer. Polymer, 51(6), 1341-1354.

109. Sahini, M., & Sahimi, M. (2014). Applications of percolation theory. CRC Press.

110. Liu, X., Krückel, J., Zheng, G., & Schubert, D. W. (2013). Mapping the electrical conductivity of poly (methyl methacrylate)/carbon black composites prior to and after shear. ACS applied materials & interfaces, 5(18), 8857-8860.

111. Starý, Z. (2014). Thermodynamics and Morphology and Compatibilization of Polymer Blends. Characterization of Polymer Blends, 93-132.

112. Pajula, K., Taskinen, M., Lehto, V. P., Ketolainen, J., & Korhonen, O. (2010). Predicting the formation and stability of amorphous small molecule binary mixtures from computationally determined Flory− Huggins interaction parameter and phase diagram. Molecular pharmaceutics, 7(3), 795-804.

113. Gedde, U. W. (2013). Polymer physics. Springer Science & Business Media.

114. Sammler, R. L., Dion, R. P., Carriere, C. J., & Cohen, A. (1992). Compatibility of high polymers probed by interfacial tension. Rheologica acta, 31(6), 554-564.

115. Schubert, D. W., & Stamm, M. (1996). Influence of chain length on the interface width of an incompatible polymer blend. EPL (Europhysics Letters), 35(6), 419.

116. Pan, Y., Liu, X., Hao, X., Starý, Z., & Schubert, D. W. (2016). Enhancing the electrical conductivity of carbon black-filled immiscible polymer blends by tuning the morphology. European Polymer Journal, 78, 106-115.

117. Xu, H. G., Qu, M. C., Pan, Y. M., & Schubert, D. W. (2019). Conductivity of Poly (methyl methacrylate)/Polystyrene/Carbon Black and Poly (ethyl methacrylate)/Polystyrene/Carbon Black Ternary Composite Films. Chinese Journal of Polymer Science, 1-10.

118. Pan, Y., Liu, X., Kaschta, J., Liu, C., & Schubert, D. W. (2017). Reversal phenomena of molten immiscible polymer blends during creep-recovery in shear. Journal of Rheology, 61(4), 759-767.

119. Liu, T., Huang, K., Li, L., Gu, Z., Liu, X., Peng, X., & Kuang, T. (2019). High performance high-density polyethylene/hydroxyapatite nanocomposites for load-bearing bone substitute: fabrication, in vitro and in vivo biocompatibility evaluation. Composites Science and Technology, 175, 100-110.

120. Elias, L., Fenouillot, F., Majesté, J. C., Alcouffe, P., & Cassagnau, P. (2008). Immiscible polymer blends stabilized with nano-silica particles: Rheology and effective interfacial tension. Polymer, 49(20), 4378-4385.

121. Fenouillot, F., Cassagnau, P., & Majesté, J. C. (2009). Uneven distribution of nanoparticles in immiscible fluids: Morphology development in polymer blends. Polymer, 50(6), 1333-1350.

122. Altstädt, V., de Freitas, L. L., & Schubert, D. W. (2004). Rheological and mechanical properties of poly (α-methylstyrene-co-acrylonitrile)/poly [(methyl acrylate-co-methyl methacrylate)] blends in miscible and phase separated regimes of various morphologies. Part IV: Influence of the morphology on the mechanical properties (IUPAC Technical Report). Pure and applied chemistry, 76(2), 389-413.

123. Cai, X., Li, B., Pan, Y., & Wu, G. (2012). Morphology evolution of immiscible polymer blends as directed by nanoparticle self-agglomeration. Polymer, 53(1), 259-266.

124. Böhm, G. G., & Nguyen, M. N. (1995). Flocculation of carbon black in filled rubber compounds. I. Flocculation occurring in unvulcanized compounds during annealing at elevated temperatures. Journal of applied polymer science, 55(7), 1041-1050.

125. Rahman, R., Soltanian, S., & Servati, P. (2016). Coupled effects of film thickness and filler length on conductivity and strain sensitivity of carbon nanotube/polymer composite thin films. IEEE Sensors Journal, 16(1), 77-87.

126. Gao, C., Zhang, S., Han, B., Sun, H., Wang, G., & Jiang, Z. (2014). Multi-walled carbon nanotube induced co-continuity of poly (ether ether ketone)/polyimide blends for high performance conductive materials. RSC Advances, 4(79), 42175-42182.

127. Jia, L. C., Li, M. Z., Yan, D. X., Cui, C. H., Wu, H. Y., & Li, Z. M. (2017). A strong and tough polymer–carbon nanotube film for flexible and efficient electromagnetic interference shielding. Journal of Materials Chemistry C, 5(35), 8944-8951.

128. Zhang, Y., Li, Z., Li, H., Gao, J., Zhang, J., & Zeng, Y. (2014). Effect of carbon nanotubes shape on the properties of multiwall carbon nanotubes/polyethylene flexible transparent conductive films. Journal of Materials Science: Materials in Electronics, 25(6), 2692-2696.

129. Zhao, B., Zhao, C., Li, R., Hamidinejad, S. M., & Park, C. B. (2017). Flexible, ultrathin, and high-efficiency electromagnetic shielding properties of poly (vinylidene fluoride)/carbon composite films. ACS applied materials & interfaces, 9(24), 20873-20884.

130. Arboleda-Clemente, L., Ares-Pernas, A., García, X., Dopico, S., & Abad, M. J. (2017). Segregated conductive network of MWCNT in PA12/PA6 composites: Electrical and rheological behavior. Polymer Composites, 38(12), 2679-2686.

131. www.surface-tension.desolid-surface-energy.htm

132. Barber, A. H., Cohen, S. R., & Wagner, H. D. (2004). Static and dynamic wetting measurements of single carbon nanotubes. Physical review letters, 92(18), 186103.

133. Burmistrov, I., Gorshkov, N., Anshin, S., Kolesnikov, E., Kuskov, K., Ilinykh, I., ... & Kuznetsov, D. (2019). Enhancement of percolation threshold by controlling the structure of composites based on nanostructured carbon filler. Journal of Electronic Materials, 48(8), 5111-5118.

134. Zhang, J., Bokov, A. A., Gao, S. L., Zhang, N., Zhuang, J., Ren, W., & Ye, Z. G. (2018). Effect of hierarchical structure on electrical properties and percolation behavior of multiscale composites modified by carbon nanotube coating. Composites Science and Technology, 164, 160-167.

135. Liu, Y. F., Feng, L. M., Chen, Y. F., Shi, Y. D., Chen, X. D., & Wang, M. (2018). Segregated polypropylene/cross-linked poly (ethylene-co-1-octene)/multi-walled carbon nanotube nanocomposites with low percolation threshold and dominated negative temperature coefficient effect: Towards electromagnetic interference shielding and thermistors. Composites Science and Technology, 159, 152-161.

136. Soares, B. G., Soares da Silva, J., SILVA, A. A., & Livi, S. (2019). Double Percolation of Melt-Mixed PS/PBAT Blends Loaded with Carbon Nanotube: Effect of Molding Temperature and the Non Covalent Functionalization of the Filler by Ionic Liquid. Frontiers in Materials, 6, 191.

137. Zhang, J., Bokov, A. A., Gao, S. L., Zhang, N., Ren, W., & Ye, Z. G. (2018). Strong Anisotropy and Ultralow Percolation Threshold in Multiscale Composites Modified by Carbon Nanotubes Coated Hollow Glass Fiber. Advanced Engineering Materials, 20(7), 1800077.

138. Jia, L. C., Yan, D. X., Cui, C. H., Ji, X., & Li, Z. M. (2016). A unique double percolated polymer composite for highly efficient electromagnetic interference shielding. Macromolecular Materials and Engineering, 301(10), 1232-1241.

139. Haghgoo, M., Hassanzadeh-Aghdam, M. K., & Ansari, R. (2019). A comprehensive evaluation of piezoresistive response and percolation behavior of multiscale polymer-based nanocomposites. Composites Part A: Applied Science and Manufacturing, 105735.

140. Chiteme, C., & McLachlan, D. S. (2003). AC and DC conductivity, magnetoresistance, and scaling in cellular percolation systems. Physical Review B, 67(2), 024206.

141. Brosseau, C. (2002). Generalized effective medium theory and dielectric relaxation in particle-filled polymeric resins. Journal of applied physics, 91(5), 3197-3204.

142. Carmona, F., Canet, R., & Delhaes, P. (1987). Piezoresistivity of heterogeneous solids. Journal of Applied Physics, 61(7), 2550-2557.

143. Deprez, N., & McLachlan, D. S. (1988). The analysis of the electrical conductivity of graphite conductivity of graphite powders during compaction. Journal of Physics D: Applied Physics, 21(1), 101.

144. Wu, J., & McLachlan, D. S. (1998). Scaling behavior of the complex conductivity of graphite-boron nitride percolation systems. Physical Review B, 58(22), 14880.

145. Kogut, P. M., & Straley, J. P. (1979). Distribution-induced non-universality of the percolation conductivity exponents. Journal of Physics C: Solid State Physics, 12(11), 2151.

146. Balberg, I. (1998). Limits on the continuum-percolation transport exponents. Physical Review B, 57(21), 13351.

147. Halperin, B. I., Feng, S., & Sen, P. N. (1985). Differences between lattice and continuum percolation transport exponents. Physical review letters, 54(22), 2391.

148. Feng, S., Halperin, B. I., & Sen, P. N. (1987). Transport properties of continuum systems near the percolation threshold. Physical review B, 35(1), 197.

149. McLachlan, D. S., Sauti, G., & Chiteme, C. (2007). Static dielectric function and scaling of the ac conductivity for universal and nonuniversal percolation systems. Physical Review B, 76(1), 014201.

150. Runyan, J., Gerhardt, R. A., & Ruh, R. (2001). Electrical properties of boron nitride matrix composites: I, Analysis of McLachlan Equation and modeling of the conductivity of boron nitride–boron carbide and boron nitride–silicon carbide composites. Journal of the American Ceramic Society, 84(7), 1490-1496

151. Kovacik, J. (1998). Electrical conductivity of two-phase composite material. Scripta materialia, 39(2), 153-157.

152. Zallen, R. (1983). The formation of amorphous solids. The physics of amorphous solids. New York: Wiley, 1-22.

153. Kassim, S. E., Achour, M. E., Costa, L. C., & Lahjomri, F. (2014). Modelling the DC electrical conductivity of polymer/carbon black composites. Journal of Electrostatics, 72(3), 187-191.

154. Weng, W., Chen, G., Wu, D., Chen, X., Lu, J., & Wang, P. (2004). Fabrication and characterization of nylon 6/foliated graphite electrically conducting nanocomposite. Journal of Polymer Science Part B: Polymer Physics, 42(15), 2844-2856.

155. Sharma, S. K., Tandon, R. P., & Sachdev, V. K. (2014). Pre-localized MWCNT network

for a low percolation threshold in MWCNT/ABS nanocomposites: experiment and theory. RSC Advances, 4(105), 60733-60740.

156. Shrivastava, N. K., Suin, S., Maiti, S., & Khatua, B. B. (2014). An approach to reduce the percolation threshold of MWCNT in ABS/MWCNT nanocomposites through selective distribution of CNT in ABS matrix. RSC advances, 4(47), 24584-24593.

157. Yi, J. Y., & Choi, G. M. (1999). Percolation behavior of conductor-insulator composites with varying aspect ratio of conductive fiber. Journal of electroceramics, 3(4), 361-369.

158. McLachlan, D. S., Chiteme, C., Park, C., Wise, K. E., Lowther, S. E., Lillehei, P. T., ... & Harrison, J. S. (2005). AC and DC percolative conductivity of single wall carbon nanotube polymer composites. Journal of Polymer Science Part B: Polymer Physics, 43(22), 3273-3287.

159. Luo, X., Qu, M., & Schubert, D. W. Electrical conductivity and fiber orientation of poly (methyl methacrylate)/carbon fiber composite sheets with various thickness. Polymer Composites.

Acknowledgment

This thesis results from my work as a Ph.D. student at the Institute for Polymer Materials of the Materials Science department at the Friedrich-Alexander-University Erlangen-Nuremberg. Therefore, I would like to thank all the people who helped me throughout my Ph.D.

I would like to thank my supervisor Prof. Dr. Dirk W. Schubert for the opportunity to be a member of his institute and to write a doctoral thesis about my scientific work during this time. I want to thank him for his support and advice during the whole period of my Ph.D. project. He gave me a great degree of freedom during this time and the opportunity to present my results at international conferences. I learned a lot of fundamental knowledge deeply on this project, e.g. Flory-Huggins parameter, spin coating, phase-separation prediction for two polymers and so on.

I have gained a lot from the personality and working attitude of Prof. Dr. Dirk W. Schubert, e.g. rigorous in work and meticulous in detail and always full of energy and enthusiasm in both working and life. I remember there was a training course at the conference in Italy, not only me but also other audiences were impressed by his full energy training course. Both in academics and daily life, I can feel his enthusiasm. This is a really good habit which I hope I can keep in my whole life.

I am sincerely grateful to Dr. Muchao Qu for his help and advice to discuss my papers. We talked about plenty of interesting things as well. I have learned a lot from him during my Ph. D. period. I express my gratitude to Dr. Yamin Pan who helped me familiar with the instruments of the institute. Dr. Xiaoqong Hao is thanked for giving suggestions for the DMTA test. I would like to thank Dr. Xianhu Liu for his kindly caring for my academic career.

I am grateful to Dr. Joachim Kaschta for his help on GPC characterization. I am deeply appreciated to M. Sc. Siegfried Werner and M. Sc. Michael Redel for revising my summary in German. My further gratitude to M. Sc. Jonas Daenicke for teaching the Gemini rheology and drying method for my samples. I am deeply thankful to M. Sc. Andreas Ziegmann for revising my abstract for a conference. I also want to acknowledge M. Sc. Franz Lanyi for discussing FTIR results. I would like to thank Dr. Mathias Bechert for his kindly offer me a book of the Ph.D. thesis. I am grateful to Tim Höhnemann for his German-style Christmas gift.

I am grateful to Ms. Jennifer Reiser for FTIR, contact angle and TGA test; Ms. Inge Herzer for DSC, Ms. Magdalena Papp for teaching me how to operate SEM, Ms. Susanne Michler for arranging all in the laboratory. Mr. Harald Rost and Mr. Marko Heyder are thanked for the technical support, they made me a model to do the thermal annealing for thin films.

M. Sc. Azeem M. Munawar is thanked for working through this thesis, I would like to thank Guanda Yang, Yiqing Qin for our scientific discussions and we had a lot of fun during our stay at LSP. Xiaoling Luo is thanked for continuing the research on conductive films. I also want to thank my colleague M. Sc. Alexander Bier, M. Sc. Bastian Wölfel, Dr. med. Dipl.-Ing. Harald von Hanstein, M. Sc. Marcus Himmler, M. Sc. Stefan Schrüfer, M. Sc. Xin Wang, M. Sc. Mirzaei Zeynab. It is a great honor to work with them.

Finally, I would like to thank my family. My parents give me constant encouragement and support for my studies. My wife (M. Sc Yang Zhang) support me and give me advice at my tough time, it is her love and encouragement makes me better.

My Ph.D. research at FAU is supported by the state scholarship fund of China Scholarship Council.